Fraunhofer ISE

University of Stuttgart
Institute for Acoustics and Building Physics
Life Cycle Engineering GaBi

FRAUNHOFER INSTITUTE FOR SOLAR ENERGY SYSTEMS, ISE
UNIVERSITY OF STUTTGART - DEPARTMENT LIFE CYCLE ENGINEERING, INSTITUTE FOR ACOUSTICS AND BUILDING PHYSICS

Working paper

MATERIAL REQUIREMENTS FOR THE ENERGY TRANSITION

Energy technology profiles and environmental impacts

Estelle Gervais, Thomas Betten, Shivenes Shammugam, Roberta Graf, Matthias Müller, Thomas Schlegl

September 2022

Supported by the German Ministry for Economic Affairs and Climate Action (BMWK)
Project number: 03ET4065

https://dx.doi.org/10.24406/publica-427

Index

Introduction		5
1	Photovoltaics	8
1.1	**PERC – Passivated Emitter and Rear Cell**	**8**
1.1.1	Description	8
1.1.2	Material efficiency	8
1.1.3	Material composition	10
1.1.4	Environmental impacts	12
1.2	**SHJ – Silicon Heterojunction Solar Cell**	**14**
1.2.1	Description	14
1.2.2	Material efficiency	15
1.2.3	Material composition	17
1.2.4	Environmental impacts	18
1.3	**CIGS – Copper Indium Gallium Selenide Solar Cell**	**21**
1.3.1	Description	21
1.3.2	Material efficiency	21
1.3.3	Material composition	23
1.3.4	Environmental impacts	24
1.4	**III-V/Si – Silicon Tandem Solar Cell**	**27**
1.4.1	Description	27
1.4.2	Material efficiency	28
1.4.3	Material composition	29
1.4.4	Environmental impacts	31
2	Wind energy	34
2.1	**EESG-DD – Electrically Excited Synchronous Generator – Direct Drive (Onshore)**	**34**
2.1.1	Description	34
2.1.2	Material efficiency	36
2.1.3	Material composition	37
2.1.4	Environmental impacts	37
2.2	**PMSG-DD – Permanent Magnet Synchronous Generator – Direct-Drive (Onshore)**	**39**
2.2.1	Description	39
2.2.2	Material efficiency	40
2.2.3	Material composition	41
2.2.4	Environmental impacts	42
2.3	**PMSG-DD – Permanent Magnet Synchronous Generator – Direct-Drive (Offshore)**	**43**
2.3.1	Description	43
2.3.2	Material efficiency	45
2.3.3	Material composition	46
2.3.4	Environmental impacts	47
2.4	**PMSG-MS – Permanent Magnet Synchronous Generator – Middle-Speed (Offshore)**	**49**

2.4.1	Description	49
2.4.2	Material efficiency	50
2.4.3	Material composition	51
2.4.4	Environmental impacts	53
3	Fuel Cell	55
3.1	**PEMFC – Proton-Exchange Membrane Fuel Cell**	**55**
3.1.1	Description	55
3.1.2	Material efficiency	56
3.1.3	Material composition	56
3.1.4	Environmental impacts	57
4	Power-to-X	59
4.1	**AEL – Alkaline Electrolysis**	**59**
4.1.1	Description	59
4.1.2	Material efficiency	60
4.1.3	Material composition	60
4.1.4	Environmental impacts	61
5	Battery	63
5.1	**VRFB – Vanadium Redox Flow Battery**	**63**
5.1.1	Description	63
5.1.2	Material efficiency	63
5.1.3	Material composition	64
5.1.4	Environmental impacts	65
5.2	**NMC – Nickel Manganese Cobalt Lithium-Ion Battery**	**66**
5.2.1	Description	66
5.2.2	Material efficiency	68
5.2.3	Material composition	69
5.2.4	Environmental impacts	70
6	Transmission grid	72
6.1	**AC – Alternating Current Line**	**72**
6.1.1	Description	72
6.1.2	Material efficiency	73
6.1.3	Material composition	74
6.1.4	Environmental impacts	74
6.2	**DC – Direct Current Line**	**76**
6.2.1	Description	76
6.2.2	Material efficiency	76
6.2.3	Material composition	76
6.2.4	Environmental impacts	77
7	Combined Cycle Power Generation	79
7.1	**NGCC – Natural Gas Combined Cycle System**	**79**
7.1.1	Description	79
7.1.2	Material efficiency	80
7.1.3	Material composition	80
7.1.4	Environmental impacts	82

8	Condensing boiler	84
8.1	**Gas Condensing Boiler**	**84**
8.1.1	Description	84
8.1.2	Material efficiency	84
8.1.3	Material composition	84
8.1.4	Environmental impacts	85
9	Heat Pump	87
9.1	**AWHP – Air to Water Heat Pump**	**87**
9.1.1	Description	87
9.1.2	Material efficiency	87
9.1.3	Material composition	88
9.1.4	Environmental impacts	88
1 0	Solar Thermal Power	90
10.1	**Solar Flat Plate Collector**	**90**
10.1.1	Description	90
10.1.2	Material efficiency	91
10.1.3	Material composition	91
10.1.4	Environmental impacts	91
1 1	Heat Storage	93
11.1	**Hot Water Tank**	**93**
11.1.1	Description	93
11.1.2	Material efficiency	93
11.1.3	Material composition	93
11.1.4	Environmental impacts	93
1 2	Building Retrofitting	95
12.1	**Insulation**	**95**
12.1.1	Description	95
12.1.2	Material efficiency	96
12.1.3	Material composition	96
12.1.4	Environmental impacts	97
1 3	Imports	98
13.1	**Electricity imports**	**98**
13.1.1	Description	98
13.1.2	Material efficiency	98
13.1.3	Material composition	98
13.1.4	Environmental impacts	98
1 4	**Material Composition of Alloys and Electronics**	**100**
1 5	**Absolute numbers of environmental impacts by technology**	**102**
1 6	References	105
1 7	Imprint	111

Introduction

The transition to low-carbon energy systems will require vast amounts of minerals, at rates and volumes which have been deemed at risk of being incompatible with how the mining industry and supply chains worked and operated in the past (Elshkaki et al., 2018; Gielen, 2021; Gregoir and van Acker, 2022; Watari et al., 2018). Material production also plays a substantial role in global greenhouse gas emissions (Hertwich, 2021) while generating social and environmental impacts locally (United Nations Environment Programme, 2020). The deployment of decarbonization technologies across the power, heat, and transport sectors as well as for storage needs to factor in these resource concerns and integrate sound mitigation strategies. To that effect, the project InteRessE – Resource Demand for the Energy Transformation: Interdisciplinary Evaluation of Scenarios to Supply Electricity and Heat – funded by BMWK has assessed the economic, social, and environmental risks associated with the material requirements for the German energy transition. The quantification of the material intensity for each energy technology and under consideration of material efficiency measures up until 2050 is hereby a central result.

As highlighted by literature reviews (Liang et al., 2022; Watari et al., 2020), studies on the metal requirements for energy technologies have multiplied over the last decade. Material intensity data are however often dispersed, as many studies focus on a specific technology such as photovoltaics (Gervais et al., 2021), wind turbine (Shammugam et al., 2019), or battery (Xu et al., 2020). Modelling the requirements for intersectoral energy scenarios is rendered significantly time-consuming. Further, the environmental impacts of material requirements for energy technologies are mostly out of scope of existing studies, despite being interlinked. Material efficiency measures resulting from technological development are not systematically considered as well (Liang et al., 2022).

This working paper addresses these gaps and represents an effort to facilitate and speed-up research work on the material requirements for the energy transition. It provides background information on 19 energy technologies for electricity and heat production, storage and transport, as well as building renovation. Each of these "technology profiles" provides a brief technology description with assumed lifetime and production location, a quantitative assessment of relevant material efficiency measures, and the dynamic material intensity until 2050. The material intensity is expressed in kg/MW (e.g., for power generation technologies), kg/kWh (e.g., for battery), kg/km of transmission line or kg/m² of renovated/built living space, depending on the technology considered. Additionally, a selection of environmental impacts is assessed. These impacts are represented by the impact on Climate Change with the Global Warming Potential as an indicator for political targets and action, and Resource Use with Abiotic Depletion Potential as an indicator for the cumulative impact of resource use totalled for metals and other abiotic resources.

The material intensities result from a literature review conducted in 2019 and 2020. The data for some technologies was reviewed and consolidated by a project advisory board of technology experts. While the focus of InteRessE lies on metals and metalloids, data on non-metallic materials is also provided when available. As for the environmental impacts, the Environmental Footprint Methodology was used in its version 3.0. The impacts are calculated with the LCA Software GaBi (Sphera, 2020). The used version is 9.2.168 with Service Pack 40. In contrast to the classic LCA approach where energy services are regarded by the provided energy, for this study the installed capacity (i.e., MW for generation, kWh for storage, km for transmission, and m² for housing retrofit)

was used. The coupling between environmental systems analysis and life cycle assessment including the consequent LCA modelling choices and the process of decarbonisation is described in (Betten et al., 2020).

The material intensity data for each technology and over time are provided in the respective chapters. The composition of alloys and electronics can further be disaggregated by constituent element as shown in Chapter 14. The LCA results are provided qualitatively in the respective chapters for each technology: The first figure shows the environmental impacts over time for Climate Change and Resource Use. The second figure shows the contribution to the Resource Use indicator by the different metals in Sb-equivalents. The values between the base years 2020, 2025, 2030, 2025, 2040, 2045 and 2050 are interpolated. The environmental impacts related to electricity imports from Europe to Germany are examined as well. The LCA results are further provided quantitatively in Chapter 15. Additional information on the relevant parameters for the environmental impacts is provided in the text for the technologies based on the LCA models.

Table 1 shows the technology profiles entailed in this working paper, along with their key built-in metals and metalloids. The selection of technologies considered is based on a trade-off between a high coverage of the technology mixes in energy systems models (BMWi, 2017; Fraunhofer ISE, 2020) and reasonable research effort. It should finally be noted that this paper is meant as a work-in-progress. Renewable energy technologies are rapidly changing. The technological landscape that could be laid out in 2019 has certainly evolved since. Therefore, the technology profiles provided need to be regularly updated and extended (e.g., TOPCon and Perovskite for PV, DFIG for wind, LFP for battery). The authors are however hopeful that this paper will encourage transparent data availability and the integration of efficiency measures and environmental impacts in material demand analyses for energy systems.

Tab. 01 Technologies considered in the working paper and their key built-in metals and metalloids. The material compositions of steel alloys and electronics is hereby not shown.

	Technology	Sub-technology	Steel alloy	Al	Cu	Pb	Zn	Ni	Ag	Bi	Si	Sn	In	Ga	Se	Cd	As	Nd	Dy	Pt	Ti	Va	Li	Mn	Co
Power and Heat Generation	PV (rooftop & ground mounted)	PERC	x	x	x	-			x	-	x	x													
		SHJ	x	x	x	-	-		x	-	x	x	-												
		CIGS	x	x	x		-					-	x	x	x	-									
		III-V/Si	x	x	x		-		x	-	x	x	x	x			x								
	Wind onshore	EESG	x	x	x																				
		PMSG-DD	x	x	x	x												x	x						
	Wind offshore	PMSG-MS		x	x	x												x	x						
		PMSG-DD	x	x	x	x												x	x						
	CHP	NGCC	x	x	x																				
	Heat pump	Air-to-water	x	x	x																				
	Boiler	Gas based	x	x	x		x																		
	Solar thermal	Flat plate	x	x	x																				
	Fuel cell	PEMFC	x		x															x	x				
Storage	Power-to-X	AEL	x	x	x			x																	
	Battery	VRF	x	x	x																	x			
		NMC Li-ion	x	x	x			x															x	x	x
	Heat storage	Water tank	x																						
Transmission	Power grid	AC line	-	x																					
		DC line	x		x	x																			
Energy demand reduction	Renovation	Retrofit from unrenovated to EnEV	x				x																		
		EnEV new construction	x				x																		
		Retrofit from unrenovated to Passive house	x				x																		
		Passive house new construction	x				x																		
		Unrenovated standard new construction	x				x																		

PV metals

Wind rare earths

Fuel cell metals

Battery metals

Base metals

x Material built-in
- Material is assumed to be substituted or used as a substitute

1 Photovoltaics

1.1 PERC – Passivated Emitter and Rear Cell

1.1.1 Description

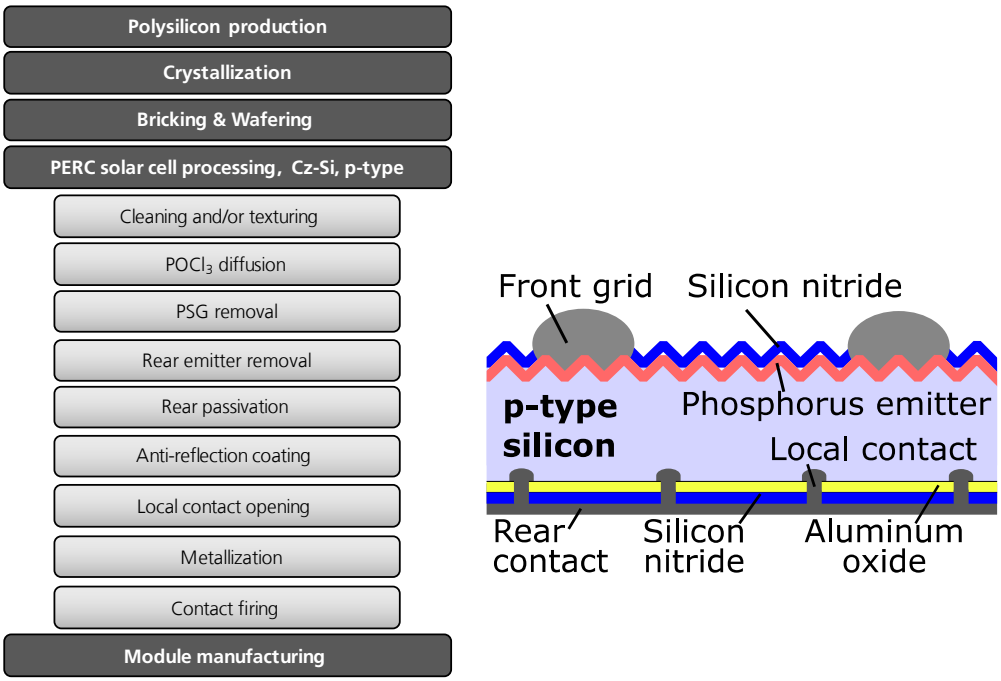


Fig. 01 Typical process flow of a PERC module with detailed cell production steps (left) and representative cross-section of a mono-facial PERC solar cell (right).

System boundaries

- PV-Module
- Inverter
- Balance-of-System (mounting structure and cabling) for rooftop and ground-mounted PV systems

Parameters for Life cycle Analysis (LCA)

- Production location of the PERC module: China
- Production location of the BOS and inverter: Germany
- PV system service life: 25 years

1.1.2 Material efficiency

Increase of the module efficiency

The material demand for PERC per MWp decreases as the module efficiency increases.

Tab. 02 Projected PERC module efficiency (expert council, personal communication, 2020)

	2018	2020	2025	2030	2035	2040	2045	2050
Module efficiency [%]	17.0	18.5	19.7	21.0	22.0	23.0	24.0	24.0

Reduction of the polysilicon usage

Polysilicon consumption can mainly be reduced through thinner Si wafers, reduced sawing losses, and lower breakage rates. As the main wafering technology, diamond wire sawing is expected to further dominate and become more efficient in the coming years. Following the projections of the International Technology Roadmap for Photovoltaics ITRPV (ITRPV, 2019), a reduction of the kerf width down to 50 µm and a reduction of the wafer thickness down to 120 µm by 2050 are assumed. Losses from ingot cropping/grinding are set constant. Considerably thinner wafer could be achieved through kerfless wafering technologies such as epitaxial growth. The adoption of such a technology remains to date associated with challenges e.g., regarding compatibility with screen printing for metallization, and has not been considered hereafter.

Tab. 03 Projected kerf width, based on (ITRPV, 2019)

	2018	2020	2025	2030	2035	2040	2045	2050
Kerf width [µm]	80	75	65	60	55	50	50	50

Tab. 04 Projected wafer thickness, based on (ITRPV, 2019)

	2018	2020	2025	2030	2035	2040	2045	2050
As-cut wafer thickness [µm]	175	169	153	140	131	125	121	120

Substitution of the aluminium frame

PV module frames are currently mainly made of aluminium. Alternative designs such as frameless modules, lightweight plastic frames, or biomaterial-based frames can however offer advantages with regards to aesthetics, ease of installation, longer lifetime by eliminating frame corrosion problems and/or reduced environmental impacts. A frameless/non-metal-framed module is therefore assumed to become market leader in the long term.

Tab. 05 Projected market shares of different module frame types, based on (ITRPV, 2019)

	2018	2020	2025	2030	2035	2040	2045	2050
Frameless/non-metal-based frame [%]	0	0	0	0	0	100	100	100
Al frame [%]	100	100	100	100	100	0	0	0

Reduction of the silver usage in metallization paste

Silver paste is typically used for contact formation on silicon solar cells and is a major cost driver in module manufacturing. In the last 10 years, the silver consumption decreased from 400 mg/cell to about 100 mg/cell (ITRPV, 2019). This trend is expected to continue in the next years, supported by developments in metallization pastes, improved screen printing e.g., with dual print, and alternative metallization designs such as thinner fingers and busbarless configuration. This is partially slowed down by the increasing market shares of n-type cell concepts that require more silver than p-type cells. Alternative metallization technologies such as direct plating enable a substitution of silver with

copper and nickel. The adoption of such a technology by the PV industry is however particularly dependent on silver prices which are currently relatively low. Silver substitution is therefore not considered here.

Tab. 06 Projected average silver amount per PERC cell, based on (ITRPV, 2019)

	2018	2020	2025	2030	2035	2040	2045	2050
Ag amount [mg/cell]	103	100	91	83	75	67	58	50

Substitution of lead

PV systems are currently excluded from the RoHS 2 EU directive and may therefore contain lead (SnPb 60/40). Accounting for a possible update of RoHS 2 and concerns about lead toxicity, a lead ban is assumed by 2030. Tin-bismuth (SnBi 50/50) is considered as a substitute.

Tab. 07 Projected market share of lead-free PERC modules

	2018	2020	2025	2030	2035	2040	2045	2050
Pb-free module [%]	0	0	0	100	100	100	100	100

1.1.3 Material composition

The material composition of a PERC module, inverter, and balance-of-system (BOS) until 2050 is shown hereafter. Metals are the focus of the present analysis. When available, data on other materials are provided as well as they remain relevant for the Life Cycle Analysis (LCA). Two technology switches can be seen for the module: Substitution of Pb with Bi from 2030 onwards, substitution of Al-frame with frameless counterparts from 2040 onwards.

Tab. 08 Projected material demand for PERC, under consideration of material efficiency measures. The material demand adds the built-in material demand with the manufacturing losses from polysilicon to module production. Based on (expert council, personal communication, 2019) and (Gervais et al., 2021)

	2018	2020	2025	2030	2035	2040	2045	2050
PERC Module [kg/MWp]								
Al (cell)	184	169	159	149	142	134	130	130
Al (frame)	8,768	8,057	7,566	7,098	6,771	0	0	0
Ag	21	18	16	13	12	10	8	7
Cu	946	869	816	766	731	689	670	670
Pb	62	57	53	0	0	0	0	0
Bi	0	0	0	54	51	48	47	47
Si	3,430	3,038	2,591	2,221	1,986	1,780	1,683	1,666
Sn	59	54	51	40	38	36	35	35
Glass	44,881	41,242	38,730	36,332	34,659	32,679	31,791	31,791
Ethylene vinyl acetate	5,058	4,648	4,365	4,095	3,906	3,683	3,583	3,583
Polyphenylene ether, Polystyrene	530	487	457	429	409	386	375	375
Polyethylene terephthalate	2,333	2,144	2,013	1,888	1,801	1,699	1,652	1,652
Polyvinyl fluoride	1,063	976	917	860	821	774	753	753
Acrylic foam	218	200	188	176	168	158	154	154

Tab. 09 Projected built-in material composition of the balance-of-system for rooftop PV systems, under consideration of PERC module efficiency increase. Based on (Fthenakis et al., 2011; Schlegl, 2013)

	2018	2020	2025	2030	2035	2040	2045	2050
Mounting structure - Rooftop [kg/MWp]								
Stainless steel	43	39	37	35	33	31	30	30
Al	53	49	46	43	41	38	37	37
Cabling - Rooftop [kg/MWp]								
Cu	792	728	683	641	612	577	561	561

Tab. 10 Projected built-in material composition of the balance-of-system for ground-mounted PV systems, under consideration of PERC module efficiency increase. Based on (Jungbluth et al., 2012; Schlegl, 2013)

	2018	2020	2025	2030	2035	2040	2045	2050
Mounting structure - Ground-mounted [kg/MWp]								
Steel	430	395	371	348	332	313	305	305
Stainless steel	18	16	15	14	14	13	13	13
Al	279	256	241	226	215	203	197	197
Cabling - Ground-mounted [kg/MWp]								
Cu	1,374	1,263	1,186	1,113	1,061	1,001	974	974

Tab. 11 Projected built-in material composition of an inverter, assumed constant. Based on (Fthenakis et al., 2011)

	2018-2050
Inverter - Rooftop [kg/MWp]	
Steel	156
Al	1,364
Cu	501
Printed circuit board	225
Inverter - Ground-mounted [kg/MWp]	
Steel	94
Al	543
Cu	288
Printed circuit board	103

1.1.4 Environmental impacts

The environmental impacts associated with the technology have been calculated based on the tables above and (IEA-PVPS Task 12, 2020; ITRPV, 2019).

The environmental impact indicators Climate Change and Resource Use of the PERC rooftop installation are shown in Figure 2.

A continuous reduction of the environmental impact of more than 75% until 2050 can be observed for Climate Change from 2020 onwards, which is mainly due to the significantly lower environmental impact of electricity (minus 85%). This circumstance results in changed relative contributions: in 2018 electricity is responsible for 76% of the environmental impact and cell production for 16%, whereas in 2050 the share of electricity decreases to 47%, while cell production contributes 42%.

In the case of Resource Use, an unsteady progression can be observed. While the environmental impact decreases continuously up to 2025 and from 2030, it increases sharply between 2025 and 2030, which is due to the substitution of lead by bismuth. Expressed in figures, this means, based on 2018 as a reference (=100%), an environmental impact of 92% (2025), 106% (2030) and 91% (2050). The relatively highest contribution in 2018 is copper with 79% and silver with 13%, in 2050 copper (66%) and bismuth (18%).

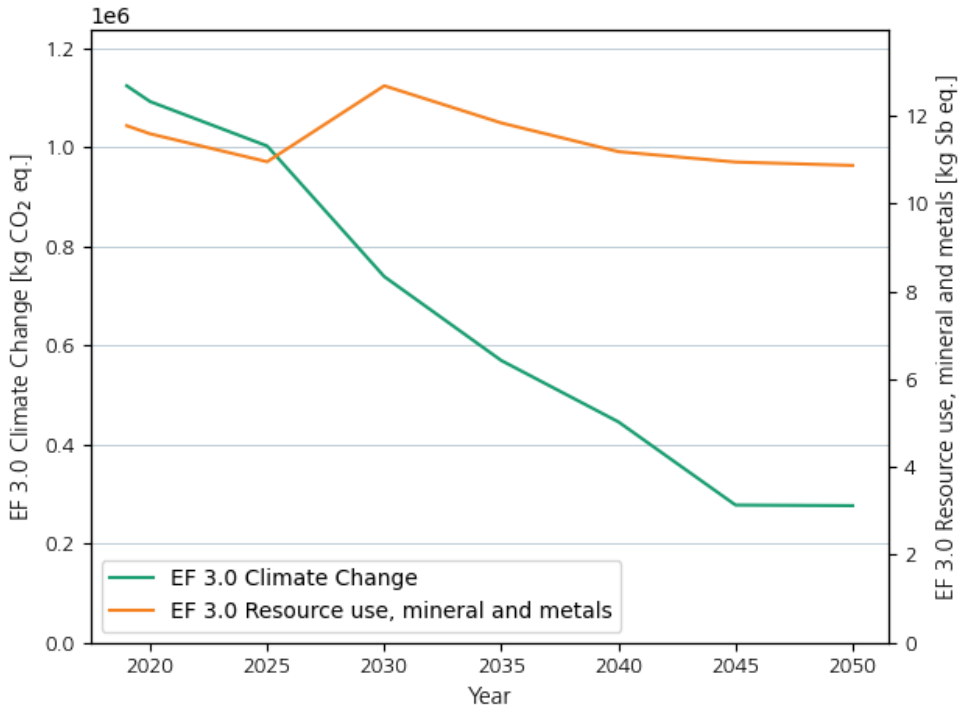


Fig. 02 Environmental impacts of PERC rooftop installation per MW of installed capacity.

Figure 3 shows the contribution of the different elements to the Resource Use indicator for rooftop installation. With the use of bismuth starting in 2030, the Resource Use increases until 2050, when it decreases again to the level of 2025.

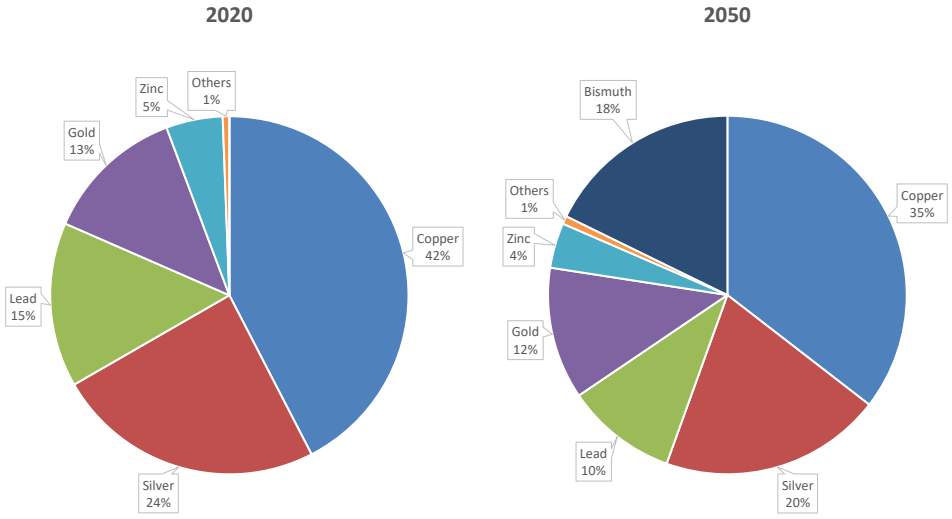


Fig. 03 Contribution of different elements to Resource Use for PERC rooftop installation.

The environmental impacts shown in Figure 4 for ground-mounted PERC solar cell installation show a very similar trajectory to that of rooftop installation (absolute and relative contributions/reductions). The absolute numbers are minimally higher due to the increased demand for copper during installation.

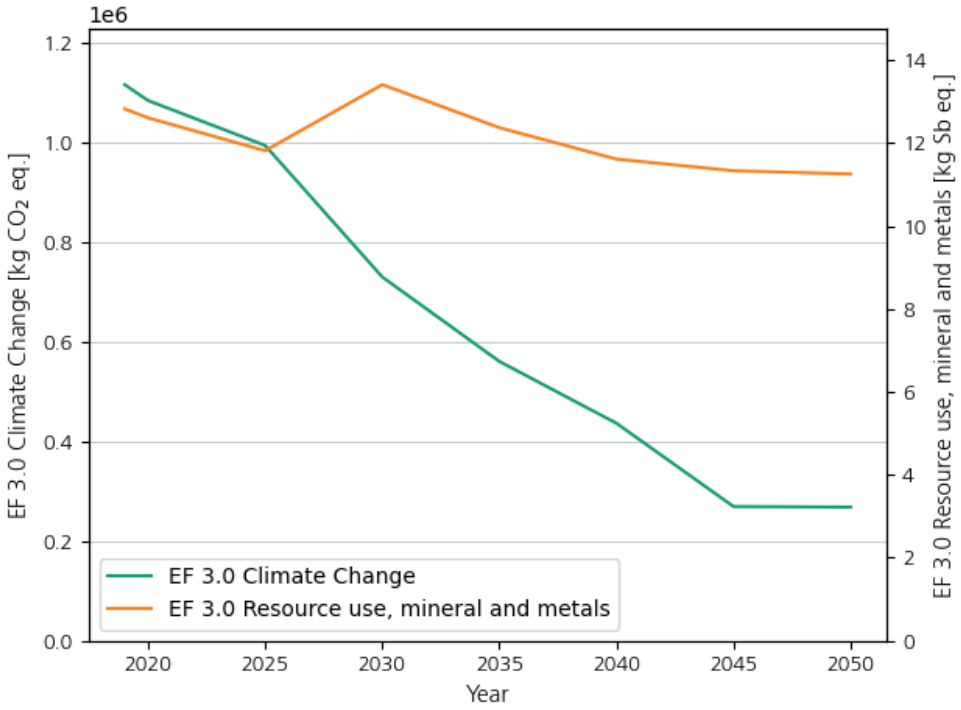


Fig. 04 Environmental impacts of PERC ground-mounted installation per MW installed.

Figure 5 shows the contribution of the different elements to the Resource Use indicator for ground-mounted installation. Again, parallels to the rooftop installation can be seen, with slightly increased absolute values of the elements used resulting in minor changes in relative contributions, as can be seen in the figure below. With the use of bismuth starting in 2030, the Resource Use increases until 2050, when it decreases again to the level of 2025.

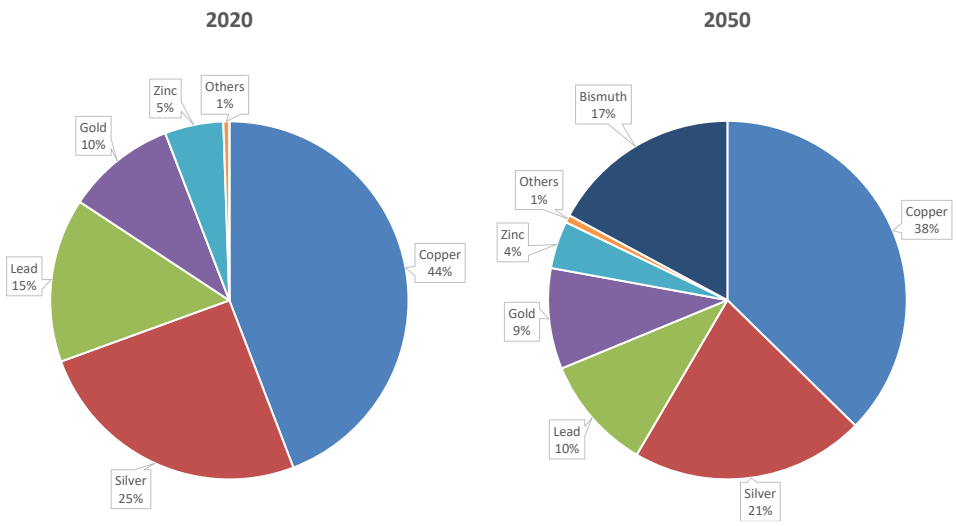


Fig. 05 Contribution of different elements to Resource Use in PERC ground-mounted installation.

1.2 SHJ – Silicon Heterojunction Solar Cell

1.2.1 Description

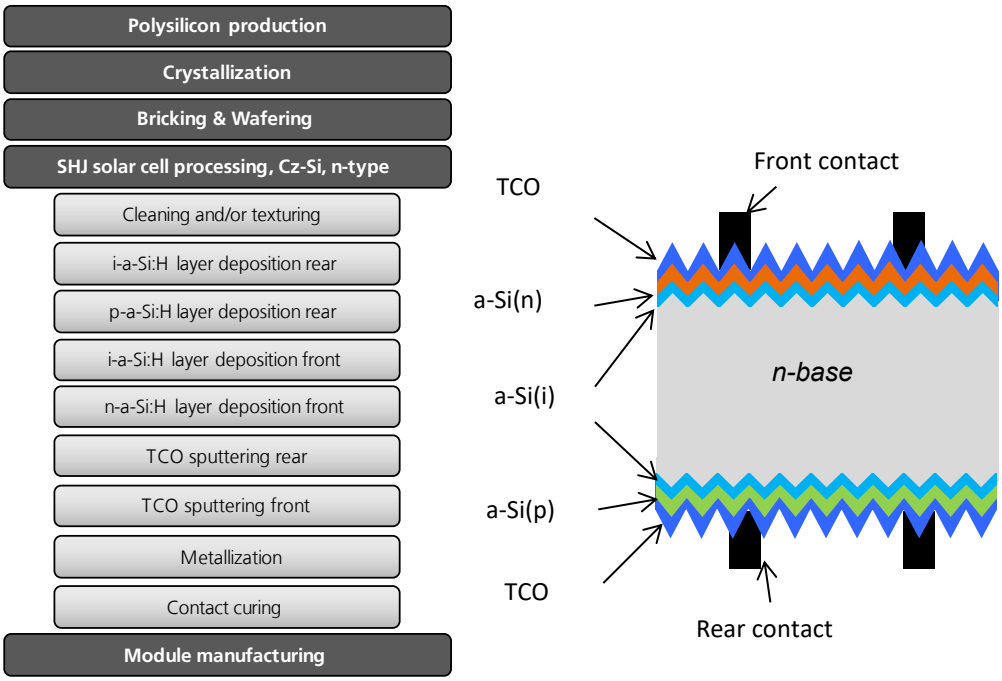


Fig. 06 Typical process flow of a SHJ module with detailed cell production steps (left) and representative cross-section of a SHJ solar cell (right).

System boundaries

- PV-Module
- Inverter

- Balance-of-System (mounting structure and cabling) for rooftop and ground-mounted PV systems

Parameters for Life cycle Analysis (LCA)

- Production location of the SHJ module: China
- Production location of the BOS and inverter: Germany
- PV system service life: 25 years

1.2.2 Material efficiency

Increase of the module efficiency

The material demand for SHJ per MWp decreases as the module efficiency increases.

Tab. 12 Projected SHJ module efficiency (expert council, personal communication, 2020)

	2018	2020	2025	2030	2035	2040	2045	2050
Module efficiency [%]	20.0	20.5	21.7	22.6	23.4	24.0	24.4	24.6

Reduction of the polysilicon usage

Polysilicon consumption can mainly be reduced through thinner Si wafers, reduced sawing losses, and lower breakage rates. As the main wafering technology, diamond wire sawing should continue to dominate and become more efficient in the coming years. Following the projections of the International Technology Roadmap for Photovoltaics ITRPV (ITRPV, 2019), a reduction of the kerf width down to 50 µm and a reduction of the wafer thickness down to 100 µm by 2050 are assumed. Losses from ingot cropping/grinding are set constant. Considerably thinner wafer could be achieved through kerfless wafering technologies such as epitaxial growth. The adoption of such a technology remains to date associated with challenges e.g., regarding compatibility with screen printing for metallization, and has not been considered hereafter.

Tab. 13 Projected kerf width, based on (ITRPV, 2019)

	2018	2020	2025	2030	2035	2040	2045	2050
Kerf width [µm]	80	75	65	60	55	50	50	50

Tab. 14 Projected wafer thickness, based on (ITRPV, 2019)

	2018	2020	2025	2030	2035	2040	2045	2050
As-cut wafer thickness [µm]	165	161	151	141	130	120	110	100

Substitution of the aluminium frame

PV module frames are currently mainly made of aluminium. Alternative designs such as frameless modules, lightweight plastic frames, or biomaterial-based frames can however offer advantages with regards to aesthetics, ease of installation, longer lifetime by reducing potential-induced degradation and eliminating frame corrosion problems and/or reduced environmental impacts. A frameless/non-metal-framed module is therefore assumed to become market leader in the long term.

Tab. 15 Projected market shares of different module frame types, based on (ITRPV, 2019)

	2018	2020	2025	2030	2035	2040	2045	2050
Frameless/non-metal-based frame [%]	0	0	0	0	0	100	100	100
Al frame [%]	100	100	100	100	100	0	0	0

Reduction of the silver usage in metallization paste

Silver paste is typically used for contact formation on silicon solar cells and is a major cost driver in module manufacturing. In the last 10 years, the silver consumption decreased from 400 mg/cell to about 100 mg/cell in PERC (ITRPV, 2019). SHJ cells require however more silver than their mono-facial, p-type counterparts. A decreasing silver usage in SHJ is nonetheless expected in the next years, supported by developments in metallization pastes, improved screen printing e.g., with dual print, and alternative metallization designs such as thinner fingers and busbarless configuration. Alternative metallization technologies such as direct plating enable a substitution of silver with copper and nickel. The adoption of such a technology by the PV industry is however particularly dependent on silver prices which remain currently relatively low. Silver substitution is therefore not considered here.

Tab. 16 Projected average silver amount per SHJ cell, based on (ITRPV, 2019)

	2018	2020	2025	2030	2035	2040	2045	2050
Ag amount [mg/cell]	275	263	232	202	171	141	110	80

Substitution of lead

PV systems are currently excluded from the RoHS 2 EU directive and may therefore contain lead (SnPb 60/40). Accounting for a possible update of RoHS 2 and concerns about lead toxicity, a lead ban is assumed by 2030 at the latest. Tin-bismuth (SnBi 50/50) is considered as a substitute.

Tab. 17 Projected market share of lead-free SHJ modules

	2018	2020	2025	2030	2035	2040	2045	2050
Pb-free module [%]	0	0	0	100	100	100	100	100

Substitution of the indium tin oxide (ITO)

The tin-doped indium oxide (In_2O_3:SnO_2 or ITO) for the transparent conductive oxide layer (TCO) is expected to be replaced by aluminium-doped zinc oxide (Al_2O_4Zn or AZO). The substitution is assumed to become standard by 2035.

Tab. 18 Projected market share of SHJ modules with indium-free TCO (expert council, personal communication, 2020)

	2018	2020	2025	2030	2035	2040	2045	2050
In-free module [%]	0	0	0	0	100	100	100	100

Reduction of the sputtering losses

When sputtering the transparent conductive oxide, around 50% of the material ends up on the cell (Marwede, 2013). The coating efficiency is assumed to increase up to 90 % by optimizing the geometry and coating of the chamber, as well as the overall process.

Tab. 19 Projected efficiency of the TCO sputtering process, based on (Marwede, 2013) and (expert council, personal communication, 2020)

	2018	2020	2025	2030	2035	2040	2045	2050
Sputtering efficiency [%]	50	50	57	64	70	76	83	90

1.2.3 Material composition

The material composition of a SHJ module, inverter, and balance-of-system (BOS) until 2050 is shown hereafter. Metals are the focus of the present analysis. When available, data on other materials are provided as well as they remain relevant for the Life Cycle Analysis (LCA). Three technology switches can be seen for SHJ modules: Substitution of ITO with AZO in 2035, substitution of Pb with Bi from 2030 onwards, substitution of Al-frame with frameless counterparts from 2040 onwards.

Tab. 20 Projected material demand for SHJ, under consideration of material efficiency measures. The material demand adds the built-in material demand with the manufacturing losses from polysilicon to module production. Based on (expert council, personal communication, 2019) and (Gervais et al., 2021)

	2018	2020	2025	2030	2035	2040	2045	2050
SHJ Module [kg/MWp]								
Ag	60	56	47	39	32	26	20	14
Cu	946	922	873	835	808	788	775	769
Pb	62	60	57	0	0	0	0	0
Bi	0	0	0	69	67	65	64	64
Si	3,144	2,934	2,505	2,193	1,928	1,699	1,531	1,378
Sn	61	59	56	39	38	37	36	36
In (TCO)	5.5	5.4	5.1	4.9	0	0	0	0
Sn (TCO	0.6	0.6	0.6	0.5	0	0	0	0
Zn (TCO)	0	0	0	0	1.5	1.4	1.2	1.1
Al (TCO)	0	0	0	0	0.02	0.02	0.02	0.02
Al (frame)	11,111	10,830	10,251	9,812	9,487	0	0	0

Tab. 21 Projected built-in material composition of the balance-of-system for rooftop PV systems, under consideration of SHJ module efficiency increase. Based on (Fthenakis et al., 2011; Schlegl, 2013)

	2018	2020	2025	2030	2035	2040	2045	2050
Mounting structure - Rooftop [kg/MWp]								
Stainless steel	36	35	33	32	31	30	30	30
Al	45	44	41	40	38	37	37	36
Cabling - Rooftop [kg/MWp]								
Cu	673	656	621	595	575	561	552	547

Tab. 22 Projected built-in material composition of the balance-of-system for ground-mounted PV systems, under consideration of SHJ module efficiency increase. Based on (Jungbluth et al., 2012; Schlegl, 2013)

	2018	2020	2025	2030	2035	2040	2045	2050
Mounting structure - Ground-mounted [kg/MWp]								
Steel	366	356	337	323	312	305	300	297
Stainless steel	15	15	14	13	13	13	12	12
Al	237	231	219	209	202	197	194	193
Cabling - Ground-mounted [kg/MWp]								
Cu	1,168	1,139	1,078	1,032	997	973	958	950

Tab. 23 Projected built-in material composition of an inverter, assumed constant. Based on (Fthenakis et al., 2011)

	2018-2050
Inverter - Rooftop [kg/MWp]	
Steel	156
Al	1,364
Cu	501
Printed circuit board	225
Inverter - Ground-mounted [kg/MWp]	
Steel	94
Al	543
Cu	288
Printed circuit board	103

1.2.4 Environmental impacts

To calculate the environmental impacts, the data given in the tables above was supplemented with data from (IEA-PVPS Task 12, 2020; ITRPV, 2019).

The environmental impact indicators Climate Change and Resource Use of the SHJ rooftop installation are shown in Figure 7. For Climate Change, there is a continuous reduction in the environmental impact of more than 75% from 2020 to 2050, which is primarily due to the significantly lower environmental impact of electricity (minus 82%). This results in changed relative contributions: in 2018, electricity is responsible for 78% of the environmental impact and cell production for 16%, whereas in 2050 the share of electricity declines to 52%, while cell production contributes 48%. In the case of Resource Use, a discontinuous course can be observed. While the environmental impact decreases continuously until 2025 and from 2030 onwards, it increases sharply between 2025 and 2030, which is caused by the substitution of lead by bismuth. Expressed in figures, this means an environmental impact of 93% (2025), 110% (2030) and 97% (2050), based on 2018 as the reference (=100%). The relatively highest contribution in 2018 is copper with 61% and silver with 31%, in 2050 copper (58%) and bismuth (23%).

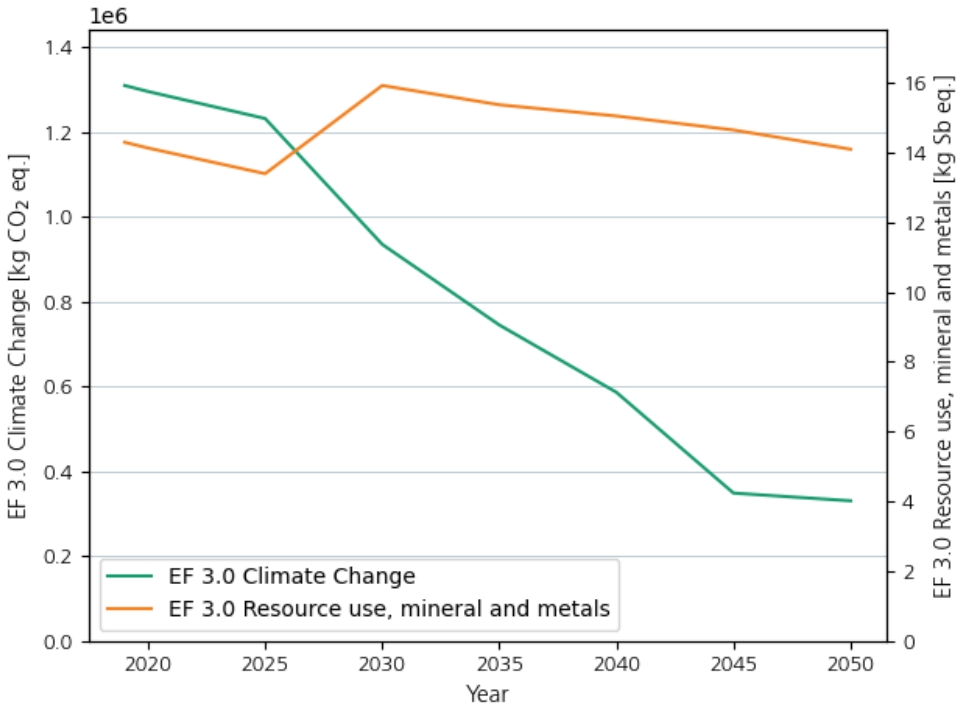


Fig. 07 Environmental impacts of SHJ rooftop PV system per MW installed capacity.

Figure 8 shows the contribution of the different elements to Resource Use in rooftop installation. With the use of bismuth from 2030 onwards, Resource Use increases in absolute terms until 2050, when it falls back to the 2025 level.

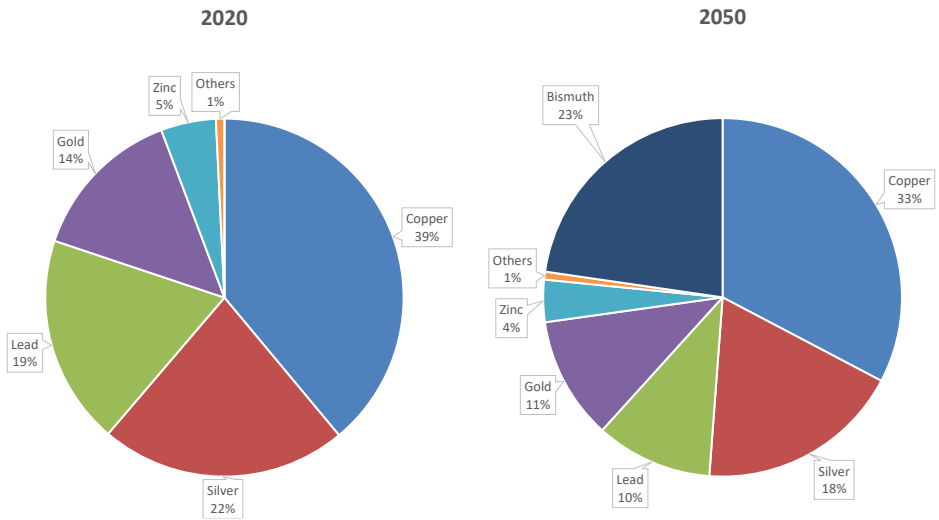


Fig. 08 Contribution of the different elements to Resource Use in SHJ rooftop installation.

The environmental impacts shown in Figure 9 for the ground-mounted PV system of SHJ solar cells show a very similar trend as for the rooftop installation (absolute and relative contributions/reductions). The absolute figures are marginally higher due to the increased demand for copper during installation.

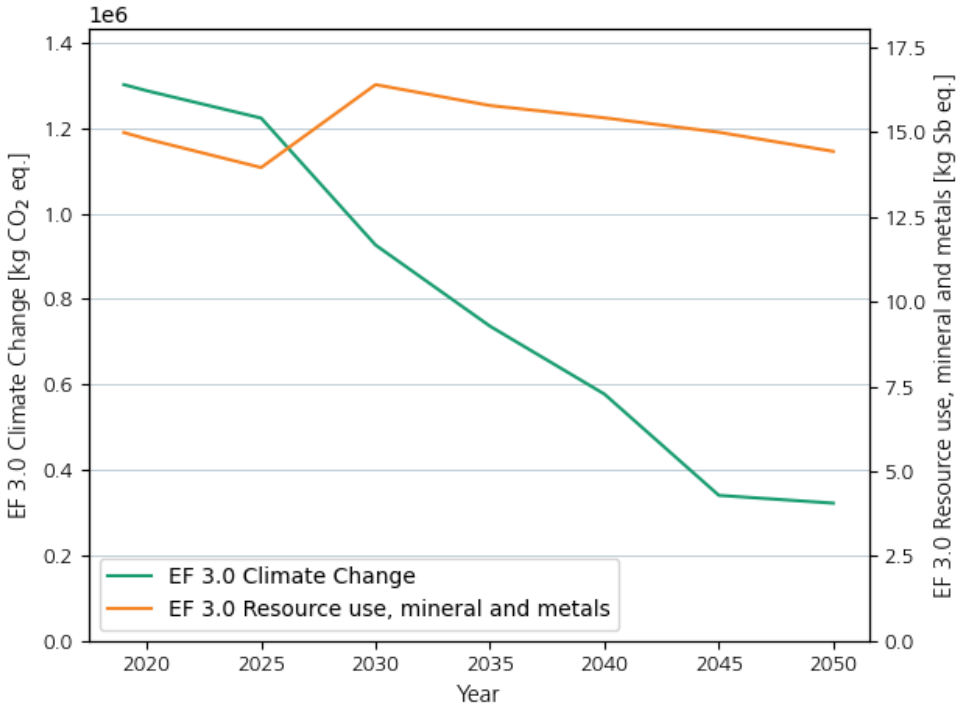


Fig. 09 Environmental impacts of SHJ ground-mounted PV system per MW installed capacity.

Figure 10 shows the Resource Use of the ground-mounted PV system. Similarly, there are parallels to the rooftop installation, with slightly higher absolute values of the elements used, which result in minor changes in the relative contributions, as shown in the following figure. With the use of bismuth, Resource Use increases until 2050, when it falls back to the level of 2025.

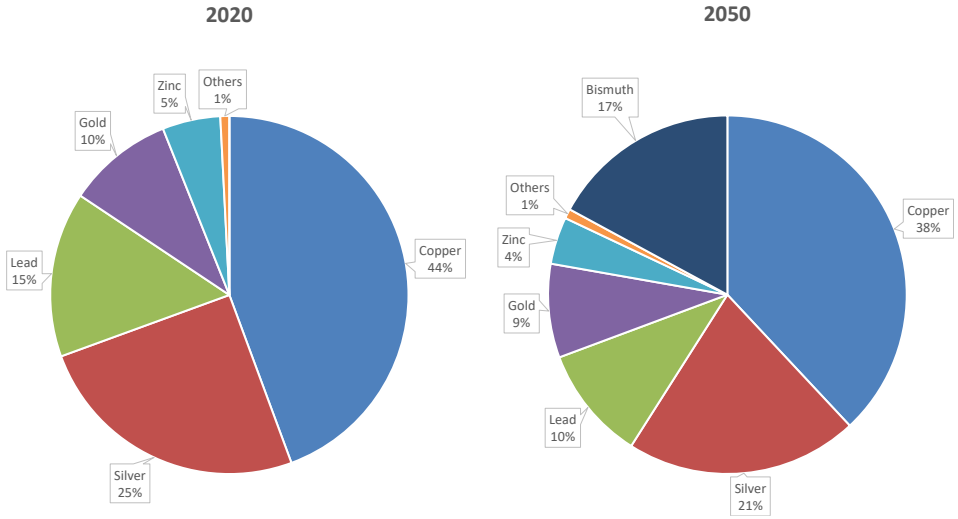


Fig. 10 Contribution of different elements to Resource Use in SHJ ground-mounted PV system.

1.3 CIGS – Copper Indium Gallium Selenide Solar Cell

1.3.1 Description

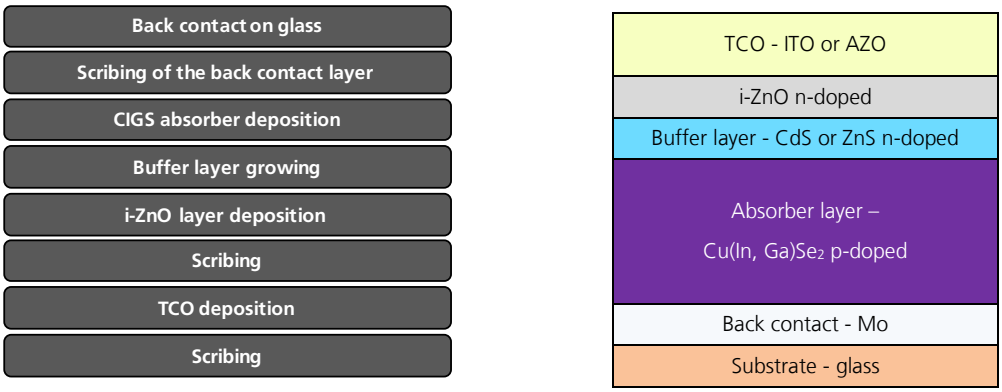


Fig. 11 Typical process flow of a CIGS module (left) and representative cross-section of a CIGS solar cell (right) (Salhi, 2022).

System boundaries

- PV-Module
- Inverter
- Balance-of-System (mounting structure and cabling) for rooftop and ground-mounted PV systems

Parameters for Life cycle Analysis (LCA)

- Production location of the CIGS module: China
- Production location of the BOS and inverter: Germany
- PV system service life: 25 years

1.3.2 Material efficiency

Increase of the module efficiency

The material demand for CIGS per MWp decreases as the module efficiency increases.

Tab. 24 Projected CIGS module efficiency (expert council, personal communication, 2019)

	2018	2020	2025	2030	2035	2040	2045	2050
Module efficiency [%]	15.6	16.0	17.0	18.0	19.0	20.0	21.0	22.0

Reduction of the absorber thickness

Copper, indium, gallium, and selenium requirements can be reduced by applying a thinner CIGS absorber layer.

Tab. 25 Projected absorber thickness, based on (Marscheider-Weidemann et al., 2016)

	2018	2020	2025	2030	2035	2040	2045	2050
Absorber thickness [µm]	1.6	1.6	1.5	1.4	1.3	1.2	1.1	1.0

Substitution of the aluminium frame

PV module frames are currently mainly made of aluminium. Alternative designs such as frameless modules, lightweight plastic frames, or biomaterial-based frames can however offer advantages with regards to aesthetics, ease of installation, longer lifetime by reducing potential-induced degradation and eliminating frame corrosion problems and/or reduced environmental impacts. Frameless thin-film modules are already commercially available (expert council, personal communication, 2020). They are therefore assumed to become standard by 2030.

Tab. 26 Projected market shares of different module frame types (expert council, personal communication, 2020)

	2018	2020	2025	2030	2035	2040	2045	2050
Frameless/non-metal-based frame [%]	0	0	0	100	100	100	100	100
Al frame [%]	100	100	100	0	0	0	0	0

Substitution of the cadmium buffer layer

Buffer layers in CIGS are mostly based on cadmium. Alternatives are being sought to avoid the use of this toxic element. Zn as a substitute has shown promising results. A replacement of CdS by ZnS is therefore assumed.

Tab. 27 Projected market share of CIGS modules with cadmium-free buffer layer, based on (Wuppertal Institut, 2014)

	2018	2020	2025	2030	2035	2040	2045	2050
Cd-free module [%]	0	0	0	100	100	100	100	100

Substitution of the indium tin oxide (ITO)

The tin-doped indium oxide (In_2O_3:SnO_2 or ITO) for the transparent conductive oxide layer (TCO) is expected to be replaced by aluminium-doped zinc oxide (Al_2O_4Zn or AZO). The substitution is assumed to become standard by 2025.

Tab. 28 Projected market share of CIGS modules with indium-free TCO, based on (Wuppertal Institut, 2014)

	2018	2020	2025	2030	2035	2040	2045	2050
In-free module [%]	0	0	100	100	100	100	100	100

Reduction of the production losses

When sputtering the transparent conductive oxide, around 50% of the material ends up on the cell (Marwede, 2013). The coating efficiency is assumed to increase up to 90% by optimizing the geometry and coating of the chamber, as well as the overall process. Similarly, the efficiency of co-evaporation – the currently most commonly used process for absorber coating – is assumed to increase up to 90%.

Tab. 29 Projected efficiency of the sputtering and co-evaporation processes, based on (Marwede, 2013) and (expert council, personal communication, 2020)

	2018	2020	2025	2030	2035	2040	2045	2050
Sputtering efficiency [%]	50	50	57	64	70	76	83	90
Co-evaporation efficiency [%]	50	50	57	64	70	76	83	90

1.3.3 Material composition

The material composition of a CIGS module, inverter, and balance-of-system (BOS) until 2050 is shown hereafter. Metals are the focus of the present analysis. When available, data on other materials are provided as well as they remain relevant for the Life Cycle Analysis (LCA). Three technology switches can be seen for CIGS modules: Substitution of ITO with AZO in 2025, substitution of CdS with ZnS from 2030 onwards, substitution of Al-frame with frameless counterparts from 2030 onwards.

Tab. 30 Projected material demand for CIGS, under consideration of material efficiency measures. The material demand adds the built-in material demand with the manufacturing losses from module production. Based on (Moss et al., 2013)

	2018	2020	2025	2030	2035	2040	2045	2050
Absorber layer [kg/MWp]								
Cu	92	90	69	55	44	36	28	23
In	50	49	38	30	24	19	16	12
Ga	26	25	20	15	12	10	8	6
Se	248	241	187	147	118	96	77	61
Buffer layer [kg/MWp]								
Cd	7.4	7.2	6.7	0	0	0	0	0
Zn	0	0	0	6.4	6.1	5.8	5.5	5.3
TCO [kg/MWp]								
In	61	59	0	0	0	0	0	0
Sn	6.6	6.4	0	0	0	0	0	0
Zn	0	0	22	18	16	14	12	11
Al	0	0	0.3	0.2	0.2	0.2	0.2	0.1
Frame [kg/MWp]								
Al	12,031	11,700	11,028	0	0	0	0	0

Tab. 31 Projected built-in material composition of the balance-of-system for rooftop PV systems, under consideration of CIGS module efficiency increase. Based on (Fthenakis et al., 2011; Schlegl, 2013)

	2018	2020	2025	2030	2035	2040	2045	2050
Mounting structure - Rooftop [kg/MWp]								
Stainless steel	46	45	42	40	38	36	34	33
Al	57	56	52	50	47	45	43	41
Cabling - Rooftop [kg/MWp]								
Cu	858	834	786	743	705	670	639	612

Tab. 32 Projected built-in material composition of the balance-of-system for ground-mounted PV systems, under consideration of CIGS module efficiency increase. Based on (Jungbluth et al., 2012; Schlegl, 2013)

	2018	2020	2025	2030	2035	2040	2045	2050
Mounting structure - Ground-mounted [kg/MWp]								
Steel	466	453	427	404	383	364	347	332
Stainless steel	19	19	18	17	16	15	14	14
Al	302	294	277	262	248	236	225	215
Cabling - Ground-mounted [kg/MWp]								
Cu	1,488	1,447	1,364	1,290	1,223	1,163	1,109	1,062

Tab. 33 Projected built-in material composition of an inverter, assumed constant. Based on (Fthenakis et al., 2011)

	2018-2050
Inverter - Rooftop [kg/MWp]	
Steel	156
Al	1,364
Cu	501
Printed circuit board	225
Inverter - Ground-mounted [kg/MWp]	
Steel	94
Al	543
Cu	288
Printed circuit board	103

1.3.4 Environmental impacts

To calculate the environmental impacts, the data in the tables above was supplemented with data from (IEA-PVPS Task 12, 2020; ITRPV, 2019).

The environmental impact indicators Climate Change and Resource Use of the CIGS rooftop installation are shown in Figure 12. The most significant contribution to the Climate Change indicator results from the required electricity. In 2018, the share is almost 73%, followed by copper (13%) and aluminium (10%) used in the module. By 2050, the environmental impact decreases continuously to 22% compared to 2018, which is due to the significant reduction in copper used (decrease of 30%) and electricity (85%), while aluminium is no longer used.

The environmental impact of the Resource Use indicator declines constantly between 2018 and 2050 to 68%. This is caused by the lower demand for copper, which has a relative contribution of over 90% to the environmental impact in each case.

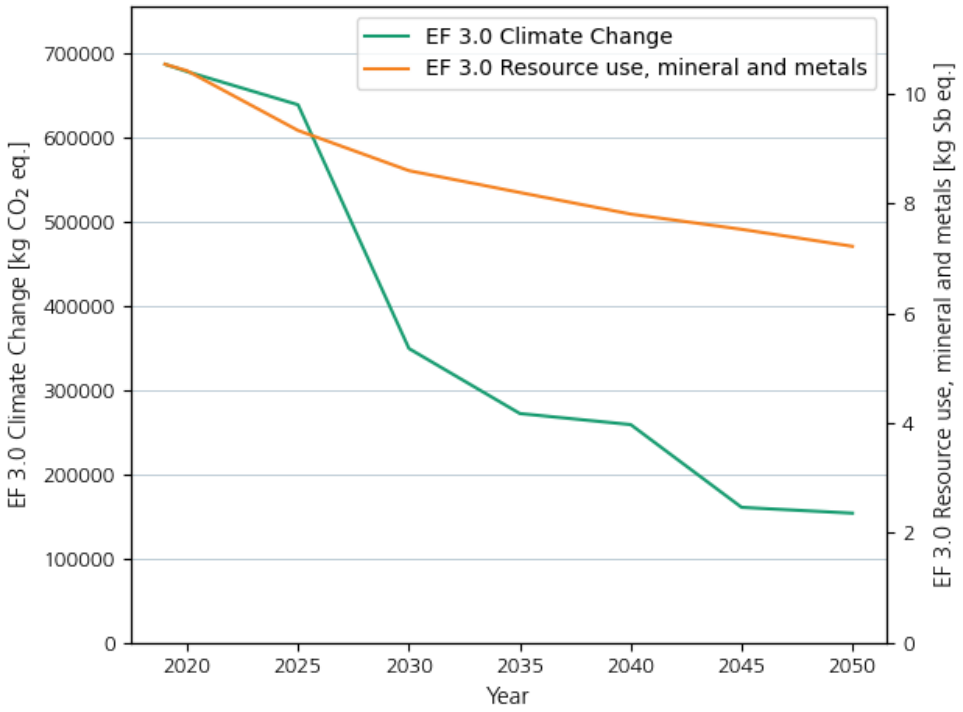


Fig. 12 Environmental impacts of CIGS rooftop installation per MW installed capacity.

Figure 13 shows the contribution of the different elements to Resource Use for rooftop installation. The absolute share of most of the elements shows decreases by 20-25% from 2020 to 2050, whereas indium is reduced by 90% and cadmium by over 98%.

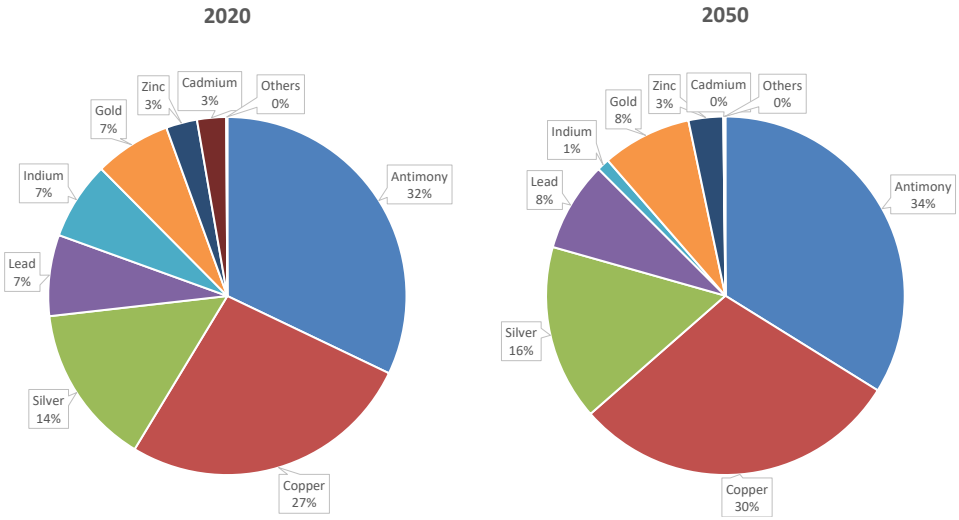


Fig. 13 Contribution of the different elements to Resource Use in CIGS rooftop installation.

The environmental impacts shown in Figure 14 for the ground-mounted installation of CIGS solar cells show a similar course as for the rooftop installation. A reduction to 27% of the initial environmental impact takes place for Climate Change between 2018 and 2050. The largest shares in 2018 are accounted for by electrical energy (72%), copper (12%) and aluminium (10%). The above-mentioned reduction in environmental impact is mainly due to a lower use of copper (minus 21%) and electricity (minus 82%) as well as aluminium, which is no longer used.

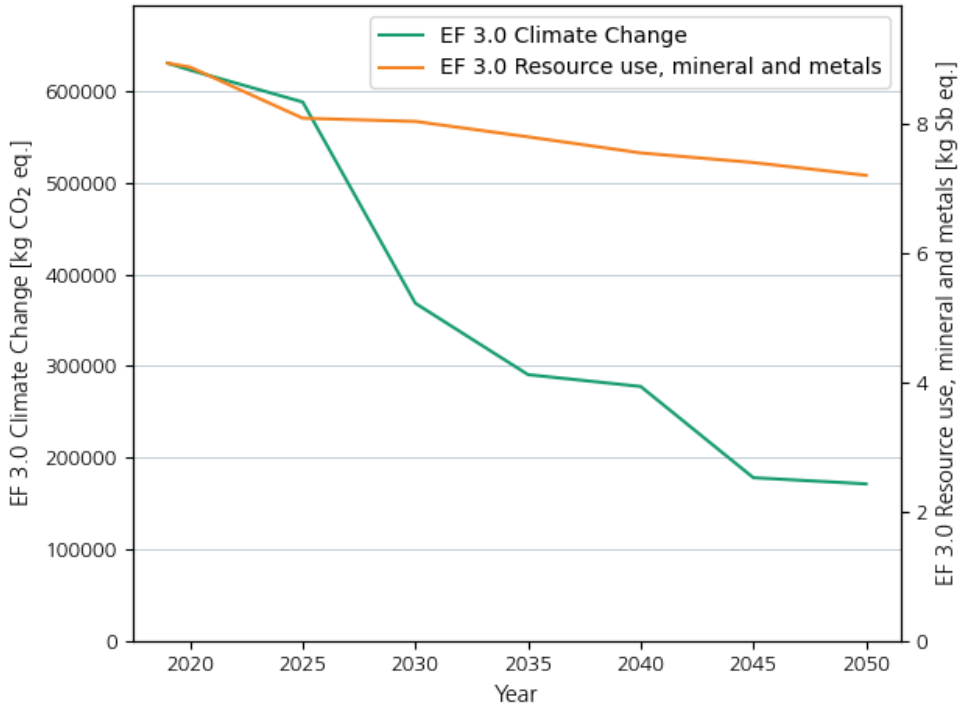


Fig. 14 Environmental impacts of CIGS ground-mounted installation per MW of installed capacity.

As shown in Figure 15, ground-mounted installation shows a similar trend for Resource Use as rooftop installation. The absolute share of most of the elements considered decreases by 5 to 15% from 2020 to 2050, whereas the indium used is reduced by almost 90% and cadmium by 98%. A corresponding impact on the relative composition can be seen in the figure below.

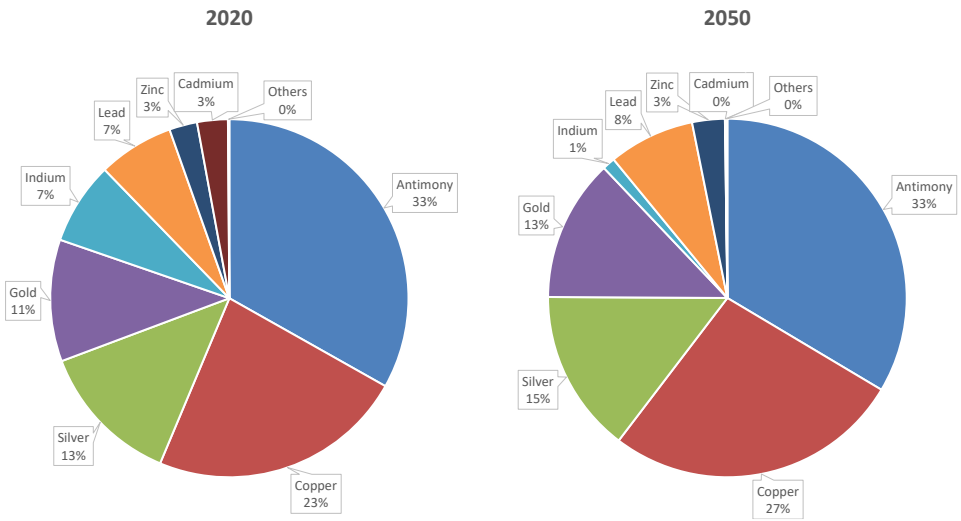


Fig. 15 Contribution of the different elements to the Resource Use in the CIGS ground-mounted installation.

1.4 III-V/Si – Silicon Tandem Solar Cell

1.4.1 Description

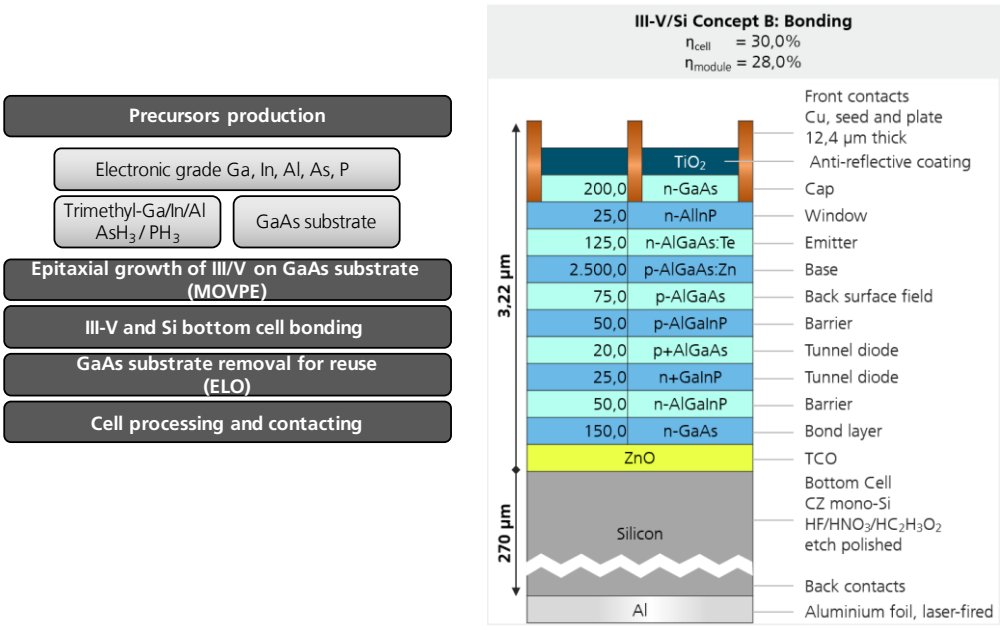


Fig. 16 Typical process flow (left) and representative cross-section of a III-V/Si solar cell (right) (Blanco et al., 2020; Mohr et al., 2007). The TiO2 layer is not included in the material composition hereafter.

System boundaries

- PV-Module
- Inverter
- Balance-of-System (mounting structure and cabling) for rooftop and ground-mounted PV systems

Parameters for Life cycle Analysis (LCA)

- Production location of the III-V/Si module: China
- Production location of the BOS and inverter: Germany
- PV system service life: 25 years

1.4.2 Material efficiency

Considering the innovation-grade of tandem solar cell concepts, III-V/Si modules are assumed to enter the market only from 2030 onwards.

Increase of the module efficiency

The material demand for III-V/Si per MWp decreases as the module efficiency increases.

Tab. 34 Projected III-V/Si module efficiency, based on (Blanco et al., 2020; Cariou et al., 2018)

	2030	2035	2040	2045	2050
Module efficiency [%]	28.0	30.0	32.0	33.0	35.0

Substitution of the aluminium frame

PV module frames are currently mainly made of aluminium. Alternative designs such as frameless modules, lightweight plastic frames, or biomaterial-based frames can however offer advantages with regards to aesthetics, ease of installation, longer lifetime by reducing potential-induced degradation and eliminating frame corrosion problems and/or reduced environmental impacts.

Tab. 35 Projected market shares of different module frame types, based on (ITRPV, 2019)

	2030	2035	2040	2045	2050
Frameless/non-metal-based frame [%]	0	0	100	100	100
Al frame [%]	100	100	0	0	0

Reduction of the production losses

When sputtering the transparent conductive oxide, around 50 % of the material ends up on the cell (Marwede, 2013). The coating efficiency is assumed to increase up to 90 % by optimizing the geometry and coating of the chamber, as well as the overall process.

The productions of the trimethyl components for the metalorganic vapour phase epitaxy (MOVPE) and of arsenic for the GaAs wafer substrate are assumed to become more efficient as well. The number of reuse cycles for the GaAs substrate until breakage is set to increase up to 300.

Tab. 36 Projected efficiency of the sputtering process, based on (Marwede, 2013) and (expert council, personal communication, 2020)

	2030	2035	2040	2045	2050
Sputtering efficiency [%]	64	70	76	83	90

Tab. 37 Projected efficiency of the trimethyl components production for MOVPE, based on (Essig et al., 2017)

	2030	2035	2040	2045	2050
Efficiency [%]	75	75	75	90	90

Tab. 38 Projected efficiency of the arsenic production for the GaAs substrate, based on (Essig et al., 2017)

	2030	2035	2040	2045	2050
Efficiency [%]	33	58	75	90	90

Tab. 39 Projected number of reuses for the GaAs substrate, based on (Essig et al., 2017)

	2030	2035	2040	2045	2050
GaAs reuse	100	100	100	300	300

Substitution of lead

PV systems are currently excluded from the RoHS 2 EU directive and may therefore contain lead (SnPb 60/40). Accounting for a possible update of RoHS 2 and concerns about lead toxicity, a lead ban is assumed by 2030 at the latest. Tin-bismuth (SnBi 50/50) is considered as a substitute.

Tab. 40 Projected market share of lead-free III-V/Si modules

	2030	2035	2040	2045	2050
Pb-free module [%]	100	100	100	100	100

1.4.3 Material composition

The material composition of a III-V/Si module, inverter, and balance-of-system (BOS) until 2050 is shown hereafter. A 0.2 µm thick AZO TCO layer was considered (Kao et al., 2019).The material requirements for the silicon bottom cell are based on the data for PERC adjusted with III-V/Si module efficiency.

Tab. 41 Projected material demand for III-V/Si, under consideration of material efficiency measures. The material demand adds the built-in material demand with the manufacturing losses from polysilicon to module production. Based on (Blanco et al., 2020) and (Gervais et al., 2021)

	2030	2035	2040	2045	2050
III-V top cell [kg/MWp]					
Ga	52	49	46	36	35
As	262	247	233	221	210
Al	19	18	17	14	13
In	15	14	13	10	10
Cu	34	32	31	29	27
GaAs substrate layer [kg/MWp]					
Ga	0.03	0.03	0.03	0.01	0.01
As	0.09	0.05	0.04	0.01	0.01
TCO [kg/MWp]					
Al	2.6	2.2	2.0	1.7	1.5
Zn	0.03	0.03	0.03	0.03	0.02
Silicon bottom cell [kg/MWp]					
Al	5	5	5	4	4
Si	2,362	2,223	2,100	1,989	1,890
Cu	574	541	511	484	460
Sn	30	28	27	25	24
Bi	40	38	36	34	32
Frame [kg/MWp]					
Al	5,323	5,010	0	0	0

Tab. 42 Projected built-in material composition of the balance-of-system for rooftop PV systems, under consideration of III-V/Si module efficiency increase. Based on (Fthenakis et al., 2011; Schlegl, 2013)

	2030	2035	2040	2045	2050
Mounting structure - Rooftop [kg/MWp]					
Stainless steel	26	24	23	22	21
Al	32	30	28	27	26
Cabling - Rooftop [kg/MWp]					
Cu	481	453	427	405	385

Tab. 43 Projected built-in material composition of the balance-of-system for ground-mounted PV systems, under consideration of III-V/Si module efficiency increase. Based on (Jungbluth et al., 2012; Schlegl, 2013)

	2030	2035	2040	2045	2050
Mounting structure - Ground-mounted [kg/MWp]					
Steel	261	246	232	220	209
Stainless steel	11	10	10	9	9
Al	169	159	150	143	135
Cabling - Ground-mounted [kg/MWp]					
Cu	834	785	742	703	668

Tab. 44 Projected built-in material composition of an inverter, assumed constant. Based on (Fthenakis et al., 2011)

	2018-2050
Inverter - Rooftop [kg/MWp]	
Steel	156
Al	1,364
Cu	501
Printed circuit board	225
Inverter - Ground-mounted [kg/MWp]	
Steel	94
Al	543
Cu	288
Printed circuit board	103

1.4.4 Environmental impacts

To calculate the environmental impacts, the data from the tables above was supplemented with data from (IEA-PVPS Task 12, 2020; ITRPV, 2019).

The environmental impact categories Climate Change and Resource Use of the III-V/Si rooftop PV system installation are shown in Figure 17. In the case of Climate Change, there is a continuous reduction in the environmental impact of over 60% by 2050, starting from 2030 as the reference. In 2030, 74% of the environmental impact is attributable to electricity and a further 18% to the production of silicon wafers. By 2050, this share changes significantly, when electricity accounts for 56% and silicon wafers for 39%.

Resource use also decreases in the period under consideration, but to a lesser extent (11% by 2050). The largest contributions to the environmental impact of Resource Use in 2030 are copper (60%), bismuth (16%) and arsenic (10%). These relative contributions hardly change by 2050 (<2%), as general efficiency improvements are accompanied by simultaneous reductions in the absolute shares.

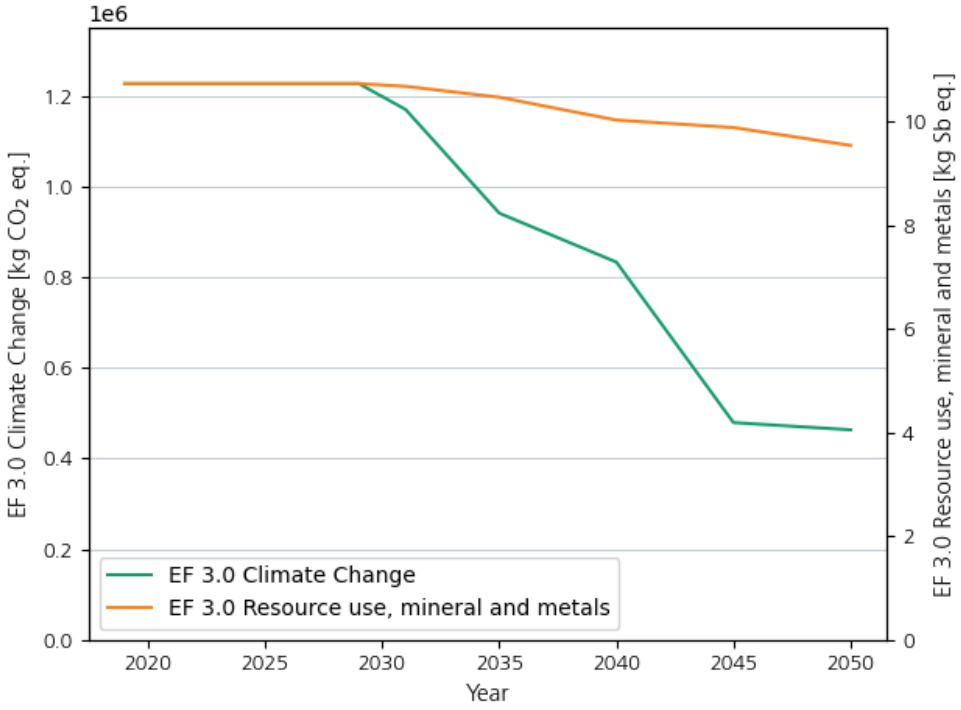


Fig. 17 Environmental impacts of III-V/Si rooftop PV system per MW installed capacity.

Figure 18 shows the contribution of the different elements to the Resource Use of the rooftop installation. The graphs show that the relative contribution of an element to Resource Use varies marginally between 2030 and 2050; in absolute terms, there is a slight decrease for most elements (5 to 20%), only the contribution of gold remains almost the same (minus 1%).

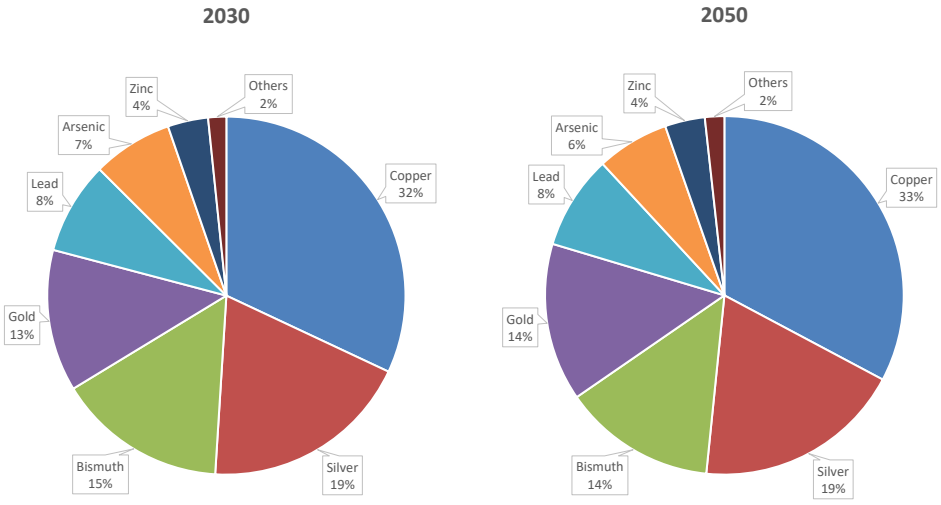


Fig. 18 Contribution of the different elements to Resource Use in the III-V/Si rooftop PV system.

The environmental impact indicators Climate Change and Resource Use shown in Figure 19 show a similar course for the ground-mounted PV system considered here as for the rooftop PV system. By 2050, there is a 63% reduction in Climate Change and the relative contributions to the environmental impact are also comparable with the rooftop PV system (electricity 76% (2030) and 60% (2050), silicon wafers 16% (2030) and 37%

(2050)). A higher absolute environmental impact compared to rooftop installation is due to higher requirements of the materials used.

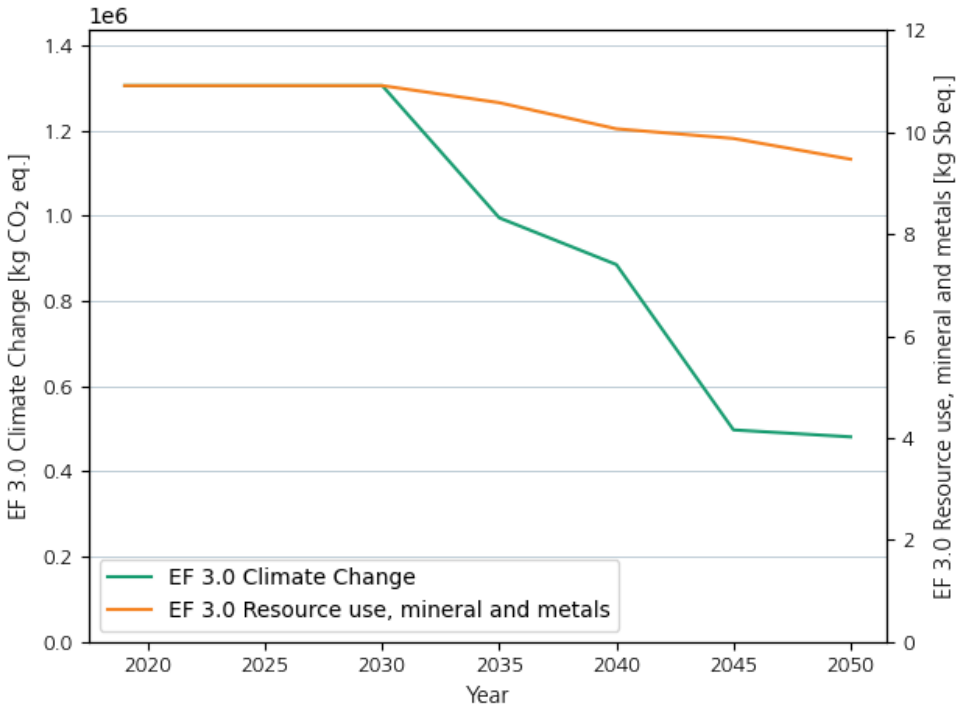


Fig. 19 Environmental impacts of III-V/Si ground-mounted PV system per MW installed capacity.

The Resource Use indicator also shows a similar result, with a slightly higher reduction of the environmental impact by 13% by 2050. The largest contribution to Resource Use in 2030 is made by copper (67%), bismuth (16%) and arsenic (10%). These relative shares barely change by 2050, as with rooftop installation, for the same reasons (<2%).

The ground-mounted PV system shows a comparable distribution for Resource Use as shown in Figure 20 as the rooftop installation with slightly higher absolute amounts, which are reduced by 10 to 20% by 2050 (exception: gold (minus 2%)). However, the effects on the relative distribution are small as shown in the following figure.

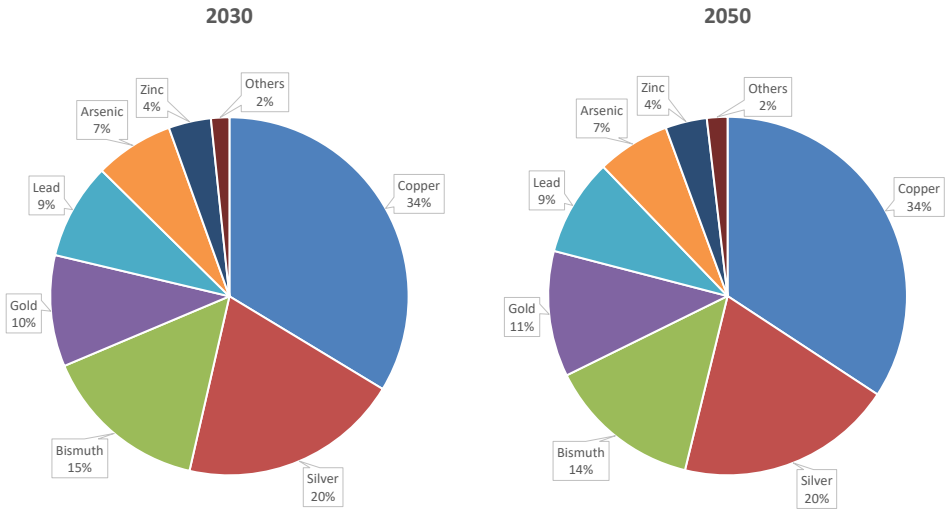


Fig. 20 Contribution of the different elements to Resource Use in the III-V/Si ground-mounted PV system.

2 Wind energy

2.1 EESG-DD – Electrically Excited Synchronous Generator – Direct Drive (Onshore)

2.1.1 Description

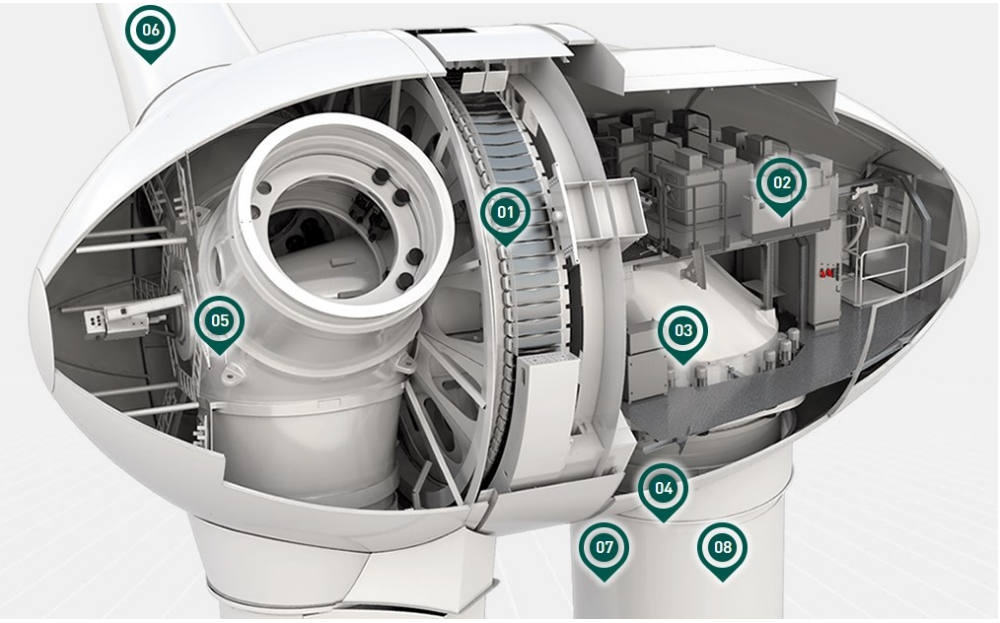


Fig. 21 Representative cross-section of an Enercon wind turbine with EESG-DD. 1: Generator, 2: Nacelle, 3: Azimuth drive, 4: E-module (not shown), 5: Rotor hub, 6: Rotor blade, 7: Tower (not shown), 8: Foundation (not shown) (Enercon).

Wind turbines with electrically excited synchronous generators and direct drive (EESG-DD) are currently used in Germany exclusively for onshore and are mostly supplied by Enercon (Bundesnetzagentur, 2019).

System boundaries

- Rotor
- Nacelle
- Tower (hybrid, based on (expert council, personal communication, 2020))
- Foundation

Parameters for Life cycle Analysis (LCA)

- Application: Onshore
- Production location of the wind turbine: Germany
- Wind turbine service lifetime: 25 years

Wind turbine dimensions

The most common rotor diameter for wind turbines with EESG-DD grew from 101 m to 115 m between 2015 and 2018. In contrast, the associated capacity remained constant at approximately 3 MW (Bundesnetzagentur, 2019). In 2019, the Enercon portfolio offered wind turbines with EESG-DD up to 4.2 MW. For larger power ranges, a technology switch to PMSG-DD is assumed to take place (Enercon, 2019).

The largest wind turbine with EESG-DD being developed as of 2019 is the E-138 EP3 E2 with a 138.25 m rotor diameter and 4.2 MW rated power. It is assumed that such dimensions will become standard in 2030.

Tab. 45 Projected dimensions of an onshore wind turbine with EESG-DD. Based on existing or under development Enercon wind turbine models. 2020: E115 EP3 - 2025: E126 EP3 - 2035 to 2050: E138 EP3

	2018	2020	2025	2030	2035	2040	2045	2050
Rotor diameter [m]	115.7	115.7	126	138	138	138	138	138
Nominal power [MW]	3.0	3.2	4.0	4.2	4.2	4.2	4.2	4.2

Wind turbine components masses

As the dimensions of a wind turbine evolve, so do the masses of its various components. To determine the masses of the rotor, nacelle, tower, and foundation, the "upscaling" approach is used. This method is commonly used to analyse the increase in mass of future wind turbines when data are not available (Caduff et al., 2012; Sieros et al., 2012). Here, the component mass M is calculated from the rotor diameter D, and a constant and scaling factor a and b.

$$M = a * D^b$$

The upscaling factors for different wind turbine types and components are provided in (Shammugam et al., 2019).

Tab. 46 Projected component mass per onshore wind turbine (WT) with EESG-DD, considering manufacturer data (Dorenbusch et al., 2019) and upscaling assumptions. This evolution applies to WTs if no material efficiency measures were implemented

	2018	2020	2025	2030	2035	2040	2045	2050
Rotor mass [t/WT]	101	101	92	116	116	116	116	116
Nacelle mass [t/ WT]	128	128	103	127	127	127	127	127
Tower mass [t/ WT]	1,306	1,306	1,719	2,304	2,304	2,304	2,304	2,304
Onshore foundation mass [t/WT]	5,372	5,372	6,697	8,912	8,912	8,912	8,912	8,912

Status-quo material composition

Tab. 47 Percentage material composition of onshore wind turbine with EESG-DD, based on the life cycle analysis of the model Enercon E82 E2 for the nacelle and hybrid tower and on averaged manufacturer data for rotor and foundation (Shammugam et al., 2019).

Rotor [% of rotor mass]	
Low alloy steel	10%
High alloy steel	9%
Cast iron	26%
Aluminium	0.1%
Copper	0.1%
Glass fibre	35%
Polymer	2%
Glass fibre reinforced plastic	1%

Epoxy resin	13%
Paint	1%
Balsa wood	1%
Adhesive	3%
Lubricant/Oil	0.1%
Nacelle [% of nacelle mass]	
Low alloy steel	9%
High alloy steel	30%
Cast iron	53%
Aluminium	1%
Copper	8%
Electronics	0.1%
Hybrid tower [% of tower mass]	
Low alloy steel	11%
Concrete	88%
Electronics	1%
Onshore foundation [% of foundation mass]	
Low alloy steel	4%
Concrete	96%

2.1.2 Material efficiency

Reduction of tower-top mass (rotor and nacelle) through copper substitution and lighter rotor blades

In the 3 MW power range, Enercon offers a compact design for wind turbines with EESG-DD. This involves replacing the traditional copper wire windings in the generator with coil elements made of aluminium. Lighter rotor blades also contribute to reducing the tower-top mass (Dorenbusch et al., 2019).

Starting in 2025, this lighter design is assumed to apply to all newly installed wind turbines with EESG-DD. The upscaling of the rotor and nacelle masses is adjusted accordingly, as well as the proportions of copper and aluminium in the generator.

Tab. 48 Projected market share of optimized compact wind turbine design

	2018	2020	2025	2030	2035	2040	2045	2050
Compact design [%]	0	0	100	100	100	100	100	100

Tab. 49 Assumed nacelle material composition for wind turbine with compact design. Copper for electrical components except generator is assumed to represent 3% of the nacelle mass (Carrascal, 2014)

Nacelle [% of nacelle mass]	
Low alloy steel	9%
High alloy steel	30%
Cast iron	53%
Aluminium	6%
Copper	3%
Electronics	0.1%

2.1.3 Material composition

The material composition of a wind turbine with EESG-DD until 2050 is shown hereafter. Metals are the focus of the present analysis. When available, data on other materials are provided as well as they remain relevant for the Life Cycle Analysis (LCA).

Tab. 50 Projected built-in material composition of onshore wind turbine with EESG-DD, under consideration of material efficiency measures. Based on (Shammugam et al., 2019)

	2018	2020	2025	2030	2035	2040	2045	2050
Rotor [t/MW]								
Glass fibre	11.8	11.0	8.0	9.7	9.7	9.7	9.7	9.7
Low alloy steel	3.3	3.1	2.2	2.7	2.7	2.7	2.7	2.7
High alloy steel	3.2	3.0	2.2	2.6	2.6	2.6	2.6	2.6
Cast iron	8.7	8.2	5.9	7.1	7.1	7.1	7.1	7.1
Al	0.030	0.029	0.021	0.025	0.025	0.025	0.025	0.025
Cu	0.026	0.024	0.018	0.021	0.021	0.021	0.021	0.021
Polymer	0.5	0.5	0.3	0.4	0.4	0.4	0.4	0.4
Glass fibre reinforced plastic	0.2	0.2	0.2	0.2	0.2	0.2	0.2	0.2
Epoxy resin	4.5	4.2	3.1	3.7	3.7	3.7	3.7	3.7
Paint	0.2	0.2	0.2	0.2	0.2	0.2	0.2	0.2
Balsa wood	0.2	0.2	0.1	0.2	0.2	0.2	0.2	0.2
Adhesive	0.9	0.9	0.6	0.8	0.8	0.8	0.8	0.8
Lubricant/Oil	0.02	0.02	0.02	0.02	0.02	0.02	0.02	0.02
Nacelle [t/MW]								
Low alloy steel	3.8	3.6	2.3	2.7	2.7	2.7	2.7	2.7
High alloy steel	12.7	11.9	7.7	9.0	9.0	9.0	9.0	9.0
Cast iron	22.4	21.0	13.5	15.9	15.9	15.9	15.9	15.9
Al	0.4	0.4	1.5	1.8	1.8	1.8	1.8	1.8
Cu	3.3	3.1	0.7	0.8	0.8	0.8	0.8	0.8
Electronics	0.055	0.052	0.033	0.039	0.039	0.039	0.039	0.039
Hybrid tower [t/MW]								
Low alloy steel	49	46	49	62	62	62	62	62
Concrete	382	358	377	481	481	481	481	481
Electronics	4.4	4.1	4.3	5.5	5.5	5.5	5.5	5.5
Onshore foundation [t/MW]								
Low alloy steel	81	76	75	95	95	95	95	95
Concrete	1,710	1,603	1,599	2,027	2,027	2,027	2,027	2,027

2.1.4 Environmental impacts

The environmental impacts of Climate Change and Resource Use of the EESG-DD wind turbine are shown in Figure 22. There is a noticeable slight reduction in Climate Change to just under 90% of the environmental impact in 2025 compared to 2018, before the maximum of 113% is reached in 2030 and stabilises at 108% from that point until 2050. The explanation for the course is that there is a non-linear relationship between the increase in the rated power of a wind turbine and the increase in the masses of the rotors, nacelle, tower, and foundation, which will result in a higher environmental impact

in the future. In 2018, concrete contributes almost 50% to Climate Change, followed by steel (11%) and ceramics (6%). In 2050, the contribution of concrete increases to 55%, while steel and ceramics are each responsible for 8%.

For Resource Use, the environmental impact reduces to 88% in 2025 compared to 2018, before stagnating at 112% from 2030. In 2018, the largest contribution is made by antimony (67%), copper (16%) and gold (10%). In 2050, the share of antimony increases to 80%, gold contributes 12%.

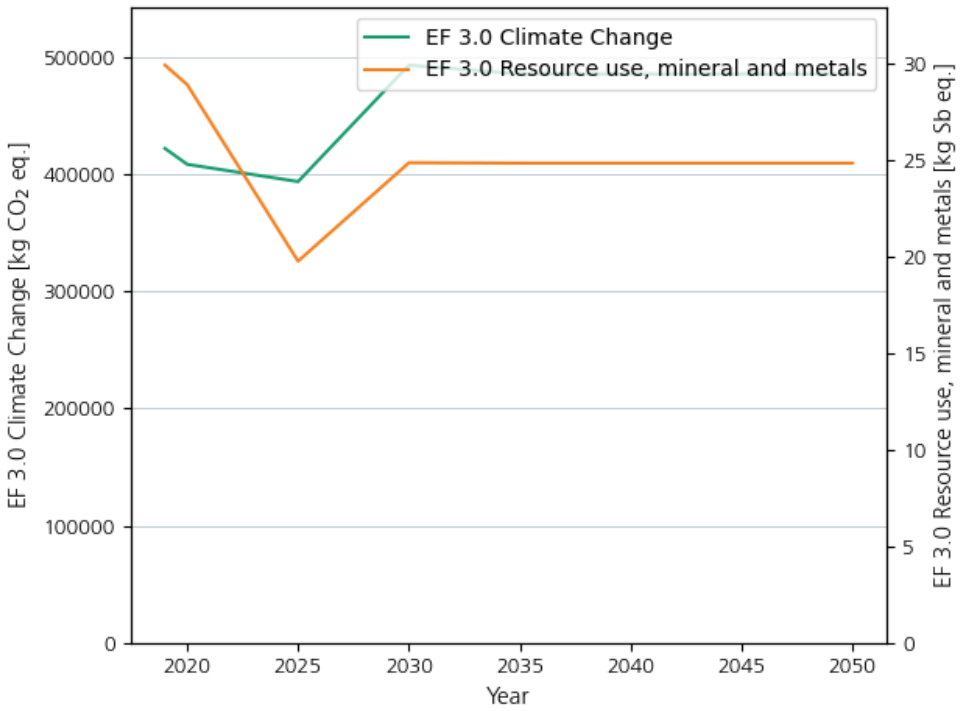


Fig. 22 Environmental impacts of the EESG-DD wind turbine per MW installed capacity.

Figure 23 shows the contribution of the different elements to Resource Use. Antimony (up 34%) and gold (up 26%) are responsible for higher Resource Use in absolute terms in 2050, while the remaining metals listed are reduced by about half. Effects on the relative composition appear in the following graph.

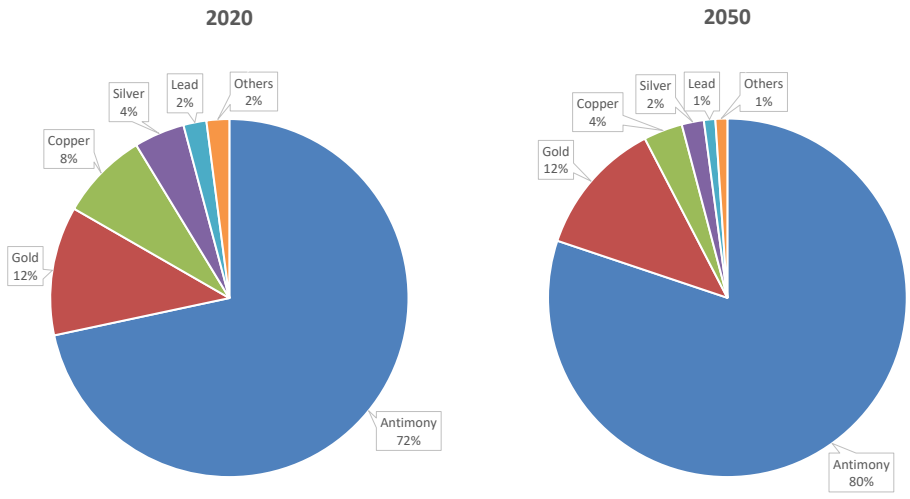


Fig. 23 Contribution of the different elements to Resource Use in the EESG-DD wind turbine.

2.2 PMSG-DD – Permanent Magnet Synchronous Generator – Direct-Drive (Onshore)

2.2.1 Description

The advantages of PMSG over induction generators or externally excited generators are smaller size, simpler manufacturing processes, and high reliability and efficiency since no external excitation is required (Bywaters et al., 2004).

System boundaries

- Rotor
- Nacelle
- Tower (hybrid, based on (expert council, personal communication, 2020))
- Foundation

Parameters for Life cycle Analysis (LCA)

- Application: Onshore
- Production location of the wind turbine: Germany
- Wind turbine service lifetime: 25 years

Wind turbine dimensions

The current trend toward larger rotor diameters for wind turbines with PMSG-DD may be restrained onshore by factors such as legally binding height restrictions, urban space competition, and infrastructure constraints associated with transporting larger components. Therefore, it is assumed that the average rotor diameter will not exceed 170 m for onshore applications.

Tab. 51 Projected dimensions of an onshore wind turbine with PMSG-DD. Based on existing or under development wind turbine models. 2020: SWT-DD-130 - 2025: E-147 EP5 - 2030: possible upgrade from E-160 EP5

	2018	2020	2025	2030	2035	2040	2045	2050
Rotor diameter [m]	130	130	147	160	170	170	170	170
Nominal power [MW]	3,6	4,3	5	5	5	5	5	5

Wind turbine components masses

As the dimensions of a wind turbine evolve, so do the masses of its various components. To determine the masses of the rotor, nacelle, tower, and foundation, the "upscaling" approach is used. This method is commonly used to analyze the increase in mass of future wind turbines when data are not available (Caduff et al., 2012; Sieros et al., 2012). Here, the component mass M is calculated from the rotor diameter D, and a constant and scaling factor a and b.

$$M = a * D^b$$

The upscaling factors for different wind turbine types and components are provided in (Shammugam et al., 2019).

Tab. 52 Projected component mass per onshore wind turbine (WT) with PMSG-DD considering upscaling assumptions. This evolution applies to WTs if no material efficiency measures were implemented.

	2018	2020	2025	2030	2035	2040	2045	2050
Rotor mass [t/WT]	118	118	161	200	234	234	234	234
Nacelle mass [t/ WT]	184	184	243	295	339	339	339	339
Tower mass [t/ WT]	1,901	1,901	2,823	3,709	4,509	4,509	4,509	4,509
Onshore foundation mass [t/WT]	7,708	7,708	11,298	14,717	17,787	17,787	17,787	17,787

Status-quo material composition

Tab. 53 Percentage material composition of onshore wind turbine with PMSG-DD (Shammugam et al., 2019). Permanent magnets are hereby not shown.

Rotor [% of rotor mass]	
Low alloy steel	10%
High alloy steel	9%
Cast iron	26%
Aluminium	0.1%
Copper	0.1%
Glass fibre	35%
Polymer	2%
Glass fibre reinforced plastic	0.7%
Epoxy resin	13%
Paint	0.7%
Balsa wood	0.6%
Adhesive	3%
Lubricant/Oil	0.1%
Nacelle [% of nacelle mass]	
Low alloy steel	9%
High alloy steel	30%
Cast iron	53%
Aluminium	1%
Copper	2%
Electronics	0.1%
Polymer	1%
Glass fibre reinforced plastic	3%
Paint	0.2%
Epoxy resin	0.3%
Lubricant/Oil	1%
Hybrid tower [% of tower mass]	
Low alloy steel	11%
Concrete	88%
Electronics	1%
Onshore foundation [% of foundation mass]	
Low alloy steel	4%
Concrete	96%

2.2.2 Material efficiency

Reduction of the rare earth content in permanent magnets

The use of permanent magnets NdFeB, which contain the rare earths neodymium and dysprosium, is associated with known supply risks. These concerns were exacerbated in

the rare earth crisis of 2011, when China imposed export restrictions on Nd and Dy. To reduce the demand for rare earths and thus mitigate supply risks in the future, material efficiency measures are being investigated. An NdFeB magnet currently consists of 2.3% dysprosium. A reduction to 1.8% could be achieved, for example, by an optimized PMSG design to lower the operating temperature of the turbine. Likewise, improved manufacturing processes could reduce the neodymium demand from 32% to 20% of the magnet mass (Pavel et al., 2017).

Substitutes for neodymium and dysprosium in NdFeB are also being investigated. The alternatives researched so far use cobalt, cerium, or terbium among others. These metals, like neodymium and dysprosium, can be considered critical and are therefore not further considered hereafter.

Tab. 54 Projected neodymium and dysprosium mass fractions in permanent magnets (Wuppertal Institut, 2014)

	2018	2025	2050
Neodymium [%]	32	25	20
Dysprosium [%]	2.3	1.8	1.8

2.2.3 Material composition

The material composition of a wind turbine with PMSG-DD until 2050 is shown hereafter. Metals are the focus of the present analysis. When available, data on other materials are provided as well as they remain relevant for the Life Cycle Analysis (LCA).

Tab. 55 Projected built-in material composition of onshore wind turbine with PMSG-DD, under consideration of material efficiency measures. Based on (Shammugam et al., 2019)

	2018	2020	2025	2030	2035	2040	2045	2050
Rotor [t/MW]								
Glass fibre	11.4	9.6	11.3	14.0	16.4	16.4	16.4	16.4
Low alloy steel	3.2	2.7	3.2	3.9	4.6	4.6	4.6	4.6
High alloy steel	3.1	2.6	3.0	3.8	4.4	4.4	4.4	4.4
Cast iron	8.4	7.1	8.3	10.3	12.1	12.1	12.1	12.1
Al	0.030	0.025	0.029	0.036	0.042	0.042	0.042	0.042
Cu	0.025	0.021	0.025	0.031	0.036	0.036	0.036	0.036
Polymer	0.5	0.4	0.5	0.6	0.7	0.7	0.7	0.7
Glass fibre reinforced plastic	0.2	0.2	0.2	0.3	0.3	0.3	0.3	0.3
Epoxy resin	4	4	4	5	6	6	6	6
Paint	0.2	0.2	0.2	0.3	0.3	0.3	0.3	0.3
Balsa wood	0.2	0.2	0.2	0.2	0.3	0.3	0.3	0.3
Adhesive	1	1	1	1	1	1	1	1
Lubricant/Oil	0.02	0.02	0.02	0.03	0.03	0.03	0.03	0.03
Nacelle [t/MW]								
Low alloy steel	4.5	3.8	4.3	5.3	6.0	6.0	6.0	6.0
High alloy steel	15.2	12.7	14.5	17.6	20.2	20.2	20.2	20.2
Cast iron	26.9	22.5	25.6	31.1	35.7	35.7	35.7	35.7
Al	0.5	0.4	0.4	0.5	0.6	0.6	0.6	0.6
Cu	1.1	0.9	1.0	1.3	1.5	1.5	1.5	1.5
Electronics	0.07	0.06	0.06	0.08	0.09	0.09	0.09	0.09
Permanent magnets NdFeB	650	650	650	650	650	650	650	650

Incl. Nd	202	202	163	163	163	163	163	130
Incl. Dy	15	15	12	12	12	12	12	12
Polymer	0.4	0.3	0.3	0.4	0.5	0.5	0.5	0.5
Glass fibre reinforced plastic	2	1	2	2	2	2	2	2
Paint	0.1	0.1	0.1	0.1	0.1	0.1	0.1	0.1
Epoxy resin	0.1	0.1	0.1	0.2	0.2	0.2	0.2	0.2
Lubricant/Oil	1	0.5	1	1	1	1	1	1
Hybrid tower [t/MW]								
Low alloy steel	60	50	64	84	102	102	102	102
Concrete	463	388	495	651	791	791	791	791
Electronics	5	4	6	7	9	9	9	9
Onshore foundation [t/MW]								
Low alloy steel	96	81	102	132	160	160	160	160
Concrete	2,045	1,712	2,158	2,811	3,397	3,397	3,397	3,397

2.2.4 Environmental impacts

The environmental impacts of Climate Change and Resource Use of the PMSG-DD onshore wind turbine are shown in Figure 24. For both indicators, a doubling (188% and 212 %; Climate Change and Resource Use, respectively) of the continuously increasing environmental impact can be observed from 2020 to 2035. Thereafter, the level of environmental impact remains constant, which can be attributed to a constant material and energy input per installed MW capacity. The largest contribution to the Climate Change indicator derives from the concrete used in the foundations, at around 50% in 2020 and 2050. Antimony has a share in Resource Use of approx. 80% for the years 2020 and 2050, gold approx. 10%.

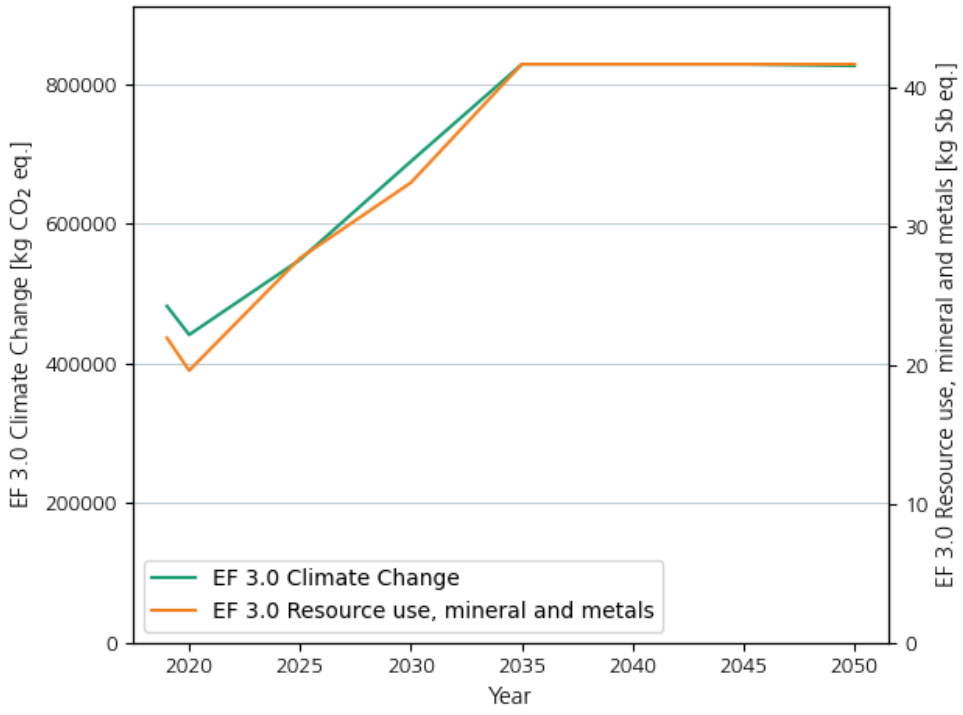


Fig. 24 Environmental impacts of the PMSG-DD onshore wind turbine per MW installed capacity.

Figure 25 shows the contribution of the different elements to Resource Use. The graphs and background data indicate that the relative contribution to the environmental impact remains practically the same when the absolute contribution is doubled for the years 2020 and 2050.

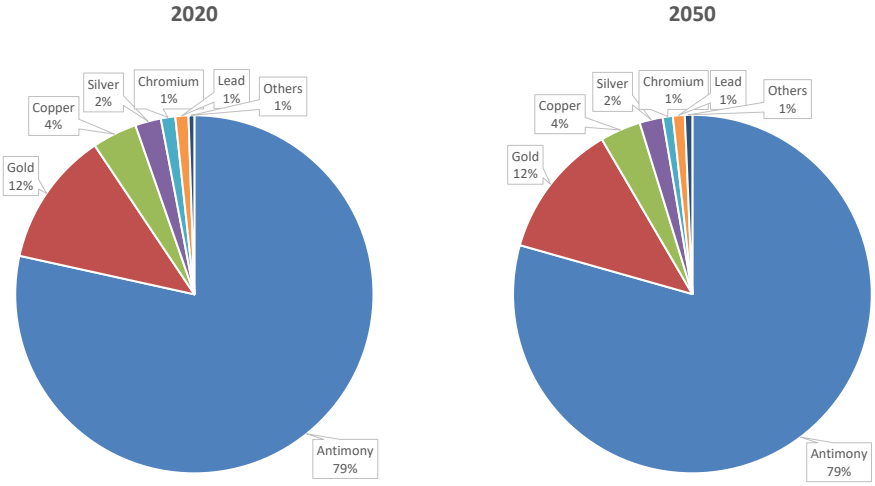


Fig. 25 Contribution of the different elements to Resource Use for the PMSG-DD onshore wind turbine.

2.3 PMSG-DD – Permanent Magnet Synchronous Generator – Direct-Drive (Offshore)

2.3.1 Description

The advantages of PMSG over induction generators or externally excited generators are smaller size, simpler manufacturing processes, and high reliability and efficiency since no external excitation is required (Bywaters et al., 2004)

System boundaries

- Rotor
- Nacelle
- Tower
- Foundation (Monopile, based on (expert council, personal communication, 2020))
- Inner-park cabling

Parameters for Life cycle Analysis (LCA)

- Application: Offshore
- Production location of the wind turbine: Germany
- Wind turbine service lifetime: 25 years

Wind turbine dimensions

In 2019, offshore wind turbine manufacturers such as Siemens-Gamesa and GE were developing wind turbines in the 10 MW+ power class with rotor diameters up to 220m, expected to be launched in 2021-2022 (GE Renewable Energy, 2019; Siemens Gamesa Renewable Energy, 2019). A strong and rapid development of the nominal power and rotor diameters of future wind turbines has therefore been assumed.

Although the technical feasibility of offshore wind turbines with 20 MW rated power has been proven, their economic attractiveness has been reported as potentially challenging (Ashuri, 2012). In contrast, the 14-16 MW power class is described as a realistic target (EU Horizon 2020) and therefore assumed to be achieved in 2040.

Tab. 56 Projected dimensions of an offshore wind turbine with PMSG-DD. Based on existing or under development wind turbine models. 2020: SWT-7.0-154 - 2025: SG 10.0-193 - 2030: Haliade X

	2018	2020	2025	2030	2035	2040	2045	2050
Rotor diameter [m]	154	154	193	220	220	250	250	250
Nominal power [MW]	6.3	7	10	12	14	16	16	16

Wind turbine components masses

As the dimensions of a wind turbine evolve, so do the masses of its various components. To determine the masses of the rotor, nacelle, tower, and foundation, the "upscaling" approach is used. This method is commonly used to analyse the increase in mass of future wind turbines when data are not available (Caduff et al., 2012; Sieros et al., 2012). Here, the component mass M is calculated from the rotor diameter D, and a constant and scaling factor a and b.

$$M = a * D^b$$

The upscaling factors for different wind turbine types and components are provided in (Shammugam et al., 2019).

Tab. 57 Projected component mass per offshore wind turbine (WT) with PMSG-DD, considering upscaling assumptions and (expert council, personal communication, 2020)). This evolution applies to WTs if no material efficiency measures were implemented

	2018	2020	2025	2030	2035	2040	2045	2050
Rotor mass [t/WT]	182	182	324	362	362	502	502	502
Nacelle mass [t/ WT]	271	271	453	611	611	819	819	819
Tower mass [t/ WT]	526	526	968	1,379	1,379	1,947	1,947	1,947
Offshore foundation mass [t/WT]	1,500	1,500	3,245	2,495	2,495	2,788	2,788	2,788

Status-quo material composition

Tab. 58 Percentage material composition of offshore wind turbine with PMSG-DD (Shammugam et al., 2019). Permanent magnets are not shown here.

Rotor [% of rotor mass]	
Low alloy steel	10%
High alloy steel	9%
Cast iron	26%
Aluminium	0.1%
Copper	0.1%
Glass fibre	35%
Polymer	2%

Glass fibre reinforced plastic	0.7%
Epoxy resin	13%
Paint	0.7%
Balsa wood	0.6%
Adhesive	3%
Lubricant/Oil	0.1%
Nacelle [% of nacelle mass]	
Low alloy steel	9%
High alloy steel	30%
Cast iron	53%
Aluminium	1%
Copper	2%
Electronics	0.1%
Polymer	1%
Glass fibre reinforced plastic	3%
Paint	0.2%
Epoxy resin	0.3%
Lubricant/Oil	1%
Steel tower [% of tower mass]	
Low alloy steel	97%
Aluminium	1%
Copper	1%
Electronics	1%
Monopile [% of foundation mass]	
Low alloy steel	100%

2.3.2 Material efficiency

Reduction of the rare earth content in permanent magnets

The use of permanent magnets NdFeB, which contain the rare earths neodymium and dysprosium, is associated with known supply risks. These concerns were exacerbated in the rare earth crisis of 2011, when China imposed export restrictions on Nd and Dy. To reduce the demand for rare earths and thus mitigate supply risks in the future, material efficiency measures are being investigated. An NdFeB magnet currently consists of 2.3% dysprosium. A reduction to 1.8% could be achieved, for example, by an optimized PMSG design to lower the operating temperature of the turbine. Likewise, improved manufacturing processes could reduce the neodymium demand from 32% to 20% of the magnet mass (Pavel et al., 2017).

Substitutes for neodymium and dysprosium in NdFeB are also being investigated. The alternatives researched so far use cobalt, cerium, or terbium among others. These metals, like neodymium and dysprosium, can be considered critical and are therefore not further considered hereafter.

Tab. 59 Projected neodymium and dysprosium mass fractions in permanent magnets (Wuppertal Institut, 2014)

	2018	2025	2050
Neodymium [%]	32	25	20
Dysprosium [%]	2.3	1.8	1.8

Use of a higher-grade steel for the tower offshore

S355 steel is commonly used for wind turbine steel towers. Higher grade steel such as S690 can be used to achieve lighter towers but comes at higher material costs. Technical challenges such as weldability, fatigue of higher-strength steels, and corrosion issues

associated with thinner tower walls need to be addressed as well (expert council, personal communication, 2020).

S500 steel is assumed to become standard for offshore towers from 2035 onwards and to lead to a 30% weight reduction, thus compensating for the cost increase with a higher strength steel (Tong, 2019). Further savings come from lower transportation costs.

Tab. 60 Projected market shares of offshore wind turbines with higher-grade steel towers (>S355), based on (expert council, personal communication, 2020))

	2018	2020	2025	2030	2035	2040	2045	2050
Higher-grade steel tower [%]	0	0	0	0	100	100	100	100

Optimization of the monopile design

Traditional monopile sizing and manufacturing methods were evaluated as conservative in an initial phase of the Pile Soil Analysis Project (PISA). The use of thinner, shorter monopiles is expected to result in steel savings of up to 30%, based on (Buist, 2015) and (expert council, personal communication, 2020).

Tab. 61 Projected market shares of offshore wind turbines with optimized monopile

	2018	2020	2025	2030	2035	2040	2045	2050
Optimized monopile [%]	0	0	0	100	100	100	100	100

2.3.3 Material composition

The material composition of an offshore wind turbine with PMSG-DD and inner park cabling until 2050 is shown hereafter. Metals are the focus of the present analysis. When available, data on other materials are provided as well as they remain relevant for the Life Cycle Analysis (LCA). Hybrid rotors are assumed to be used from 2030 onwards.

Tab. 62 Projected built-in material composition of offshore wind turbine with PMSG-DD, under consideration of material efficiency measures. Based on (Shammugam et al., 2019)

	2018	2020	2025	2030	2035	2040	2045	2050
Rotor [t/MW]								
Glass fibre	10.1	9.1	7.3	8.5	7.2	8.8	8.8	8.8
Carbon fibre	-	-	-	2.1	1.8	2.2	2.2	2.2
Low alloy steel	2.8	2.5	3.2	3.0	2.5	3.1	3.1	3.1
High alloy steel	2.7	2.4	3.1	2.8	2.4	3.0	3.0	3.0
Cast iron	7.4	6.7	8.4	7.8	6.7	8.1	8.1	8.1
Al	0.026	0.023	0.029	0.027	0.023	0.028	0.028	0.028
Cu	0.022	0.020	0.025	0.023	0.020	0.024	0.024	0.024
Polymer	0.4	0.4	0.5	0.5	0.4	0.5	0.5	0.5
Glass fibre reinforced plastic	1	1	1	1	1	1	1	1
Epoxy resin	4	3	4	4	3	4	4	4
Paint	0.2	0.2	0.2	0.2	0.2	0.2	0.2	0.2
Balsa wood	0.2	0.2	0.2	0.2	0.2	0.2	0.2	0.2
Adhesive	1	1	1	1	1	1	1	1
Lubricant/Oil	0.02	0.02	0.02	0.02	0.02	0.02	0.02	0.02
Nacelle [t/MW]								
Low alloy steel	3.8	3.4	4.0	4.5	3.9	4.6	4.6	4.6

High alloy steel	12.8	11.5	13.5	15.2	13.0	15.3	15.3	15.3
Cast iron	22.6	20.3	23.8	26.8	23.0	26.9	26.9	26.9
Al	0.4	0.3	0.4	0.5	0.4	0.5	0.5	0.5
Cu	0.9	0.8	1.0	1.1	0.9	1.1	1.1	1.1
Electronics	0.06	0.05	0.06	0.07	0.06	0.07	0.07	0.07
Permanent magnets NdFeB	650	650	650	650	650	650	650	650
Incl. Nd	202	202	163	163	163	163	163	130
Incl. Dy	15	15	12	12	12	12	12	12
Polymer	0.3	0.3	0.3	0.4	0.3	0.4	0.4	0.4
Glass fibre reinforced plastic	1	1	1	2	1	2	2	2
Paint	0.1	0.1	0.1	0.1	0.1	0.1	0.1	0.1
Epoxy resin	0.1	0.1	0.1	0.1	0.1	0.1	0.1	0.1
Lubricant/Oil	0.5	0.4	0.5	0.6	0.5	0.6	0.6	0.6
Hybrid tower [t/MW]								
Low alloy steel	81	73	94	112	77	95	95	95
Al	0.8	0.7	0.9	1.1	0.9	1.2	1.2	1.2
Cu	0.8	0.7	0.9	1.1	0.9	1.1	1.1	1.1
Electronics	0.9	0.8	1.0	1.2	1.0	1.3	1.3	1.3
Monopile [t/MW]								
Low alloy steel	190	171	142	137	118	143	143	143

Tab. 63 Projected built-in material composition of offshore inner park cabling, adapted from data on the EnBW Baltic 1 project and considering 33kV HVAC cable of 12.2 kg/m and 2km cabling length. Based on (BERR, 2008; Birkeland, 2011; ENBW, 2020)

	2018	2020	2025	2030	2035	2040	2045	2050
Inner-park cabling [t/MW]								
Low alloy steel	1.3	1.2	0.8	0.7	0.6	0.5	0.5	0.5
Cu	1.49	1.34	0.94	0.78	0.67	0.59	0.59	0.59
Pb	0.69	0.62	0.43	0.36	0.31	0.27	0.27	0.27
Polyethylene	0.34	0.31	0.22	0.18	0.15	0.14	0.14	0.14
Transformer platform [t/MW]								
Low alloy steel	29.8	29.8	29.8	29.8	29.8	29.8	29.8	29.8
Cu	5.4	5.4	5.4	5.4	5.4	5.4	5.4	5.4
Concrete	18.9	18.9	18.9	18.9	18.9	18.9	18.9	18.9

2.3.4 Environmental impacts

The environmental impacts of Climate Change and Resource Use of the PMSG-DD offshore wind turbine are depicted in Figure 26. An increase in the environmental impact can be seen for both indicators by 2030 in relation to 2020 (Climate Change +16%, Resource Use +6%). In 2035, the environmental impacts per MW of installed capacity reach a minimum (101% for Climate Change, 96%) before settling at 120 and 103% from 2040 (Climate Change and Resource Use, respectively). This is due to the fact that in 2035 (apart from 2020) the lowest material input, with which the environmental impacts correlate, occurs per installed capacity (non-linear correlation). The largest contribution to the Climate Change indicator is accounted for by the copper used in the

transformer and marine cables, at around 50% in 2020 and 2050. Copper has a share in Resource Use of approx. 75% for the years 2020 and 2050, lead approx. 20%.

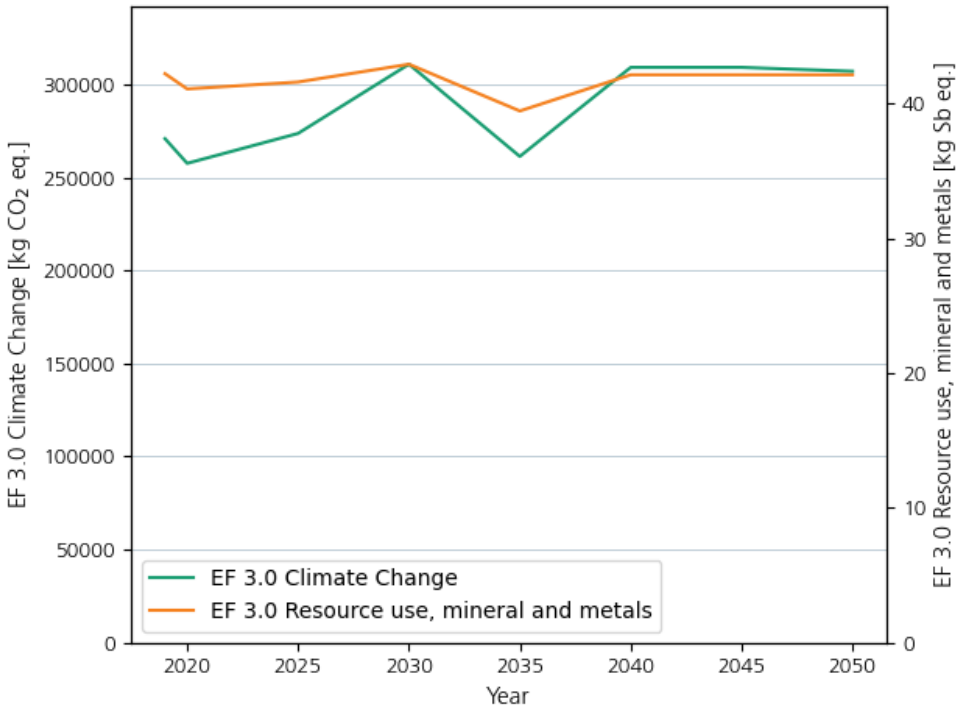


Fig. 26 Environmental impacts of the PMSG-DD offshore wind turbine per MW installed capacity.

Figure 27 shows the contribution of the different elements to Resource Use. It can be seen from the graphs and background data that the relative contribution to the environmental impact remains almost the same for the years 2020 and 2050, because the absolute values hardly change (0 - 10%), with the exception of gold (plus 62%) and chromium (minus 23%).

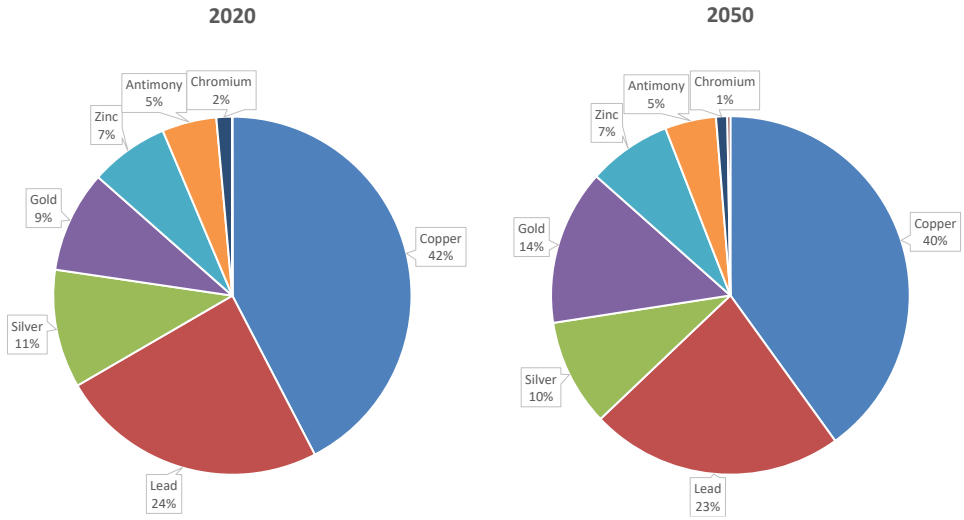


Fig. 27 Contribution of the different elements to Resource Use in the PMSG-DD offshore wind turbine.

2.4 PMSG-MS – Permanent Magnet Synchronous Generator – Middle-Speed (Offshore)

2.4.1 Description

The advantages of PMSG over induction generators or externally excited generators are smaller size, simpler manufacturing processes, and high reliability and efficiency since no external excitation is required (Bywaters et al., 2004). In 2019, the PMSG for the medium speed range was exclusively manufactured by MHI Vestas.

System boundaries

- Rotor
- Nacelle
- Tower
- Foundation (Monopile, based on (expert council, personal communication, 2020))
- Inner-park cabling

Parameters for Life cycle Analysis (LCA)

- Application: Offshore
- Production location of the wind turbine: Germany
- Wind turbine service lifetime: 25 years

Wind turbine dimensions

In 2018, 56 wind turbines from MHI Vestas were installed at the Borkum Riffgrund 2 Park in the North Sea (Bundesnetzagentur, 2019). These wind turbines have a rated power of 8.3 MW and a rotor diameter of 164 m. The trend towards larger and more powerful offshore wind turbines will prevail until 2050.

Tab. 64 Projected dimensions of an offshore wind turbine with PMSG-MS. Based on existing or under development wind turbine models. 2020: V164-9.5 - 2025: possible upgrade from V174-9.5

	2018	2020	2025	2030	2035	2040	2045	2050
Rotor diameter [m]	164	164	174	200	220	250	250	250
Nominal power [MW]	8.3	9.5	10	12	14	16	16	16

Wind turbine components masses

As the dimensions of a wind turbine evolve, so do the masses of its various components. To determine the masses of the rotor, nacelle, tower, and foundation, the "upscaling" approach is used. This method is commonly used to analyse the increase in mass of future wind turbines when data are not available (Caduff et al., 2012; Sieros et al., 2012). Here, the component mass M is calculated from the rotor diameter D, and a constant and scaling factor a and b.

$$M = a * D^b$$

The upscaling factors for different wind turbine types and components are provided in (Shammugam et al., 2019).

Tab. 65 Projected component mass per offshore wind turbine (WT) with PMSG-MS, considering upscaling assumptions and (expert council, personal communication, 2020). This evolution applies to WTs if no material efficiency measures were implemented

	2018	2020	2025	2030	2035	2040	2045	2050
Rotor mass [t/WT]	195	195	199	284	362	502	502	502
Nacelle mass [t/ WT]	313	313	358	492	611	819	819	819
Tower mass [t/ WT]	624	624	732	1,066	1,379	1,947	1,947	1,947
Offshore foundation mass [t/WT]	1,200	1,200	1,288	1,289	1,647	2,288	2,288	2,288

Status-quo material composition

Tab. 66 Percentage material composition of offshore wind turbine with PMSG-MS (Shammugam et al., 2019). Permanent magnets are not shown here.

Rotor [% of rotor mass]	
Low alloy steel	10%
High alloy steel	9%
Cast iron	26%
Aluminium	0.1%
Copper	0.1%
Glass fibre	28%
Carbon fibre	7%
Polymer	2%
Glass fibre reinforced plastic	0.7%
Epoxy resin	13%
Paint	0.7%
Balsa wood	0.6%
Adhesive	3%
Lubricant/Oil	0.1%
Nacelle [% of nacelle mass]	
Low alloy steel	10%
High alloy steel	39%
Cast iron	42%
Aluminium	0.9%
Copper	2.1%
Electronics	0.4%
Polymer	1%
Glass fibre reinforced plastic	3%
Paint	0.1%
Epoxy resin	0.3%
Lubricant/Oil	1%
Steel tower [% of tower mass]	
Low alloy steel	97%
Aluminium	1%
Copper	1%
Electronics	1%
Monopile [% of foundation mass]	
Low alloy steel	100%

2.4.2 Material efficiency

Reduction of the rare earth content in permanent magnets

The use of permanent magnets NdFeB, which contain the rare earths neodymium and dysprosium, is associated with known supply risks. These concerns were exacerbated in

the rare earth crisis of 2011, when China imposed export restrictions on Nd and Dy. To reduce the demand for rare earths and thus mitigate supply risks in the future, material efficiency measures are being investigated. An NdFeB magnet currently consists of 2.3% dysprosium. A reduction to 1.8% could be achieved, for example, by an optimized PMSG design to lower the operating temperature of the turbine. Likewise, improved manufacturing processes could reduce the neodymium demand from 32% to 20% of the magnet mass (Pavel et al., 2017).

Substitutes for neodymium and dysprosium in NdFeB are also being investigated. The alternatives researched so far use cobalt, cerium, or terbium among others. These metals, like neodymium and dysprosium, can be considered critical and are therefore not further considered hereafter.

Tab. 67 Projected neodymium and dysprosium mass fractions in permanent magnets (Wuppertal Institut, 2014)

	2018	2025	2050
Neodymium [%]	32	25	20
Dysprosium [%]	2.3	1.8	1.8

Use of a higher-grade steel for the tower offshore

S355 steel is commonly used for wind turbine steel towers. Higher grade steel such as S690 can be used to achieve lighter towers but comes at higher material costs. Technical challenges such as weldability, fatigue of higher-strength steels, and corrosion issues associated with thinner tower walls need to be addressed as well (expert council, personal communication, 2020).

S500 steel is assumed to become standard for offshore towers from 2035 onwards and to lead to a 30% weight reduction, thus compensating for the cost increase with a higher strength steel (Tong, 2019). Further savings come from lower transportation costs.

Tab. 68 Projected market shares of offshore wind turbines with higher-grade steel towers (>S355), based on (expert council, personal communication, 2020)

	2018	2020	2025	2030	2035	2040	2045	2050
Higher-grade steel tower [%]	0	0	0	0	100	100	100	100

Optimization of the monopile design

Traditional monopile sizing and manufacturing methods were evaluated as conservative in an initial phase of the Pile Soil Analysis Project (PISA). The use of thinner, shorter monopiles is expected to result in steel savings of up to 30%, based on (Buist, 2015) and (expert council, personal communication, 2020).

Tab. 69 Projected market shares of offshore wind turbines with optimized monopile

	2018	2020	2025	2030	2035	2040	2045	2050
Optimized monopile [%]	0	0	0	100	100	100	100	100

2.4.3 Material composition

The material composition of an offshore wind turbine with PMSG-MS until 2050 is shown hereafter. Metals are the focus of the present analysis. When available, data on other materials are provided as well as they remain relevant for the Life Cycle Analysis (LCA).

Tab. 70 Projected built-in material composition of offshore wind turbine with PMSG-MS, under consideration of material efficiency measures. Based on (Shammugam et al., 2019)

	2018	2020	2025	2030	2035	2040	2045	2050
Rotor [t/MW]								
Glass fibre	6.6	5.7	5.6	6.6	7.2	8.8	8.8	8.8
Carbon fibre	1.6	1.4	1.4	1.7	1.8	2.2	2.2	2.2
Low alloy steel	2.3	2.0	1.9	2.3	2.5	3.1	3.1	3.1
High alloy steel	2.2	1.9	1.9	2.2	2.4	3.0	3.0	3.0
Cast iron	6.1	5.3	5.1	6.1	6.7	8.1	8.1	8.1
Al	0.021	0.019	0.018	0.021	0.023	0.028	0.028	0.028
Cu	0.018	0.016	0.015	0.018	0.020	0.024	0.024	0.024
Polymer	0.4	0.3	0.3	0.4	0.4	0.5	0.5	0.5
Glass fibre reinforced plastic	0.2	0.1	0.1	0.2	0.2	0.2	0.2	0.2
Epoxy resin	3	3	3	3	3	4	4	4
Paint	0.2	0.1	0.1	0.2	0.2	0.2	0.2	0.2
Balsa wood	0.1	0.1	0.1	0.1	0.2	0.2	0.2	0.2
Adhesive	1	1	1	1	1	1	1	1
Lubricant/Oil	0.02	0.01	0.01	0.02	0.02	0.02	0.02	0.02
Nacelle [t/MW]								
Low alloy steel	4.0	3.4	3.7	4.2	4.5	5.3	5.3	5.3
High alloy steel	15.4	12.9	14.1	16.1	17.2	20.1	20.1	20.1
Cast iron	16.2	13.7	14.9	17.0	18.1	21.3	21.3	21.3
Al	0.3	0.3	0.3	0.4	0.4	0.4	0.4	0.4
Cu	0.8	0.7	0.8	0.9	0.9	1.1	1.1	1.1
Electronics	0.14	0.12	0.13	0.15	0.15	0.18	0.18	0.18
Permanent magnets NdFeB	160	160	160	160	160	160	160	160
Incl. Nd	50	50	40	40	40	40	40	32
Incl. Dy	4	4	3	3	3	3	3	3
Polymer	0.3	0.2	0.3	0.3	0.3	0.4	0.4	0.4
Glass fibre reinforced plastic	1	1	1	1	1	2	2	2
Paint	0.1	0.0	0.1	0.1	0.1	0.1	0.1	0.1
Epoxy resin	0.1	0.1	0.1	0.1	0.1	0.1	0.1	0.1
Lubricant/Oil	0.4	0.4	0.4	0.5	0.5	0.6	0.6	0.6
Hybrid tower [t/MW]								
Low alloy steel	73	64	71	86	77	95	95	95
Al	0.7	0.6	0.7	0.8	0.9	1.2	1.2	1.2
Cu	0.7	0.6	0.7	0.8	0.9	1.1	1.1	1.1
Electronics	0.8	0.7	0.8	0.9	1.0	1.3	1.3	1.3
Monopile [t/MW]								
Low alloy steel	145	126	129	107	118	143	143	143

Tab. 71 Projected built-in material composition of offshore inner park cabling, adapted from data on the EnBW Baltic 1 project and considering 33kV HVAC cable of 12.2 kg/m and 2km cabling length. Based on (BERR, 2008; Birkeland, 2011; ENBW, 2020)

	2018	2020	2025	2030	2035	2040	2045	2050
Inner-park cabling [t/MW]								
Low alloy steel	1.0	0.9	0.8	0.7	0.6	0.5	0.5	0.5
Cu	1.1	1.0	0.9	0.8	0.7	0.6	0.6	0.6
Pb	0.5	0.5	0.4	0.4	0.3	0.3	0.3	0.3
Polyethylene	0.3	0.2	0.2	0.2	0.2	0.1	0.1	0.1
Transformer platform [t/MW]								
Low alloy steel	29.8	29.8	29.8	29.8	29.8	29.8	29.8	29.8
Cu	5.4	5.4	5.4	5.4	5.4	5.4	5.4	5.4
Concrete	18.9	18.9	18.9	18.9	18.9	18.9	18.9	18.9

2.4.4 Environmental impacts

The environmental impacts of Climate Change and Resource Use of the PMSG-MS wind turbine are presented in Figure 28. For both indicators, an increasing environmental impact is visible from 2020 to 2040 (+ 35% for Climate Change, + 12% for Resource Use), whereas the environmental impacts remain constant from 2040 to 2050. This is caused by larger towers, nacelles and foundations, whose environmental impact increases disproportionately per MW of installed capacity.

The largest contribution to the Climate Change indicator is made by the copper used in the transformer and marine cables, at around 50% in 2020 and 2050. Copper accounts for almost 75% of Resource Use in 2020 and 2050.

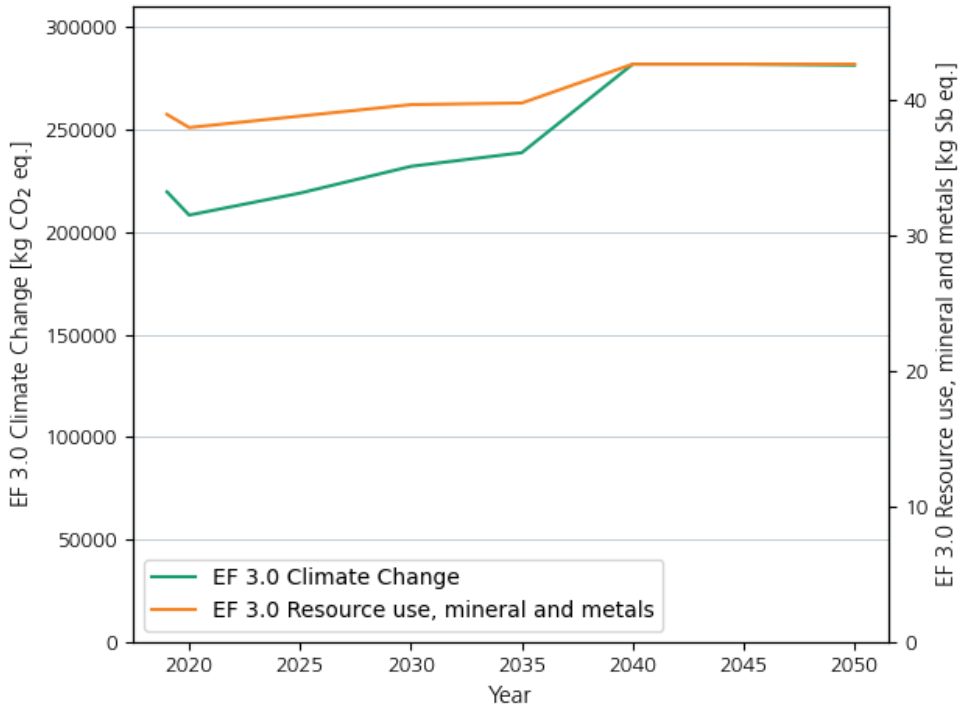


Fig. 28 Environmental impacts of the PMSG-MS wind turbine per MW installed capacity.

Figure 29 demonstrates the contribution of the different elements to Resource Use. Based on the graphs and background data, both relative and absolute contributions (plus 0-7%, exception: antimony plus 86%) to the environmental impact remain almost the same for the years 2020 and 2050.

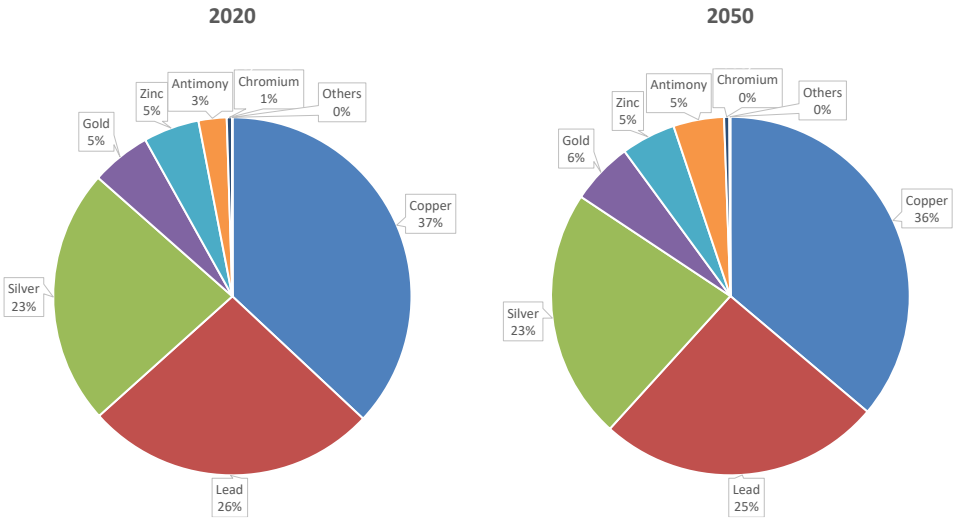


Fig. 29 Contribution of the different elements to Resource Use in the PMSG-MS wind turbine.

3 Fuel Cell

3.1 PEMFC – Proton-Exchange Membrane Fuel Cell

3.1.1 Description

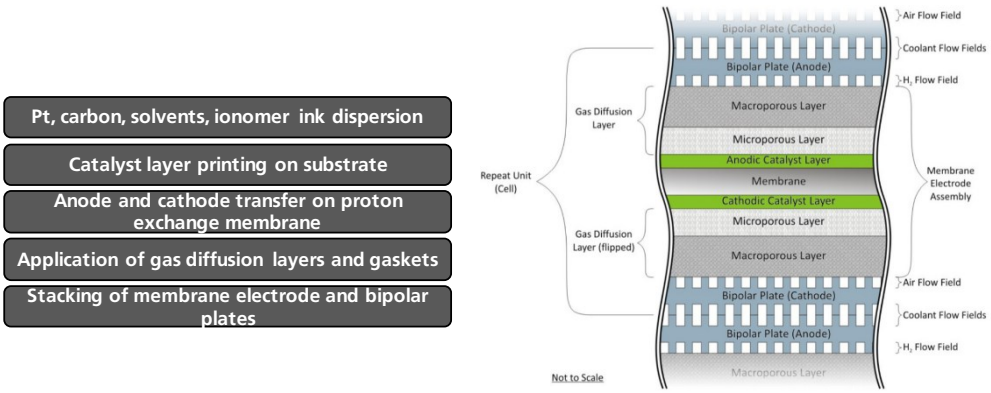


Fig. 30 Typical process flow (left) and representative cross-section of a of a PEMFC stack (right) (James et al., 2010).

System boundaries

- Stack

Parameters for Life cycle Analysis (LCA)

- Production location of the PEMFC stack: Asia/USA
- PEMFC stack service lifetime: 15 years

Technical parameters

Tab. 72 Projected PEMFC stack properties, based on (James, 2018; James et al., 2017)

	2018	2030	2040
Stack Power Net/Gross [kW]	88.5/114	80/87.1	80/87.1
Cell Voltage [V]	0.6	0.663	0.663
Total active area [m²]	9.91	7.0	5.8
Fuel cell efficiency [%]	48	53	53
Active-to-Total-Area Ratio	0.4	0.625	0.65
Number cells per stack	370	377	377
Membrane thickness [µm]	17	10	10
GDL Macroporous layer thickness [µm]	172	105	105

3.1.2 Material efficiency

Reduction of the platinum loading in the catalyst layer

The roadmap of (James, 2018) sees Pt loadings of 0.125 mgPt/cm² and 0.088 mgPt/cm² for 2018 and 2025, respectively, based on next-generation technologies and PtCo alloys. The durability of these Pt alloys remains however a challenge, as they rapidly degrade by dissolution of Pt and the alloy components (Sneed et al., 2018) compared to pure Pt catalysts. It is therefore assumed that pure Pt catalysts will be used, and targeted Pt loadings will be achieved in the medium to long-term.

Tab. 73 Projected platinum loading in the catalyst layer, based on (James, 2018)

	2018	2020	2025	2030	2035	2040	2045	2050
Power density (mW/cm²)	1150			1250		1500		
Total platinum loading (mg/cm²))	0,3			0,125		0,088		
- For the cathode	0,275			0,107		0,07		
- For the anode	0,025			0,0018		0,018		
Total Platinum (g/kW$_{net}$)	0,336	0,279	0,198	0,126	0,099	0,075	0,050	0,035

Use of steel-based bipolar plates

Bipolar plates generally use either injection moulded graphite plates or embossed stainless steel metal foils. (James et al., 2017) indicates however that the metallic alternative may become more prevalent. Although metal plates are more susceptible to fuel cell corrosion and more expensive than graphite plates, they have favourable properties for mass production and compact stack designs. According to (Lakshmanan, 2017), stainless steel plates should become thinner to remain competitive.

Tab. 74 Stainless steel content in bipolar plates, based on (Lakshmanan, 2017)

	2018	2025	2030	2050
Stainless steel [g/kW$_{net}$]	400	275	150	150

3.1.3 Material composition

The material composition of a PEMFC stack until 2050 is shown hereafter. Metals are the focus of the present analysis. When available, data on other materials are provided as well as they remain relevant for the Life Cycle Analysis (LCA).

Tab. 75 Projected built-in material composition of PEMFC stack, under consideration of material efficiency measures. The composition is assumed constant until 2050, unless stated otherwise. Based on (Miotti et al., 2017)

	2018	2020	2025	2030	2035	2040	2045	2050
Catalyst layer [g/kW]								
Platinum	0.336	0.279	0.198	0.126	0.099	0.075	0.050	0.035
Carbon particles	0.78							
Polytetrafluoroethylene (PTFE)	0.01							
Solvent	3.70							
Membrane [g/kW]								
Tetrafluoroethylene (TFE)	8.24							
Sulfuric Trioxide	0.39							
Expanded PTFE (ePTFE)	0.83							

Gas diffusion layer [g/kW]								
Carbon paper	29.81							
PTFE	2.49							
Carbon black for microporous layer	5.71							
PTFE for microporous layer	1.79							
Solvent	0.56							
Membrane-electrode-unit [g/kW]								
Gasket	42.84							
Bipolar plates [g/kW]								
Stainless steel	400	400	275	150	150	150	150	150
Titanium nitride (anti-corrosion layer)	12.75	12.75	12.7	12.64	12.64	12.64	12.64	12.64
Graphite	12.75	12.75	12.7	12.64	12.64	12.64	12.64	12.64
Screen-printed gaskets	1.86							
End plate [g/kW]								
Glass fiber	9.88							
Epoxy	9.88							
Current collector [g/kW]								
Copper	18.15	17.29	16.06	15.07	14.82	14.60	14.39	14.32
Compression bands [g/kW]								
Stainless steel	11.46	10.92	10.14	9.51	9.36	9.22	9.08	9.04
Housing [g/kW]								
Polypropylene	49.14							

3.1.4 Environmental impacts

The environmental impact indicators Climate Change and Resource Use of the PEM fuel cell are shown in Figure 31. In the case of Climate Change, there is a continuous, rapid decline in the environmental impact of around 60% by 2030, followed by a weaker decline of a further 20% by 2050. This is almost exclusively due to the reduced use of platinum, which is responsible for 81% of the environmental impact in 2018 and for 43% in 2050, followed by the gaseous diffusion layer (27%).

A similar picture emerges for Resource Use. Both the reduction in environmental impact and the contribution of platinum are comparable. In addition to platinum, copper has a high contribution to the environmental impact in 2050 with 39%.

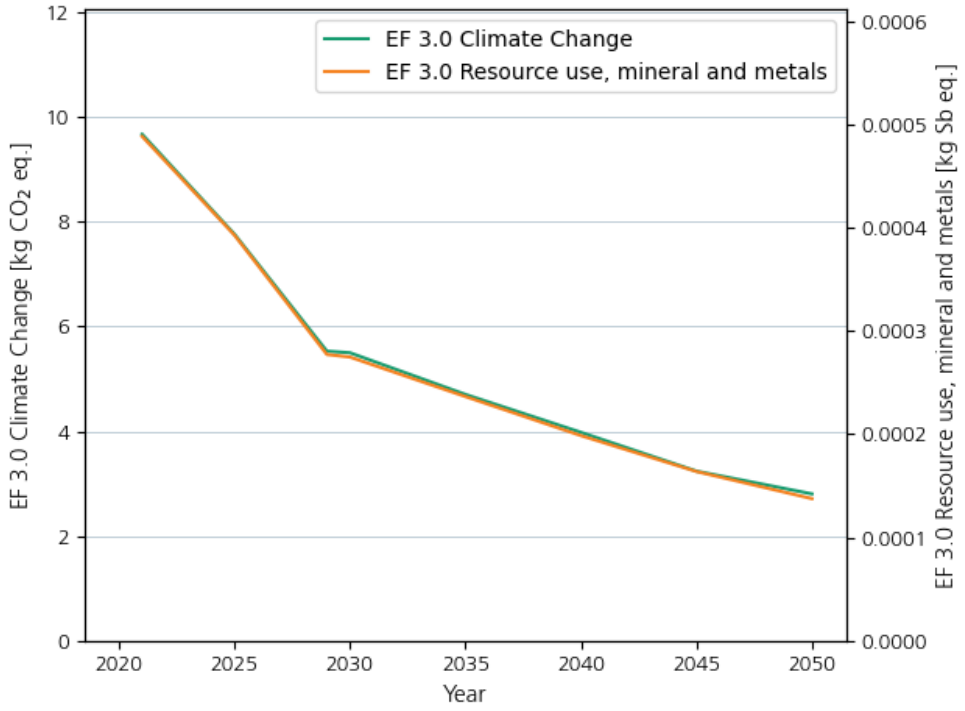


Fig. 31 Environmental impact of the PEM fuel cell per MW installed capacity.

Figure 32 shows the contribution of the different elements to Resource Use. The graphs show that the relative share of antimony increases from 7% in 2020 to 19% in 2050. This is due to an increasing absolute share of antimony, while the other metals, with the exception of gold, are less used.

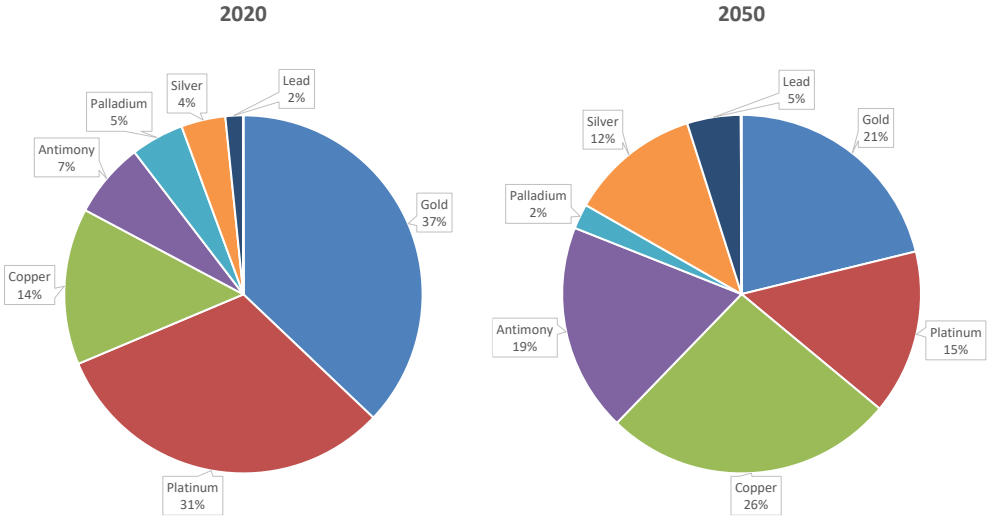


Fig. 32 Contribution of the different elements to resource utilisation in the PEM fuel cell.

4 Power-to-X

4.1 AEL – Alkaline Electrolysis

4.1.1 Description

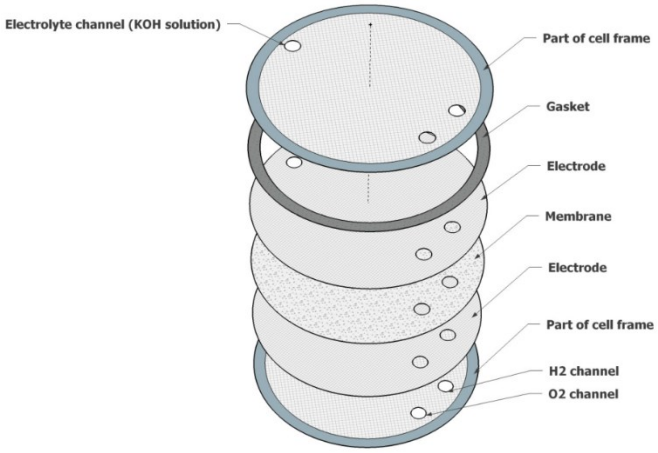


Fig. 33 Alkaline electrolysis cell set-up (Koj et al., 2017).

In a stack configuration, AEL cells are connected in series. The production of AEL does not require scarce or toxic raw materials. Since the ban on the use of asbestos at the European level in 2005, ZrO2 polysulfone has become the accepted material for the membrane. Nickel is commonly used as anode and cathode material, which provides good electrochemical activity and resistance in alkaline environments (Smolinka et al., 2018). To reduce the required cell voltage, the electrodes can be coated with a coating of Raney nickel (alloy Ni-Al).

System boundaries

- Stack

Parameters for Life cycle Analysis (LCA)

- Production location of the AEL stack: China
- AEL service lifetime: 10 years

Technical parameters

Tab. 76 Properties of the reference AEL stack (Koj et al., 2017)

	Reference value 2018
System power [MW]	6
Efficiency [%]	65.7
Number of cells per stack	139

4.1.2 Material efficiency

Increase of the efficiency

For low-temperature electrolysis such as AEL, an efficiency of about 65% (LHV) is common (Koj et al., 2017; Smolinka et al., 2018). By 2050, an efficiency increase up to 70% is assumed (Sterchele, 2019).

Tab. 77 Projected AEL efficiency, based on (Koj et al., 2017; Sterchele, 2019)

	2020	2030	2040	2050
Efficiency [%]	65.7	65.7	68.0	70.0

4.1.3 Material composition

The material composition of an AEL stack until 2050 is shown hereafter. Metals are the focus of the present analysis. When available, data on other materials are provided as well as they remain relevant for the Life Cycle Analysis (LCA).

Tab. 78 Projected material demand for AEL stack, under consideration of material efficiency measures. Based on the LCA of (Koj et al., 2017), it includes all material inputs for the stack production. The data is for a total of 8 stacks. 4 stacks for the initial construction of the plant and 4 stacks that will be replaced during the considered lifetime. The composition is assumed constant unless stated otherwise.

	2018	2040	2050
Stack and cells frame [kg/MW]			
Unalloyed steel	33,333	32,206	31,286
Cu	333	322	313
Cells			
- **Electrodes [kg/MW]**			
Ni	5,117	4,944	4,802
Al	75	72	70
Carbon monoxid	25		
- **Membran [kg/MW]**			
Zirconium oxide	183		
Polyphenelene sulfide	57		
Polysulfones	43		
N-Methyl-2-pyrrolidone	217		
- **Gaskets [kg/MW]**			
Polytetrafluoroethylene	13		
Graphite	72		
Acrylonitrile butadiene styrene	27		
Lubricating oil	0.1		
Aniline	8		
Acetic anhydride	9		
Terephtalic acid	15		
Nitric acid	6		
Hydrochloric acid	22		
- **Others [kg/MW]**			
Calendered rigid plastic	130		
Decarbonized water	1,833		
Deionized water	14,333		

4.1.4 Environmental impacts

The environmental impact indicators Climate Change and Resource Use of the AEL are shown in Figure 34. The level of the environmental impact Climate Change decreases continuously by a total of 20% from 2020 to 2050, which is almost exclusively due to a lower demand for nickel and electrical energy. Moreover, these two factors contribute significantly to the environmental impact both in 2020 and 2050 (nickel 65% / 76%, 2020 / 2050; electricity 22% / 6%). In both 2020 and 2050, copper contributes to almost 99% of the environmental impact.

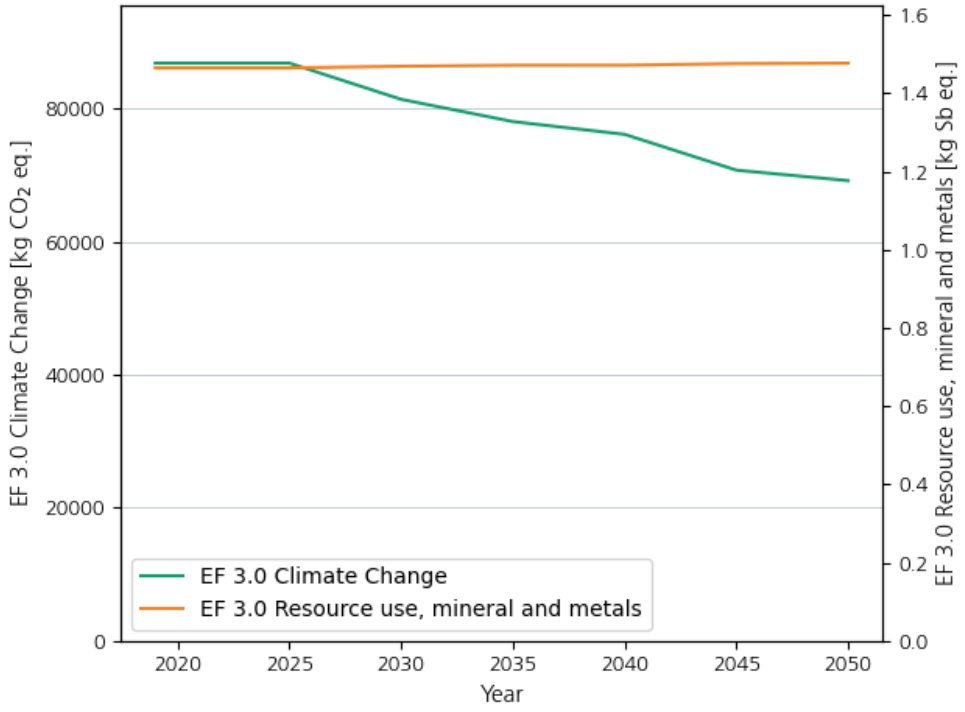


Fig. 34 Environmental impacts of AEL per MW of installed capacity.

Figure 35 shows the contribution of the various elements to the environmental impact of Resource Use. This increases slightly for the elements used between 2020 and 2050 (1 to 7%), with the exception of nickel, for which a reduction of 6% can be observed. This has an insignificant influence on the relative shares of the environmental impact, as shown in the graph.

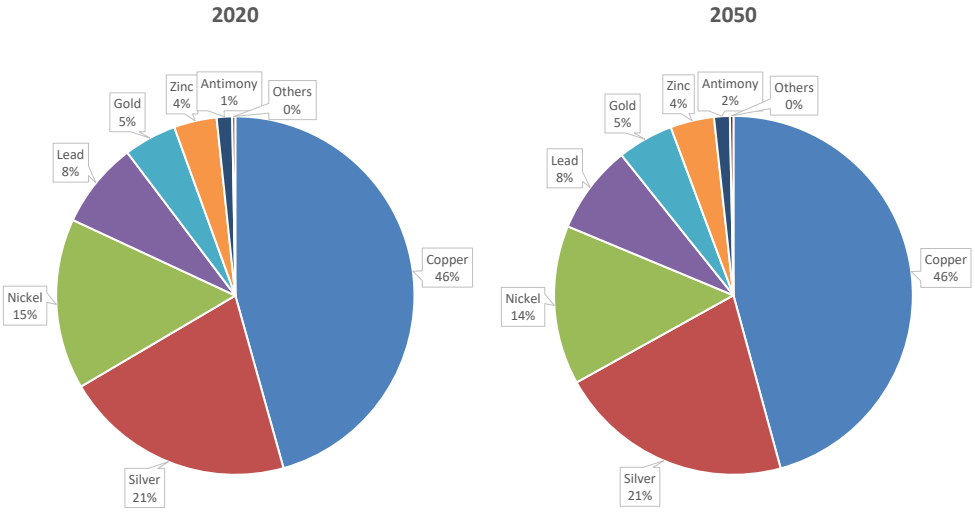


Fig. 35 Contribution of the different elements to the Resource Use of the AEL per MW installed capacity.

5 Battery

5.1 VRFB – Vanadium Redox Flow Battery

5.1.1 Description

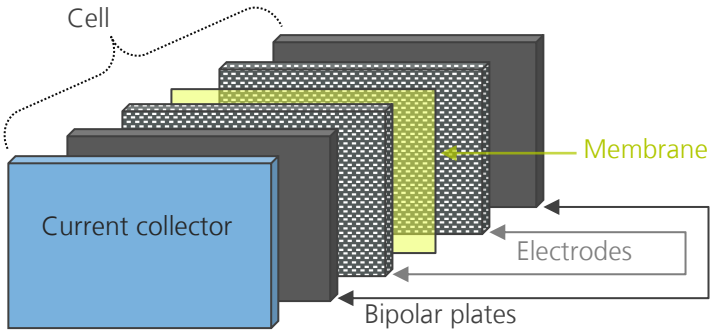


Fig. 36 Schematic representation of a VRF cell (Minke, 2016).

Redox flow batteries are mainly used as stationary storage technology at the grid operator level. The second largest end-users are commercial and industrial applications of electrical storage.

System boundaries

- Stack
- Battery management system (BMS)

Parameters for Life cycle Analysis (LCA)

- Production location of VRFB: Germany
- VRFB service lifetime: 20 years

Technical parameters

Tab. 79 VRFB properties (Abbas et al., 2020; Kim, 2019; Nadeem et al., 2019)

	Reference value 2019
Energy density [gravimetric] [Wh/kg]	20-70
Energy density [volumetric] [kWh/m³]	25-35
Power density [gravimetric] [W/kg]	20-150
Full cycle number [pcs.]	13,000-20,000
Self-discharge [%]	1%/a
Operating temperature [C°]	0 bis +40
Efficiency (DC-DC) [%]	70-80

5.1.2 Material efficiency

Increase of the power density

The improvement of battery performances has been the primary focus of R&D activities. An increase in power density from 80 mW/cm² today to 100-120 mW/cm² in the future

is therefore assumed (Thielmann et al., 2017). A material demand reduction of 4.57% annually is further derived from the assumed energy density increase from 10 Wh/kg in 2019 to 40 Wh/kg in 2050. As VRFB is still a relatively young technology, the annual material improvement rates of 4.6% are assumed only until 2030, as research progress will be concentrated on this period and development beyond this is not yet foreseeable.

5.1.3 Material composition

The material composition of a VRFB until 2050 is shown hereafter. Metals are the focus of the present analysis. When available, data on other materials are provided as well as they remain relevant for the Life Cycle Analysis (LCA).

Tab. 80 Projected built-in material demand for VRFB, under consideration of material efficiency measures. The composition is assumed constant unless stated otherwise. Based on (Minke, 2016; UBA, 2016)

	2018	2020	2025	2030	2035	2040	2045	2050
Electrolyte [kg/kWh]								
Vanadium	1.95	1.77	1.40	1.11	1.11	1.11	1.11	1.11
Vanadium Pentoxide	6.68	6.09	4.82	3.81	3.81	3.81	3.81	3.81
Sulfuric acid	0.90	0.82	0.65	0.51	0.51	0.51	0.51	0.51
Phosphoric acid	0.0006	0.0005	0.0004	0.0003	0.0003	0.0003	0.0003	0.0003
Electrode [kg/kWh]								
Carbon felt	0.05	0.05	0.04	0.03	0.03	0.03	0.03	0.03
Stack [kg/kWh]								
Bipolar plate								
Graphite	0.58	0.53	0.42	0.33	0.33	0.33	0.33	0.33
Membrane								
Nafion®	0.02	0.02	0.01	0.01	0.01	0.01	0.01	0.01
Conductor								
Copper	0.24	0.22	0.17	0.14	0.14	0.14	0.14	0.14
Gasket								
FKM	0.05							
Stack housing								
Steel	0.15	0.14	0.11	0.09	0.09	0.09	0.09	0.09
Cell housing [kg/kWh]								
PVC	0.04							
Tank [kg/kWh]								
Glass fibre	3.93							
Pumps [kg/kWh]								
Plastic coated steel	0.07	0.06	0.05	0.04	0.04	0.04	0.04	0.04
Pipes [kg/kWh]								
Teflon® coated steel	0.04	0.04	0.03	0.02	0.02	0.02	0.02	0.02
Inverter [kg/kWh]								
Copper	0.34	0.31	0.24	0.19	0.19	0.19	0.19	0.19
PVC	0.02							
Cable [kg/kWh]								
Copper	0.02	0.02	0.02	0.01	0.01	0.01	0.01	0.01

Heat exchanger [kg/kWh]								
Stainless steel	0.27	0.25	0.19	0.15	0.15	0.15	0.15	0.15
Process control system (PCS) / BMS [kg/kWh]								
Aluminium	0.077	0.077	0.077	0.077	0.077	0.077	0.077	0.077
Iron	0.020	0.020	0.020	0.020	0.020	0.020	0.020	0.020
Copper	0.009	0.009	0.009	0.009	0.009	0.009	0.009	0.009
Silicone	0.016	0.016	0.016	0.016	0.016	0.016	0.016	0.016
Glass fibre	0.006	0.006	0.006	0.006	0.006	0.006	0.006	0.006
Epoxy resin	0.005	0.005	0.005	0.005	0.005	0.005	0.005	0.005
Plastic	0.006	0.006	0.006	0.006	0.006	0.006	0.006	0.006

5.1.4 Environmental impacts

The environmental impact indicators Climate Change and Resource Use of a VRF battery are shown in Figure 37. While the level of environmental impacts for Climate Change decreases by more than 40% between 2018 and 2030, which is explained by lower amounts of vanadium used, the relative contribution of vanadium to the indicator remains almost identical at approx. 95%. Between 2030 and 2050, there is no further reduction in the share of vanadium or other materials used, since, as described above, the development beyond 2030 is not yet foreseeable.

A similar picture emerges for the Resource Use indicator. By 2030, the environmental impact decreases by approx. 40%, before it remains constant from then on for the reason mentioned above. During the entire period under consideration, almost 92% of the environmental impact is attributable to the copper used in the inverter and stack.

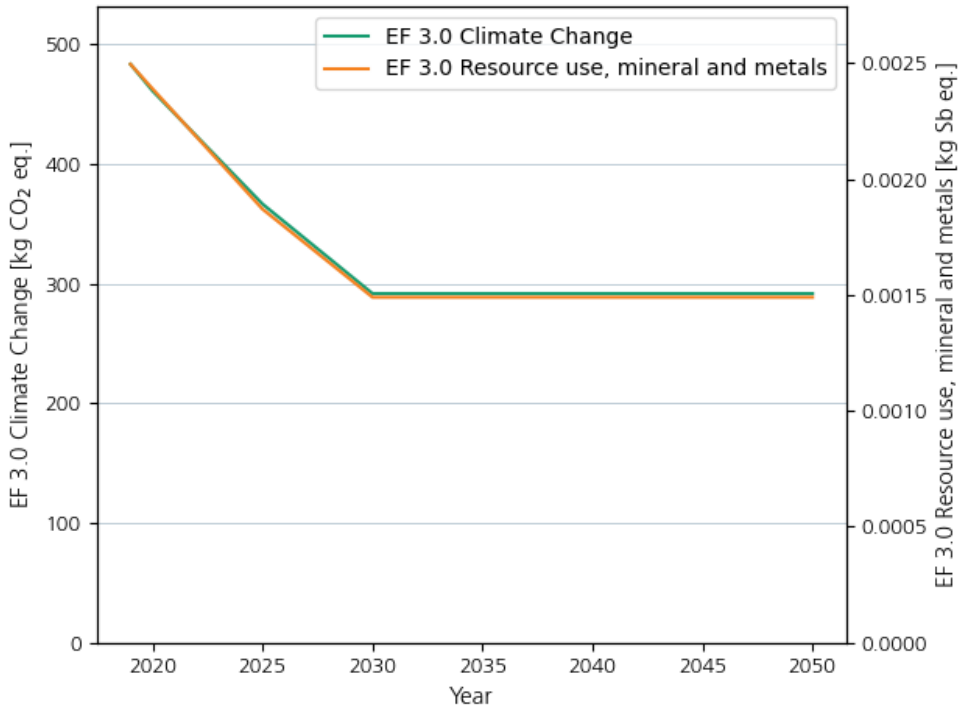


Fig. 37 Environmental impact of the VRF battery per kWh of storage capacity.

Figure 38 shows the contribution of the different elements to the indicator Resource Use. The relative share of all elements in the environmental impact remains almost the same, while their absolute share decreases to 62 to 64%.

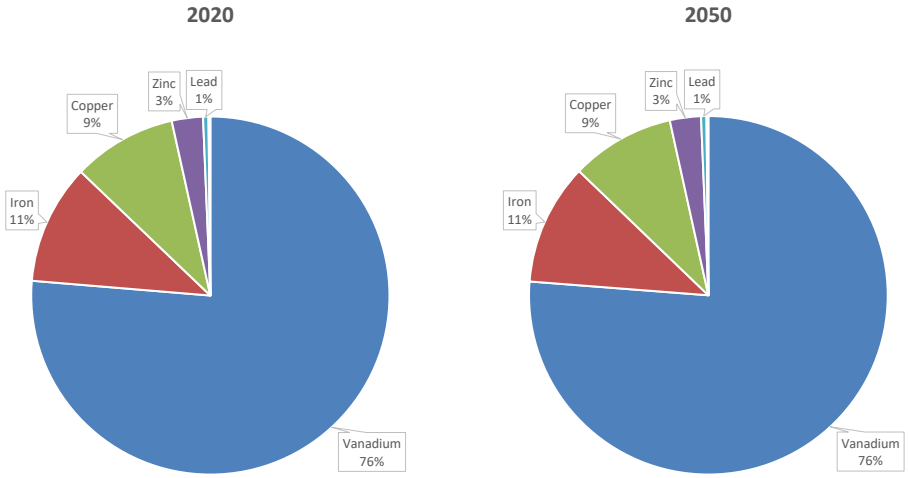


Fig. 38 Contribution of the different elements to Resource Use in the VRF battery.

5.2 NMC – Nickel Manganese Cobalt Lithium-Ion Battery

5.2.1 Description

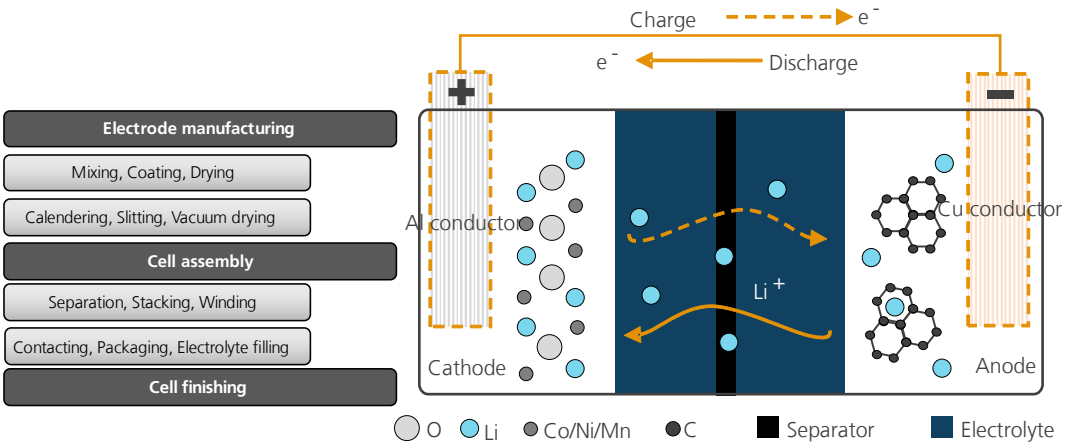


Fig. 39 Typical process flow (left) and schematic representation (right) of a Li-ion battery cell (RWTH Aachen and VDMA, 2015; Stenzel et al., 2015).

System boundaries

- Battery cell (prismatic)
- Battery housing
- Battery management system (BMS)

Parameters for Life cycle Analysis (LCA)

- Production location of NMC: China
- NMC service lifetime: 5-20 years

Tab. 81 Energy demand by production step for a 40 Ah Li-ion cell using water-based electrode manufacturing processes. Based on (Pettinger and Dong, 2017; Thomitzek et al., 2019)

	Process energy for a 40 Ah-Cell (Wh/Wh)	Process energy for 113 cells in a 7,5 kWh-Pack (kWh)	Process energy for 1 kWh battery capacity (kWh/kWh)
Cells			
Slurry prep. cathode	11.3	9.6	1.3
Slurry prep. anode	11.3	9.6	1.3
Anode coating (incl. solvent/water drying)	57.5	48.7	6.5
canode coating (incl. solvent/water drying)	90.5	76.7	10.2
Anode slitting	2.9	2.5	0.3
Cathode slitting	2.9	2.5	0.3
Anode calendering	28.5	24.2	3.2
Cathode calendering	28.5	24.2	3.2
Anode notching	21.9	18.5	2.5
Cathode notching	21.9	18.5	2.5
Cell assembly	57.2	48.5	6.5
Drying	57.2	48.5	6.5
Filling	14.8	12.5	1.7
Formation	27.3	23.2	3.1
End suction	4.1	3.5	0.5
Cell total	437.8	371.2	49.5
Rack		5.1	5.1
Battery assembly		17.3	17.3
Inverter		8.7	8.7
Total		402.3	80.6

Technical parameters

Tab. 82 NMC properties (Shammugam, 2019)

	Reference value 2019
Energy density [gravimetric] [Wh/kg]	140-200
Energy density [volumetric] [Wh/l]	240-290
Power density [W/kg]	270-1,400
Full cycle number [pcs.]	3,000-10,000
Thermal runaway [°c]	210
Operating temperature [°c]	-40 bis +65
Efficiency [%]	95
Battery cost (Pack) [€/kWh]	200-410

5.2.2 Material efficiency

Increase of the power density

The improvement of battery performances has been the primary focus of R&D activities. An increase in gravimetric energy density from 235 Wh/kg today to 400 Wh/kg in the future can be expected (Meeus, 2018). Although the material requirement per kWh of a Li-ion battery is thus reduced, there is a technical lower limit to the material reduction. For lithium in Li-ion battery, this is around 70g per kWh (Kushnir and Sandén, 2012). Taking into account the energy density improvements and the technical material lower limit for lithium, an annual material efficiency improvement of the cell components of 1.73% is assumed.

Substitution of cobalt in the cathode

A material substitution of cobalt by nickel is expected in the next years. The proportion of cobalt will be successively reduced from a one-to-one ratio of nickel, manganese and cobalt (NMC 111) to 80% nickel, 10% manganese and 10% cobalt (NMC 811) (Bongartz et al., 2021). For reasons of data availability and current marketability, only NMC 611 is hereby considered.

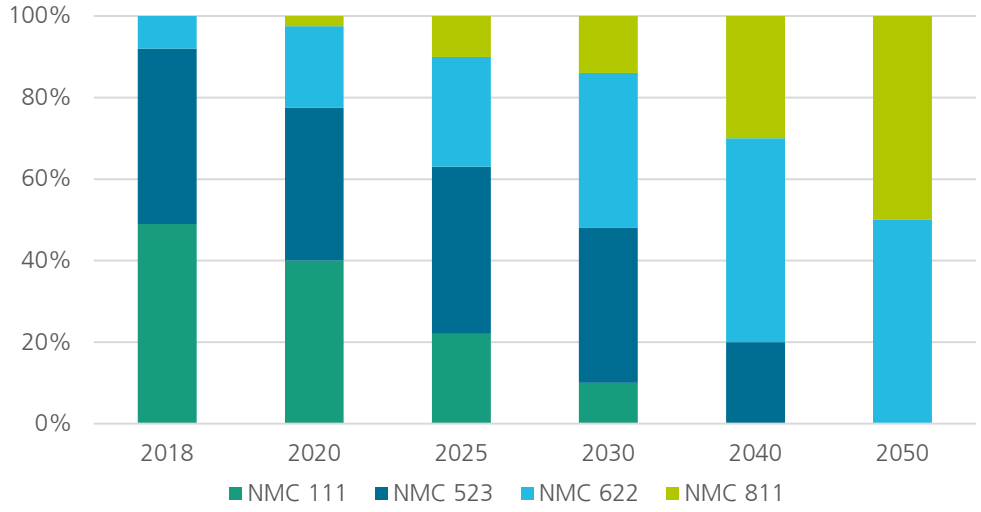


Fig. 40 Projected substitution of cobalt with nickel in NMC batteries, based on (Pillot, 2017).

Substitution measures not included

- Anode

The anode used in the NMC battery is typically made of graphite. Some studies project that anodes with a 5-10% silicon content will enter the market starting in 2020 (NPE, 2016).

- Electrolyte

The conducting salt lithium hexafluorophosphate (LiPF6) is the most commonly used electrolyte material. Although it could in principle also be replaced by lithium bisoxalatoborate, an electrolyte composition other than LiPF6 is not expected to establish (Buchert et al., 2019; UBA, 2016).

- Conductor film

The aluminium-based conductor foil could be replaced by copper. The disadvantage of the higher weight of copper could be compensated by its better conductivity (Buchert et al., 2019; Graedel and Nassar, 2015).

- Cell housing

The standard material for the cell housing is aluminium. Due to the low weight of aluminium, no substitution is expected.

- Separator

No material substitution of the separator consisting of polypropylene and polyethylene is known (UBA, 2016).

5.2.3 Material composition

The material composition of an NMC 622 until 2050 is shown hereafter. Electrolytes typically consist of lithium hexafluorophosphate (LiPF6) dissolved in mixed carbonate solvents selected from ethylene carbonate (EC), propylene carbonate (PC), ethyl methyl carbonate (EMC), dimethyl carbonate (DMC), and diethyl carbonate (DEC). An electrolyte system with LiPF6 in a weight ratio of 3:7 of EC and DEC as solvents with addition of vinylene carbonate as additive is hereby used (Qian et al., 2019). Metals are the focus of the present analysis. When available, data on other materials are provided as well as they remain relevant for the Life Cycle Analysis (LCA).

Tab. 83 Projected built-in material composition of NMC 622 battery cells, under consideration of material efficiency measures. The composition is assumed constant unless stated otherwise. Based on (ANL, 2018; Bongartz et al., 2021; Buchert et al., 2011; Marscheider-Weidemann et al., 2016; Olivetti et al., 2017; Pertti, 2017; Reuter et al., 2014; Thielmann et al., 2015; UBA, 2016)

	2018	2020	2025	2030	2035	2040	2045	2050
Cathode [kg/kWh]								
Lithium	0.13	0.12	0.11	0.1	0.09	0.09	0.08	0.07
Manganese	0.2	0.19	0.18	0.16	0.15	0.14	0.12	0.11
Cobalt	0.21	0.2	0.18	0.17	0.15	0.14	0.13	0.12
Nickel	0.63	0.61	0.56	0.51	0.47	0.43	0.39	0.36
Aluminium (conductor foil)	0.83	0.8	0.74	0.67	0.62	0.57	0.52	0.48
Binder (Polyvinylidene fluoride - PVDF)	0.35							
Anode [kg/kWh]								
Graphite	1.28	1.23	1.13	1.03	0.95	0.87	0.8	0.73
Copper (conductor foil)	0.46	0.44	0.4	0.37	0.34	0.31	0.28	0.26
Binder (Polyvinylidene fluoride - PVDF)	0.1							

Electrolyte [kg/kWh]								
Solvent	0.6							
Additive	0.001							
LiPF6	0.1							
Of which Lithium	0.005	0.004	0.004	0.004	0.003	0.003	0.003	0.003
Of which Phosphor	0.025							
Of which Fluorine	0.075							
Cell housing [kg/kWh]								
Aluminium	0.24	0.24	0.24	0.24	0.24	0.24	0.24	0.24
Separator [kg/kWh]								
Polyolefine (PO) membranes	0.1							

Tab. 84 Projected material composition of NMC Li-ion battery housing, based on (UBA, 2016)

	2018	2020	2025	2030	20335	2040	2045	2050
Cable [kg/kWh]								
Aluminium	0.016	0.016	0.016	0.016	0.016	0.016	0.016	0.016
Copper	0.15	0.15	0.15	0.15	0.15	0.15	0.15	0.15
Stainless steel	0.083	0.083	0.083	0.083	0.083	0.083	0.083	0.083
Frame [kg/kWh]								
Plastic	1.24							
Stainless steel	0.08	0.08	0.08	0.08	0.08	0.08	0.08	0.08
Housing [kg/kWh]								
Stainless steel	2.31	2.31	2.31	2.31	2.31	2.31	2.31	2.31

Tab. 85 Projected material composition of battery management system (BMS), based on (UBA, 2016)

	2018	2020	2025	2030	2035	2040	2045	2050
BMS [kg/kWh]								
Aluminium	0.23	0.23	0.23	0.23	0.23	0.23	0.23	0.23
Iron	0.060	0.060	0.060	0.060	0.060	0.060	0.060	0.060
Copper	0.026	0.026	0.026	0.026	0.026	0.026	0.026	0.026
Silicone	0.050	0.050	0.050	0.050	0.050	0.050	0.050	0.050
Glass fibre	0.018	0.018	0.018	0.018	0.018	0.018	0.018	0.018
Epoxy resin	0.014	0.014	0.014	0.014	0.014	0.014	0.014	0.014
Plastic	0.019	0.019	0.019	0.019	0.019	0.019	0.019	0.019

5.2.4 Environmental impacts

The environmental impact indicators Climate Change and Resource Use of the NMC cells are shown in Figure 41. The environmental impact of Climate Change decreases continuously from 2018 to 2050 to approximately 50%, which is primarily due to the lower contribution of electricity. In 2018, this is responsible for almost 40% of the environmental impact, followed by graphite (11%). In 2050, polyamide (18%) contributes most to Climate Change, followed by electricity (15%) and graphite (12%).

Resource consumption decreases constantly between 2018 and 2050 by a total of more than 30%. Copper accounts for the highest share with over 80% of the environmental impact, followed by cobalt with nearly 15 % during the period under review.

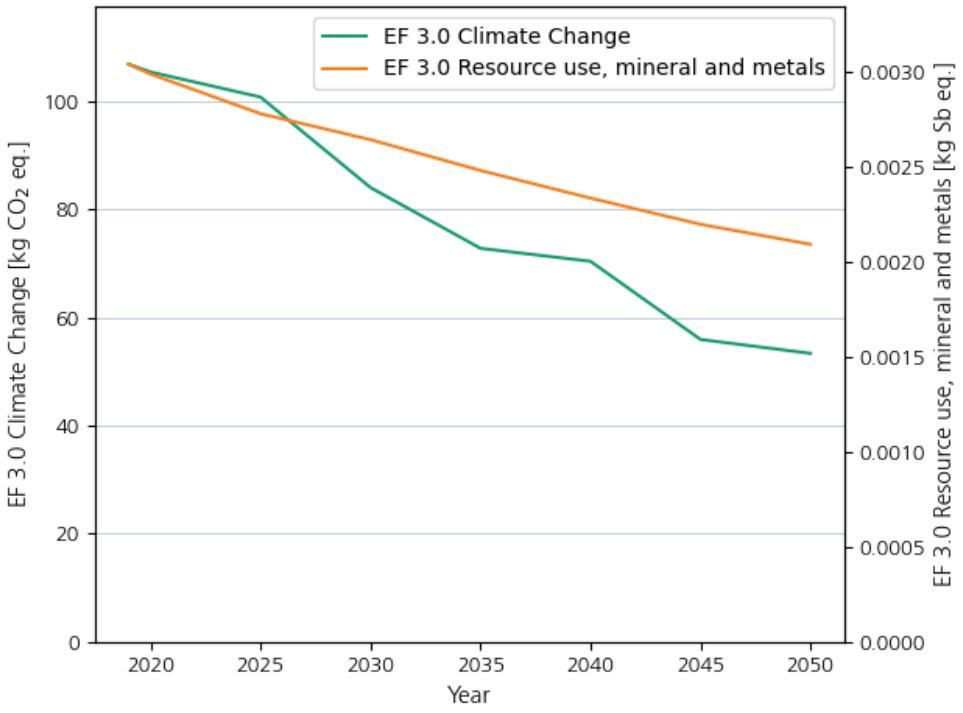


Fig. 41 Environmental impacts of the NMC cell per kWh of storage capacity.

Figure 42 shows the contribution of the different elements to Resource Use. The graphs indicate that the relative share of the elements used remains constant, as the absolute values decrease accordingly (approx. 30% for all metals shown, 40% for sulphur).

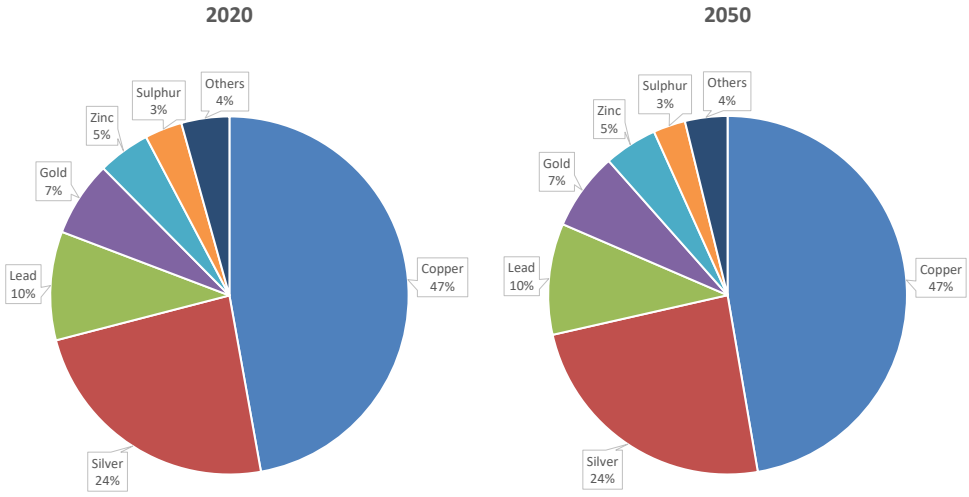


Fig. 42 Contribution of the different elements to Resource Use in the NMC cell.

6 Transmission grid

6.1 AC – Alternating Current Line

6.1.1 Description

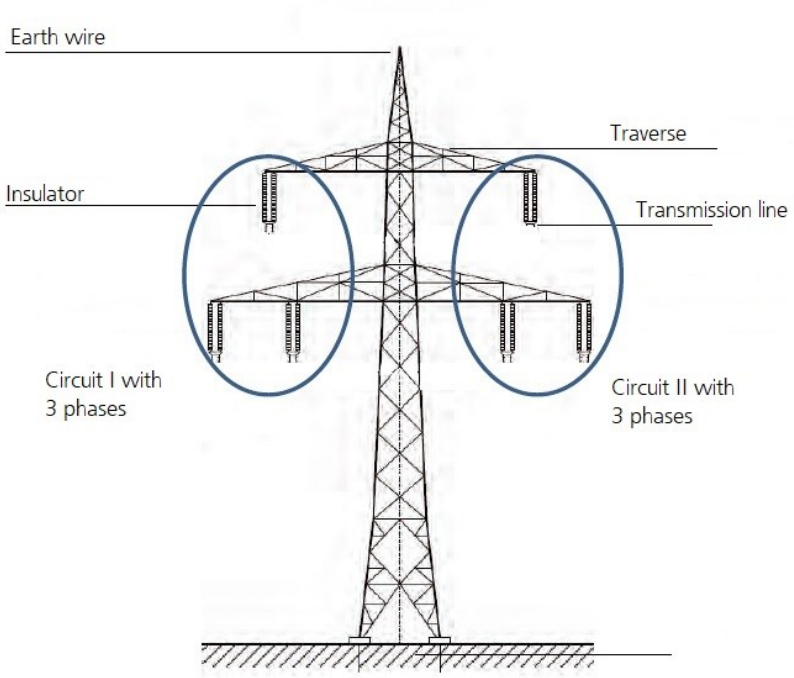


Fig. 43 Schematic representation of a transmission tower with 2 AC circuits, adapted from (Bundesnetzagentur, 2016).

The German transmission grid has a length of more than 35,000 km (system kilometers) and transports electricity at the highest voltage level up to 380 kV from power plants over long distances to the distribution grids in the regions. These "electricity highways" also connect the German power grid with those of neighbouring countries. Four transmission system operators, 50Hertz, Amprion, TenneT, and TransnetBW, are responsible for reliable and secure supra-regional power exchange. The transmission grid is mainly equipped with 380 kV alternating current. High-voltage power is transmitted almost exclusively via overhead lines (Leprich et al., 2011). The main reasons for this are the lower investment and maintenance costs of overhead lines compared to underground cables, as well as the ability of overhead lines to transmit high power, since the heat generated by the current flow can be easily dissipated to the surrounding air.

An overhead line pole carries at least 2 circuits, each of which includes three phases. Insulators made of porcelain, glass, or ceramic are suspended from the grounded pole to dissipate the high voltages of the cables from the pole. ACSR (Aluminum Conductor Steel Reinforced) overhead line cables are commonly used for this purpose. They consist of a steel core and an aluminium sheath, each with spirally wound individual wires. For the 380 kV voltage, a bundle of four ropes per phase is usually used.

System boundaries

- 380 kV AC circuits for overhead transmission lines

Parameters for Life cycle Analysis (LCA)

- Production location: Germany
- Service lifetime of conductor cables and insulators: 40 years

6.1.2 Material efficiency

Use of High Temperature Low Sag (HTLS) Conductors

HTLS have a core made of composite material or special steel alloys that cause less sag as conductor temperatures increase, thus exhibiting 50 to 100% higher transmission capacity (Ropenus et al., 2018). Materials for HTLS include STACIR (Super Thermal Alloy Conductor Invar Reinforced), ACCC (Aluminium Conductor Composite Core), or GZTACSR (Gap-type Super Thermal Resistant Aluminium Alloy Conductor Steel Reinforced).

In Germany, HTLS are already in use. If one follows the grid development plan 2030, the further use of HTLS is only planned in isolated cases. The main reason for this is the associated higher costs. However, the grid expansion requirements of long-term energy scenarios (BMWi, 2017) are to be covered predominantly by replacing existing circuits with HTLS. Grid expansion with 380 kV HTLS AC circuits is therefore assumed from 2030 onwards.

Since the ACCC is currently one of the HTLS power conductors with the best overall performance (Chen, 2019), its material composition is considered. The HTLS consists of a hybrid core of carbon and glass fibres bonded in an epoxy resin matrix. The central carbon fibres are surrounded by boron-free glass fibres, which prevent corrosion between the carbon fibres and the aluminium. The aluminium strands conduct electricity. Because of the lightweight composite core, ACCC can contain about 28% more aluminium than the conventional ACSR for a comparable weight, enabling better conductivity (CTC Global, 2011).

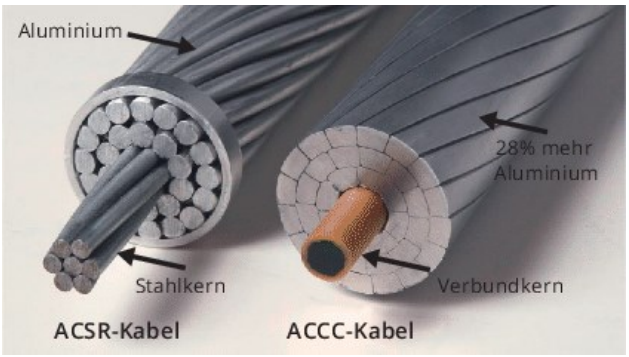


Fig. 44 ACSR line (left) with core of steel and ACCC line (right) with composite core and using 28% more aluminium (Wietschel et al., 2015).

The use of superconductors such as MgB2 and high-temperature superconductors in the transmission grid also offers promising properties such as higher performance and lower power losses (Thomas et al., 2016). Due to the current lack of commercial applications, superconductors for power transmission are not considered here.

6.1.3 Material composition

The material composition of a 380 kV AC circuit until 2050 is shown hereafter. Metals are the focus of the present analysis. When available, data on other materials are provided as well as they remain relevant for the Life Cycle Analysis (LCA).

Tab. 86 Projected material composition of a 380 kV AC circuit, under consideration of material efficiency measures. HTLS conductors are used from 2030 onwards. Based on (Jorge et al., 2012)

	2020-2030	2030-2050
AC circuit [kg/km]		
Steel	4,320	0
Aluminium	11,940	15,283
Mineral oil	378	0
Composite core	0	977

6.1.4 Environmental impacts

The environmental impacts of the AC grid are shown in Figure 45 using the indicators Climate Change and Resource Use. The level of environmental impacts remains constant until 2030 and then increases to 126% (Climate Change) and 190% (Resource Use) by 2035 compared to 2020. While the Climate Change indicator decreases marginally to 114% by 2050, the Resource Use indicator shows a further slight increase to 200%. On the one hand, the different material mixes before and after 2030 are responsible for these changes, as is the different high contribution of electricity to the respective environmental impact.

The largest contributions to the Climate Change indicator in 2020, 2035 and 2050 are made by electricity (58%, 55%, 50%) and aluminium (42%, 42%, 47%). The increases are primarily caused by a higher share of aluminium, which replaces steel and mineral oils from 2030 onwards.

A similar picture can be observed in the Resource Use. In the reference year 2020 and the comparison years 2035 and 2050, electricity accounts for the majority of the environmental impact (80%, 86%, 87%), followed by aluminium (19%, 13%, 12%).

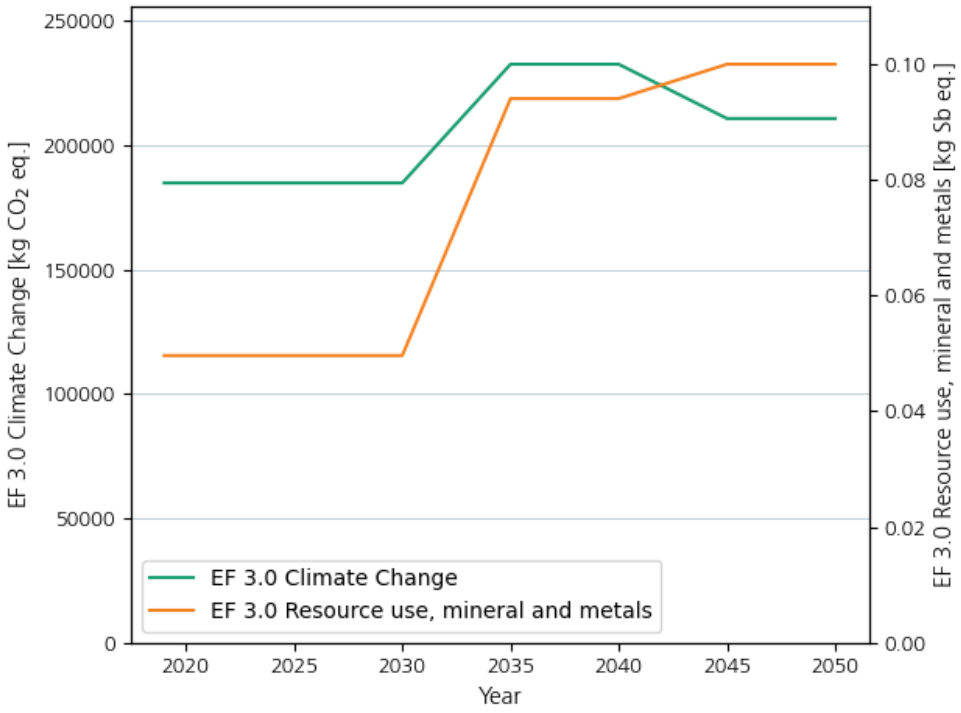


Fig. 45 Environmental impacts of the AC grid per km of installed power line.

Figure 46 shows the contribution of the different elements to the environmental impact Resource Use for the AC power grid. Between 2020 and 2050, the absolute amount of the mapped elements used increases between 150% (sulphur) and 230% (gold, copper, molybdenum), which has an impact on the composition of the relative shares in the percentage range.

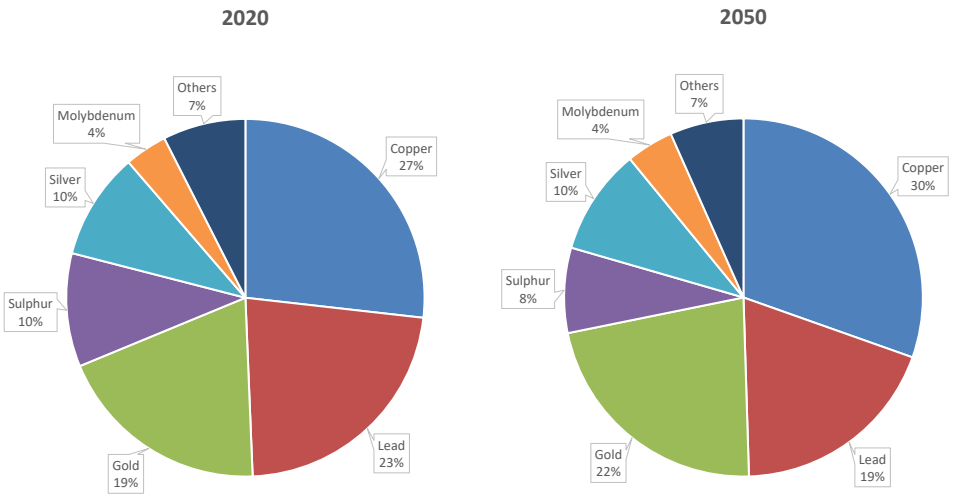


Fig. 46 Contribution of the different elements to the Resource Use of the AC grid per km of installed power line.

6.2 DC – Direct Current Line

6.2.1 Description

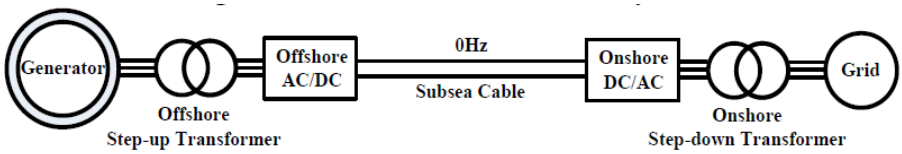


Fig. 47 Example of a transmission structure for an offshore wind farm (Xiang et al. 2016).

In Germany, electricity produced in the north of the country, e.g., from offshore wind farms, needs to be transported to the south, where electricity consumption is the highest. The existing grid, equipped with AC, does not provide the necessary capacity, which means that excessive amounts of energy are lost during transmission between long distances. High-voltage direct current (HVDC) transmission enables the lowest cable weight per MW transmission and low energy losses (NKT, 2017). HVDC lines can be used as an active network element to control power flows, thus providing more stability to the network (Hofmann and Lutz, 2015). Once the electricity has arrived at its destination, it is converted back to alternating current in converter stations, as only alternating current can be further converted to medium and low voltage.

Since 2016, according to the Federal Requirements Plan Act, direct current lines must be built primarily as underground cables instead of overhead lines. Submarine cables, which are used to transport electricity from offshore wind farms but also between countries, usually bridge very long distances in Germany and are also laid as HVDC cables. (Bundesamt für Seeschifffahrt und Hydrographie).

System boundaries

- High-voltage DC circuit for underground and submarine cables

Parameters for Life cycle Analysis (LCA)

- Production location: Germany
- Service lifetime of conductor cables and insulators: 40 years

6.2.2 Material efficiency

The use of superconductors such as MgB2 and high-temperature superconductors in the transmission grid offers promising properties such as higher performance and lower power losses (Thomas et al., 2016). Due to the current lack of commercial applications, superconductors for power transmission are not considered here.

6.2.3 Material composition

The material composition of a high-voltage DC circuit until 2050 is shown hereafter. The main difference between DC underground cables and submarine cables is the amount of steel required: steel armouring is used to mechanically protect the cables from damage, e.g., from ship anchors. The production of one kilometre of submarine cable thus requires 15,800 kg of steel against 3,400 kg of steel for an underground cable (Jorge et al., 2012).

The length of the submarine cables needed to expand the electricity grid is typically not known from energy scenarios. Based on the expansion of offshore wind energy in Germany, it is assumed that 15% of the total length of DC cables is required offshore. An average steel demand for HVDC is considered.

Metals are the focus of the present analysis. When available, data on other materials are provided as well as they remain relevant for the Life Cycle Analysis (LCA).

Tab. 87 Projected material composition of a high-voltage DC circuit for underground and submarine applications. Based on (Jorge et al., 2012)

	2020-2050
DC circuit [kg/km]	
Copper	14,700
Insulation (e.g. paper)	5,000
Mineral oil	3,900
Lead	14,200
Steel	5,260
Polyethylene	2,600

6.2.4 Environmental impacts

The environmental impact indicators Climate Change and Resource Use of the HVDC grid are shown in Figure 48. The level of the environmental impacts of Climate Change and Resource Use remains almost constant between 2020 and 2050 (minus 1% and plus 0.001%, respectively), as only the contribution of electricity to the environmental impact changes minimally. The largest contribution to the Climate Change indicator in the years 2020 and 2050 is made by copper (approx. 63%) and lead (21%).

A similar picture can be seen for Resource Use. In both 2020 and 2050, copper is responsible for approximately 65% of the environmental impacts, with the remaining impact mainly attributable to lead (35%).

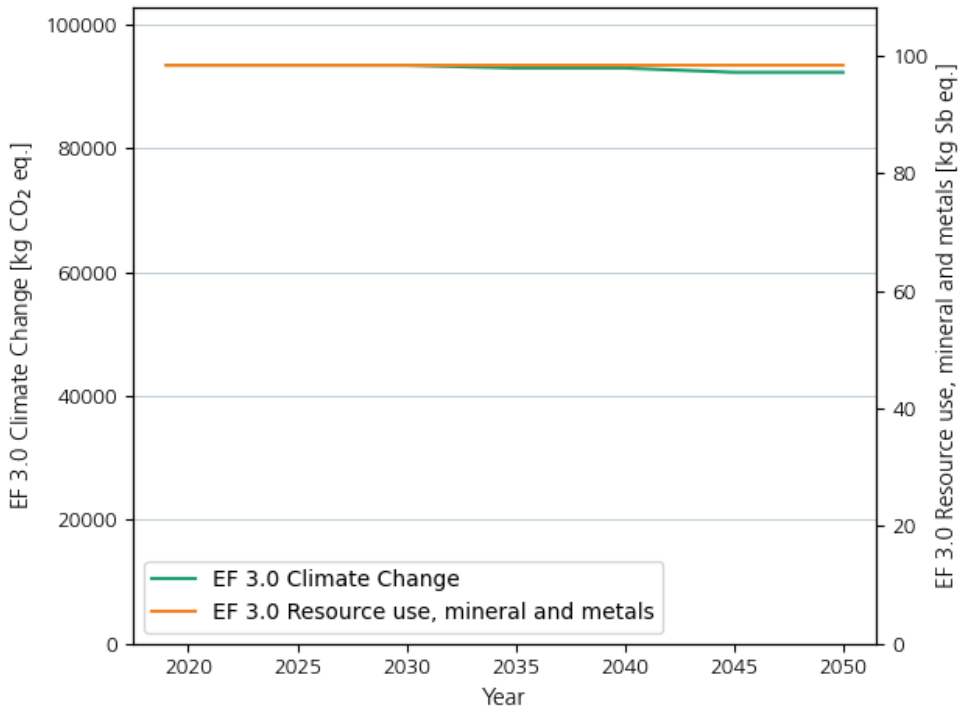


Fig. 48 Environmental impacts of the HVDC grid per km of installed power line.

Figure 49 shows the contribution of the different elements to the environmental impact of Resource Use in an HVDC power grid. Since the absolute amount of elements used

remains the same between 2020 and 2050, their relative contribution to the environmental impact does not change either.

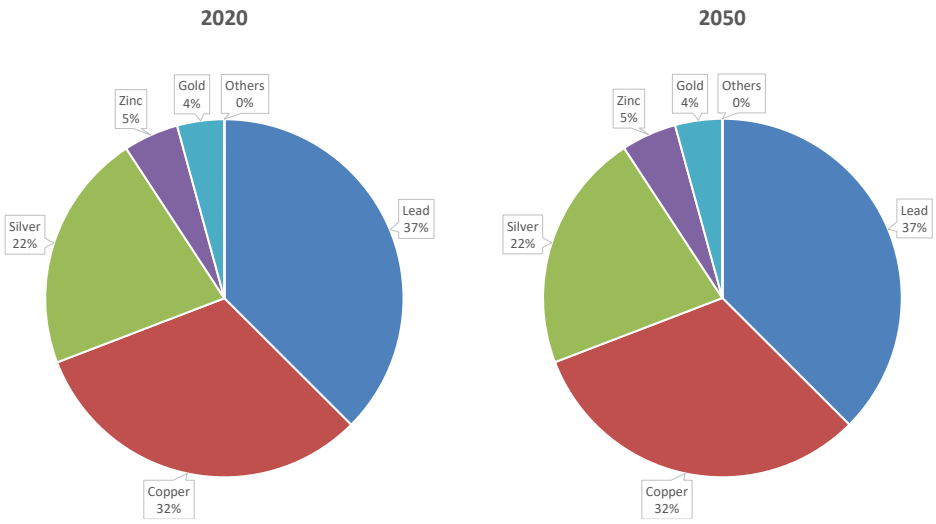


Fig. 49 Contribution of the different elements to the Resource Use of the HVDC grid per km of installed power line.

7 Combined Cycle Power Generation

7.1 NGCC – Natural Gas Combined Cycle System

7.1.1 Description

Gas and steam turbines are mainly made of steel alloys. Their material requirements are rarely investigated in the literature, as they are of less interest compared to technologies containing critical metals. Nonetheless, the efficiency of fossil fuel-fired power plants increases with operating temperature and pressure. Under these conditions, special alloying metals are added to bulk metals such as steel to improve thermal resistance, prevent corrosion, and prevent premature component wear (Dilthey, 2005).

Different types of steel are used in the construction of a NGCC plant. Although compositions might vary for each alloy type, a composition was chosen to represent each of these specific alloys.

Tab. 88 Composition of different steel alloys used in a NGCC (Georg Grimm Edelstahlhandel; PCC Energy Group, 2020; Steel Grades)

	Low alloy steel	**High alloy steel with chromium**	**High alloy steel with chromium-nickel**
	28NiCrMo4	X22CrMoV12	NiCr20Co18Ti
Al [%]			1.35
C [%]	0.24	0.24	0.03
Cr [%]	1.0	12.5	24.5
Co [%]			20
Fe [%]	97.04	83.47	51.02
Mn [%]	0.3	0.9	
Mo [%]	0.2	1.2	0.1
Nb [%]			1.5
Ni [%]	1.0	0.8	
P [%]	0.035	0.025	
S [%]	0.035	0.015	
Si [%]	0.15	0.5	0.15
Ti [%]			1.35
V [%]		0.35	

- Low alloy steel - 28NiCrMo4

Low alloy steel often contains less than 5% alloying element. The 28NiCrMo4 belongs to the heat resistant steels and can reduce the decarburization tendency, even at elevated temperatures, by forming resistant carbides. In addition to power plants, this steel is often used for mechanical components with larger cross-sectional dimensions such as missiles, weapons, and railroads (Bleck and Moeller, 2018).

- High alloy steel with chromium - X22CrMoV12

X22CrMoV12 is a standard steel for high-temperature components such as steam turbines (Schmidt, 2013). The addition of vanadium causes an increase in the elongation and creep rupture strength of this steel grade. In general, steam conditions of up to 610°C are achieved with steels containing about 12% chromium. By using coatings on Ni-chromium steel, it is possible to increase steam conditions to about 640°C.

- High alloy steel with chromium-nickel - NiCr20Co18Ti

This alloy was developed specifically for the power generation industry. With even higher chromium content than the X22CrMoV12, this alloy offers a significant improvement in resistance to high temperature corrosion mechanisms. The alloy was originally intended for use as boiler tubes in the superheater sections of plants but was then adapted for use as a material for steam headers (Moss et al., 2013). With niobium, aluminium, and titanium, the NiCr20Co18Ti alloy exhibits both high strength and good thermal stability (PCC Energy Group, 2020; Schmidt, 2013).

System boundaries

- Gas turbine
- Steam turbine
- Generator
- Heat recovery steam generator
- Condenser
- Piping, valves
- Electrical components (transformer, high-voltage switchgear, emergency power system, batteries)
- Civil engineering (construction and foundation)

Parameters for Life cycle Analysis (LCA)

- Production location: Germany
- NGCC service lifetime: 40 years

7.1.2 Material efficiency

Increase of the efficiency

The electrical efficiency of a NGCC plant is assumed to increase from 60.5% in 2020 to 65% by 2050. The specific material requirements are set to decrease linearly with the efficiency increase.

Tab. 89 Projected efficiency of an NGCC plant. Based on (Görner and Sauer, 2016; Kwon et al., 2019) and (expert council, personal communication, 2020)

	2020	2030	2040	2050
Efficiency [%]	60.5	62.0	63.5	65.0

7.1.3 Material composition

The material composition of a NGCC until 2050 is shown hereafter. Metals are the focus of the present analysis. When available, data on other materials are provided as well as they remain relevant for the Life Cycle Analysis (LCA).

Tab. 90 Projected material composition of a NGCC plant, under consideration of material efficiency measures. Based on (Parthey, 2010) and a reference power plant with 825 MWel nominal capacity (gas turbine SCC5-4000F, generator SGT5-4000F, steam turbine SGen5-3000W)

	2018	2020	2030	2040	2050
Gas turbine [kg/MWel]					
Steel	119.4	111.5	108.8	106.2	103.8
Low alloy steel - 28NiCrMo4	157.3	146.9	143.4	140.0	136.8
High alloy steel with Cr - X22CrMoV12	118.5	110.6	108.0	105.4	103.0

High alloy steel with Cr-Ni - NiCr20Co18Ti	165.3	154.3	150.6	147.1	143.7
Cast iron	167.0	156.0	152.2	148.6	145.2
Cu	0.7	0.6	0.6	0.6	0.6
Other metals	0.02	0.02	0.02	0.02	0.02
Inorganic materials, ceramics	1.3	1.2	1.2	1.2	1.1
Plastics	0.2	0.2	0.2	0.2	0.2
Other materials	0.04	0.04	0.04	0.04	0.04
Organic materials	3.0	2.8	2.7	2.6	2.6
Steam turbine [kg/MWel]					
Steel	815.7	761.7	743.3	725.8	709.0
Low alloy steel - 28NiCrMo4	8.4	7.8	7.7	7.5	7.3
High alloy steel	3.8	3.6	3.5	3.4	3.3
High alloy steel with Cr - X22CrMoV12	72.3	67.5	65.8	64.3	62.8
High alloy steel with Cr-Ni - NiCr20Co18Ti	139.2	130.0	126.9	123.9	121.0
Cast iron	209.8	195.9	191.2	186.7	182.3
Generator [kg/MWel]					
Steel	88.0	82.2	80.2	78.3	76.5
Low alloy steel - 28NiCrMo4	585.8	547.0	533.8	521.2	509.2
High alloy steel with Cr - X22CrMoV12	1.9	1.8	1.8	1.7	1.7
High alloy steel with Cr-Ni - NiCr20Co18Ti	22.1	20.7	20.2	19.7	19.2
Cast iron	10.4	9.7	9.4	9.2	9.0
Cu	111.1	103.8	101.3	98.9	96.6
Ceramics	1.6	1.5	1.5	1.5	1.4
Plastics	11.7	10.9	10.6	10.4	10.1
Other materials	8.7	8.2	8.0	7.8	7.6
Heat recovery steam generator [kg/MWel]					
Steel	8,578.9	8,011.7	7,817.9	7,633.2	7,457.1
High alloy steel with Cr - X22CrMoV12	2,327.3	2,173.4	2,120.8	2,070.7	2,022.9
Mineral fibres	327.8	306.1	298.7	291.6	284.9
Condenser [kg/MWel]					
Steel	0.2	0.2	0.2	0.2	0.2
High alloy steel with Cr-Ni - NiCr20Co18Ti	0.2	0.2	0.2	0.2	0.2
Piping and valves [kg/MWel]					
Steel	218.1	203.7	198.7	194.0	189.6
Low alloy steel - 28NiCrMo4	372.1	347.5	339.1	331.1	323.5
High alloy steel with Cr - X22CrMoV12	187.2	174.9	170.6	166.6	162.7
High alloy steel with Cr-Ni - NiCr20Co18Ti	82.1	76.6	74.8	73.0	71.3
Cu	0.01	0.01	0.01	0.01	0.01
Inorganic materials, ceramics	0.1	0.1	0.1	0.1	0.1
Plastics	60.5	56.5	55.1	53.8	52.6
Electrical components [kg/MWel]					
Steel	767.2	716.5	699.2	682.6	666.9
Cast iron	21.9	20.5	20.0	19.5	19.1
Cu	293.0	273.6	267.0	260.7	254.7
Inorganic materials, ceramics	46.9	43.8	42.8	41.8	40.8
Plastics	19.8	18.5	18.1	17.6	17.2
Wood	75.1	70.2	68.5	66.9	65.3
Civil engineering [kg/MWel]					
Iron	3,988.1	3,724.4	3,634.3	3,548.5	3,466.6
Cu	4.0	3.8	3.7	3.6	3.5
Inorganic materials, ceramics	12.3	11.5	11.2	11.0	10.7
Plastics	95.4	89.1	86.9	84.9	82.9
Organic materials	1.1	1.0	1.0	1.0	0.9
Concrete, mortar, plaster	93,056.9	86,904.3	84,801.8	82,798.6	80,887.9

Bitumen, asphalt	994.8	929.1	906.6	885.2	864.7
Gravel	2,387.9	2,230.0	2,176.1	2,124.6	2,075.6
Sand	5.4	5.0	4.9	4.8	4.7
Shuttering	0.3	0.3	0.3	0.3	0.3
Gypsum	0.9	0.8	0.8	0.8	0.8

7.1.4 Environmental impacts

The environmental impact indicators Climate Change and Resource Use of the NGCC power plant are shown in Figure 50. The environmental impacts of Climate Change and Resource Use decrease continuously by 10% and 7%, respectively, from 2020 to 2050, which is mainly due to a lower environmental impact of electricity and material efficiency measures. In 2020 and 2050, the largest contributions to the environmental impact of Climate Change are made by cement (25% / 28%), electricity (23% / 16%) and steam generation (18% each).

In terms of Resource Use, the main drivers in both 2020 and 2050 are copper (approx. 70%) and steam generation (14%) (half of which is attributable to the metals ferrochrome and molybdenum).

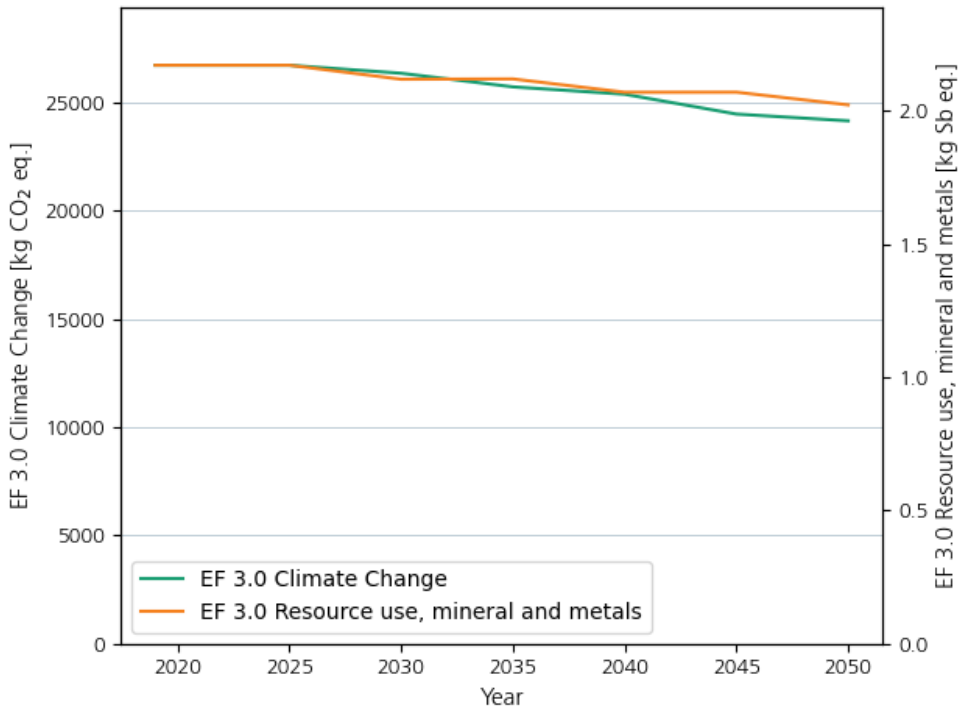


Fig. 50 Environmental impacts in a NGCC power plant per MW of installed capacity.

Figure 51 shows the contribution of the different elements to the Resource Use in NGCC power plants. Since a steady absolute reduction (7%) of the elements used can be observed between 2020 and 2050, their relative contribution to the environmental impact remains constant.

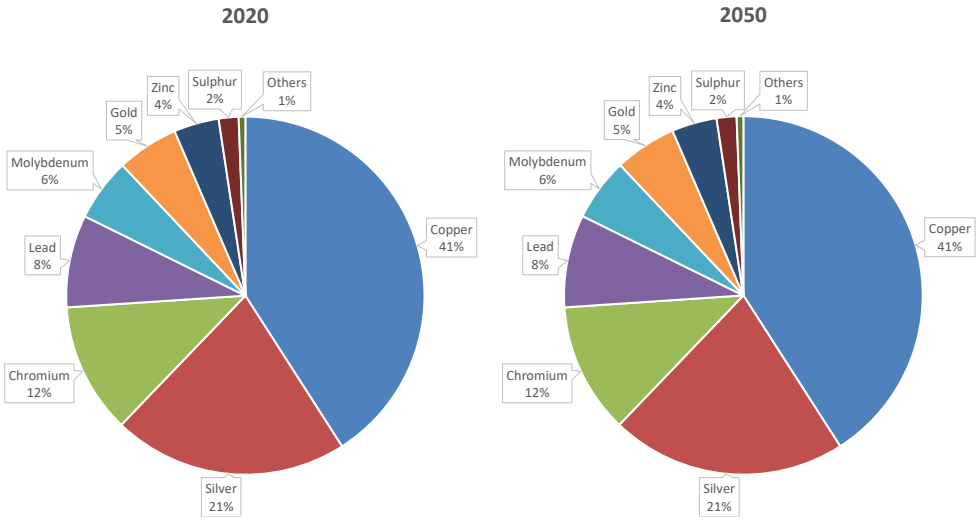


Fig. 51 Contribution of the different elements to Resource Use in a NGCC power plant.

8 Condensing boiler

8.1 Gas Condensing Boiler

8.1.1 Description

System boundaries

- Natural gas condensing boiler including water tank

Parameters for Life cycle Analysis (LCA)

- Production location: Germany
- Service lifetime: 20 years

Technical parameters

Tab. 91 Technical properties of the gas condensing boiler taken as reference for the material composition analysis (Vignali, 2017)

	Reference value
Electrical power [kWel]	0.12
Nominal heat input [kWth]	26.7
Minimum heat input [kWth]	3.2
Nominal heat output [kWth]	23.6
Minimum heat output [kWth]	3
Heating efficiency at 100% of nominal output [%]	108.1
Heating efficiency at 30% of nominal production [%]	102.1
Continuous supply capacity with ΔT 30°C [L/min]	12.9
Minimum pressure for sanitary hot water [bar]	0.3
Minimum hot water supply [L/min]	1.5
Weight of the boiler filled with water [kg]	42.4

8.1.2 Material efficiency

Gas condensing boilers were already identified by the European Commission in 2012 as the best available technology on the market, as they offer limited opportunities for efficiency improvements (Garcia Pardo et al., 2012). No material efficiency measure is therefore considered. The material composition is set constant over the years.

8.1.3 Material composition

The material composition of a gas condensing boiler until 2050 is shown hereafter. Metals are the focus of the present analysis. When available, data on other materials are provided as well as they remain relevant for the Life Cycle Analysis (LCA).

Tab. 92 Projected material composition of a gas condensing boiler. Based on (Vignali, 2017)

	2018 - 2050
Gas condensing boiler [g/kW]	
Silicone	4.9
EPDM	2.7
ABS	49.6
PVC	0.2
Al	80.7
Steel	969.4
High alloy steel	285.4
Brass	136.2
Cu	107.0
Electronics	10.5

8.1.4 Environmental impacts

The environmental impact indicators Climate Change and Resource Use of a gas condensing boiler are shown in Figure 52. Between 2020 and 2050, there is a minimal reduction in Climate Change of 3 percentage points, which is exclusively due to the lower share of electricity. The largest contribution to Climate Change during the period under consideration is made by steel with almost 40%, followed by stainless steel (24%) and electricity (approx. 10%).

The environmental impact of Resource Use hardly increases between 2020 and 2050 (0.02%). In 2020, as in 2050, over 80% is accounted for copper.

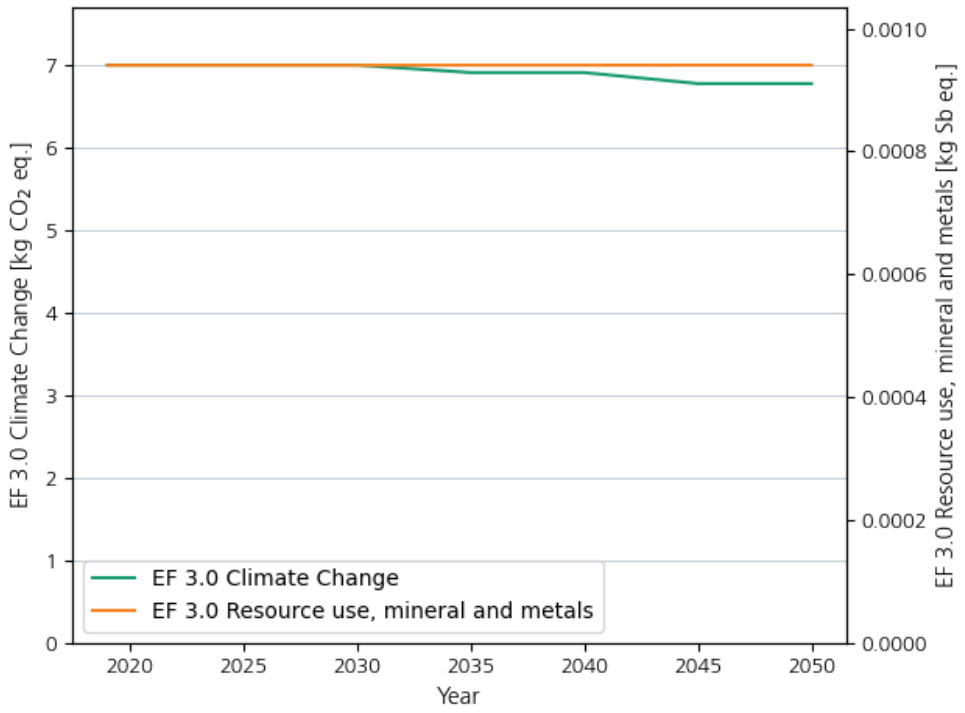


Fig. 52 Environmental impacts of the gas condensing boiler installation per MW of installed capacity.

Figure 53 shows the contribution of the various elements to the Resource Use indicator. Since no reduction in the elements used can be observed in absolute terms between 2020 and 2050, the relative contribution of the individual elements to the environmental impact also remains constant.

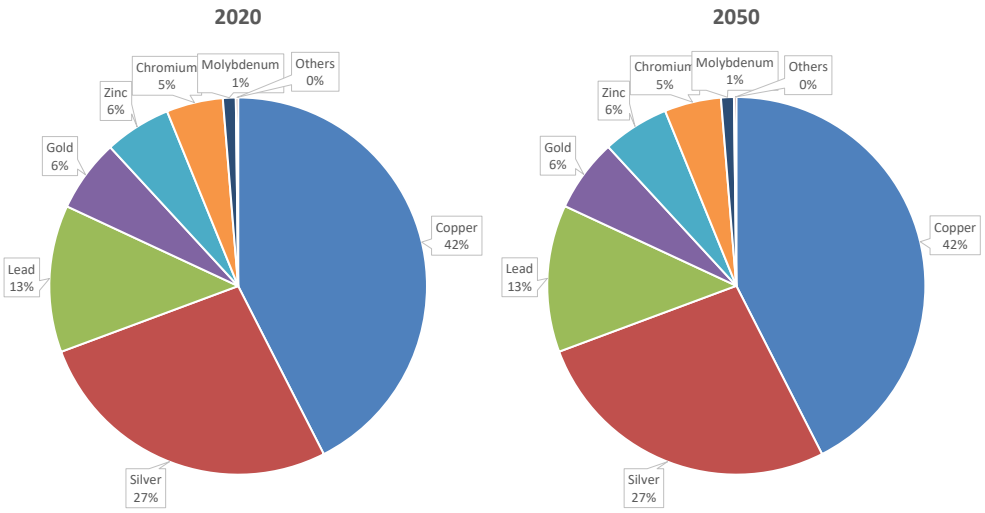


Fig. 53 Contribution of the various elements to Resource Use of the gas condensing boiler installation.

9 Heat Pump

9.1 AWHP – Air to Water Heat Pump

9.1.1 Description

Heat pumps are mainly made of steel and copper. Their material requirements are rarely investigated in the literature, as they are of less interest compared to technologies containing critical metals.

Tab. 93 Literature on the material composition of heat pumps (not exhaustive)

Source	(Shah et al., 2008)	(Johnson , 2011)	(Greening and Azapagic, 2012)	(Zheng et al., 2016)	(Huelman et al., 2016)	(Aquino et al., 2017)	(Lozano Miralles et al., 2018)
Heat pump type	Air-Air	Air-Water	Air-Water	Air-Air	Sole-Water	Sole-Water	Air-Air
Heating capacity [kWhth]	26.25	10	10	10.98	14	17	25
Electricity consumption [kWhel]	11.94	2.56	2.56	4.39	4.08	-	5.7

The Life cycle Analysis (LCA) of (Greening and Azapagic, 2012) shows a high level of detail on the material composition of an air-water heat pump. It is used as the reference material composition for 2018.

System boundaries

- Air to water heat pump system including air fan, evaporator, compressor, condenser, and refrigerant

Parameters for Life cycle Analysis (LCA)

- Production location: Germany
- Service lifetime: 20 years

9.1.2 Material efficiency

Increase of the heat pump performance

The development of the Coefficient of Performance (COP) and of the Seasonal Performance Factor (SPF) of heat pumps in Germany from 1993 to 2012 has been compiled by (Born et al., 2017) based on test results from accredited test centres. A simple extrapolation of these values results in a COP and an SPF value of 4.3 and 3.3 in 2019 and 5 and 3.8 in 2030, respectively – i.e., an increase of 1.2% until 2030. The assumptions for the development of the COP are within the forecast of (FfE, 2017). The maximum plant size is set to remain at 20 MW, with a lifetime of 20 years. Since no data is available beyond 2030, it is assumed that the COP and the SPF remain constant beyond 2030.

Following the COP and SPF increase trends, the material efficiency is assumed to increase linearly at a rate of 1.2%/a through 2030. No material efficiency measures are assumed after that.

9.1.3 Material composition

The material composition of an air-to-water heat pump system until 2050 is shown hereafter. Metals are the focus of the present analysis. When available, data on other materials are provided as well as they remain relevant for the Life Cycle Analysis (LCA).

Tab. 94 Projected material composition of an air-to-water heat pump system, under consideration of material efficiency measures. Based on (Greening and Azapagic, 2012)

	2020	2025	2030	2050
Condenser [kg/kWth]				
Low alloy steel	2.9	2.7	2.5	2.5
Copper	0.1	0.1	0.1	0.1
Evaporator [kg/kWth]				
Copper	1.6	1.5	1.4	1.4
Aluminium	0.4	0.4	0.3	0.3
Compressor [kg/kWth]				
Steel	3	2.7	1.5	1.5
Housing [kg/kWth]				
Erythropoetic Protoporphyrite (EPP)	8.5	6.7	5	5
Motor. wiring. Valve [kg/kWth]				
Copper	4.8	4.5	4.2	4.2
Insulation piping [kg/kWth]				
Elastomer	0.2	0.15	0.13	0.13
Air fan [kg/kWth]				
HDPE	0.1	0.1	0.1	0.1
Refrigerant R-134a [kg/kWth]	0.2	0.2	0.2	0.2
Electronics [kg/kWth]	0.2	0.2	0.2	0.2

9.1.4 Environmental impacts

The environmental impact indicators Climate Change and Resource Use of the heat pump system are shown in Figure 54. They decrease by 15 and 12% respectively between 2020 and 2030, which is due to the material efficiency measures. While the environmental impact of the Climate Change indicator continues to decrease slightly (2 percentage points) from 2030 to 2050, it remains constant for Resource Use. In 2020, the largest contribution to the Climate Change indicator is made by copper (approx. 55%) and stainless steel (18%). In 2050, the relative share of copper increases slightly to 59%, while the share of stainless steel remains unchanged. In terms of Resource Use, 98% of the environmental impact in 2020 and 2050 is accounted for by the copper used.

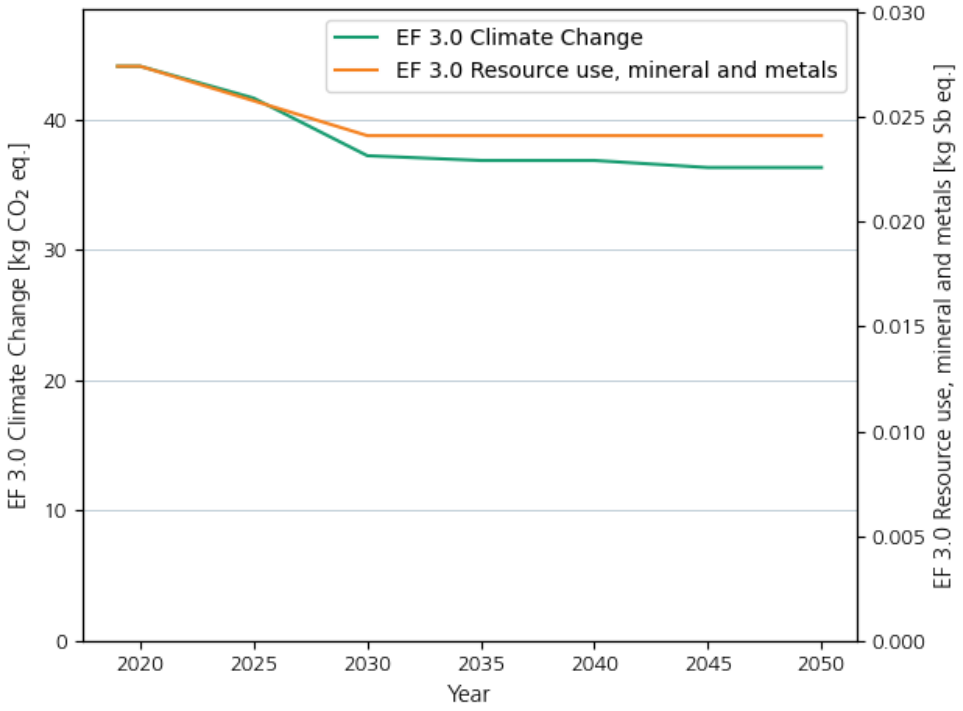


Fig. 54 Environmental impact of the heat pump system per kW of installed capacity.

Figure 55 shows the contribution of the different elements to the environmental impact of Resource Use for heat pumps. Since a constant absolute reduction of all elements considered can be observed between 2020 and 2050 (minus 12%), the relative contribution to the environmental impact remains constant.

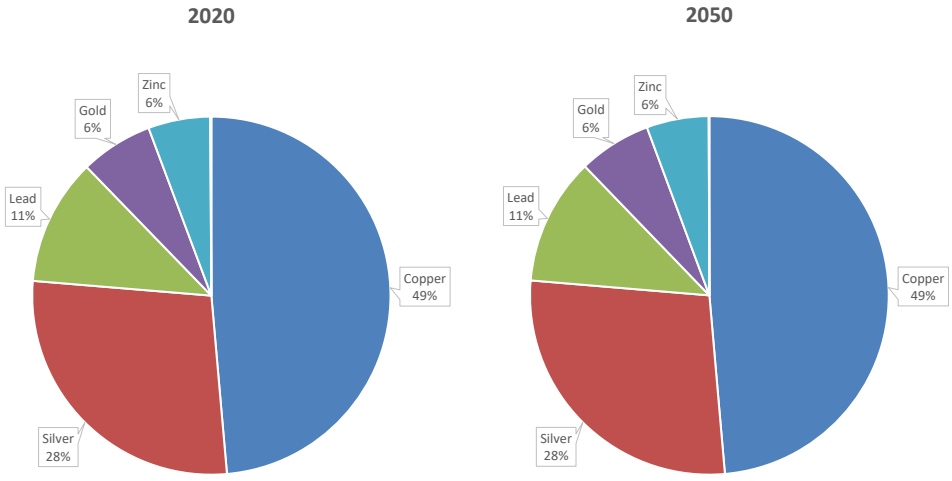


Fig. 55 Contribution of the different elements to Resource Use in the heat pump system.

1 0 Solar Thermal Power

10.1 Solar Flat Plate Collector

10.1.1 Description

The absorber – central component of the collector converting the solar radiation into heat – typically includes materials such as copper, aluminium sheet, or coated glass. The absorber is coated to distribute the solar radiation efficiently and to reduce radiation (BDH, 2011). Literature on the material composition of flat plate collectors for solar thermal systems is limited. This is probably because aluminium and copper are considered non-critical metals.

Tab. 95 Literature on the material composition of solar thermal systems (not exhaustive)

Source	(Altun-Çiftçioğlu et al., 2016)	(Stucki, Matthias: Jungbluth, Niels, 2012)	(Ardente et al., 2005)	(Greening and Azapagic, 2014)	(Carnevale et al., 2014)
Type of solar thermal system	Flat plate	Flat plate	Flat plate	Flat plate	Flat plate
Size [m²]	4	5	2,13	4	2,13
Absorber [kg/m²]					
Alloyed Steel				32.00	
Galvanised steel			15.92		15.92
Solar glass			4.93	9.12	4.93
Aluminium					
Copper	2.00	1.61	3.85	2.82	3.63
Sheet rolling				2.82	
Heat transfer medium [kg/m²]					
Propylene glycol	3.28	1.91		1.01	2.54
Frame [kg/m²]					
Stainless steel			2.86	4.14	2.86
Glass Wool					
Rock Wool				2.43	
Aluminium		1.60	1.88	3.93	1.88
Balance of System (i.e. piping, manifold, insulation) [kg/m²]					
Copper	2.00	1.60		8.00	
Elastomere		0.97		4.00	
Steel	2.00				

The Life cycle Analysis (LCA) of (Greening and Azapagic, 2014) shows a high level of detail on the material composition of a 2.8 kW capacity solar flat plate collector. It is used as the reference material composition.

System boundaries

- Flat plate collector system including pump, expansion tank, heat storage tank, heat transfer medium, and Balance of System (piping, manifold, insulation)

Parameters for Life cycle Analysis (LCA)

- Production location: Germany
- Service lifetime: 20 years

10.1.2 Material efficiency

No material efficiency measures are assumed for the solar thermal plant. A constant specific material composition is therefore considered until 2050.

10.1.3 Material composition

The material composition of a solar flat plate collector system until 2050 is shown hereafter. Metals are the focus of the present analysis. When available, data on other materials are provided as well as they remain relevant for the Life Cycle Analysis (LCA).

Tab. 96 Projected material composition of a solar flat plate collector system. Based on (Greening and Azapagic, 2014)

	2018 - 2050
Absorber [kg/kW]	
Cu	4.0
Low alloy steel	49.7
Low iron solar glass	13.0
Frame [kg/kW]	
Al	5.6
Mineral wool	3.5
Stainless steel	5.9
Heat transfer medium [kg/kW]	
Propylene glycol	1.4
Balance of System [kg/kW]	
Cu	2.86
Elastomer	1.43
Pump [kg/kW]	
Al	0.02
Cu	0.22
Cast iron	1.07
Stainless steel	0.82
Polyvinylchloride	0.03
Synthetic rubber	0.01
Expansion tank [kg/kW]	
Carboard	0.18
Low alloy steel	1.68
Butyl acrylate	0.25
Polypropylene	0.01
Hot water tank (250 L) [kg/kW]	
Glass wool	3.0
Low alloy steel	32.8
Stainless steel	6.0
Polyvinyl chloride	0.3

10.1.4 Environmental impacts

The environmental impact indicators Climate Change and Resource Use of the solar thermal power plant are shown in Figure 56. The level of the environmental impact of Climate Change remains constant until 2030 and then gradually decreases by a total of approx. 2.5% until 2050. This is solely due to a decreasing contribution of electricity; the contributions of the remaining products and processes remain unchanged. Over the entire period considered, steel (approx. 40%), aluminium (12%) and electricity (initially

10%, decreasing to 7% by 2050) account for the largest share of the environmental impact.

For Resource Use, there is a marginal increase (0.02%) in the environmental impact between 2020 and 2050, which is due to the higher impact of electricity. The main drivers in both 2020 and 2050 are copper (approx. 55%) and molybdenum (30%).

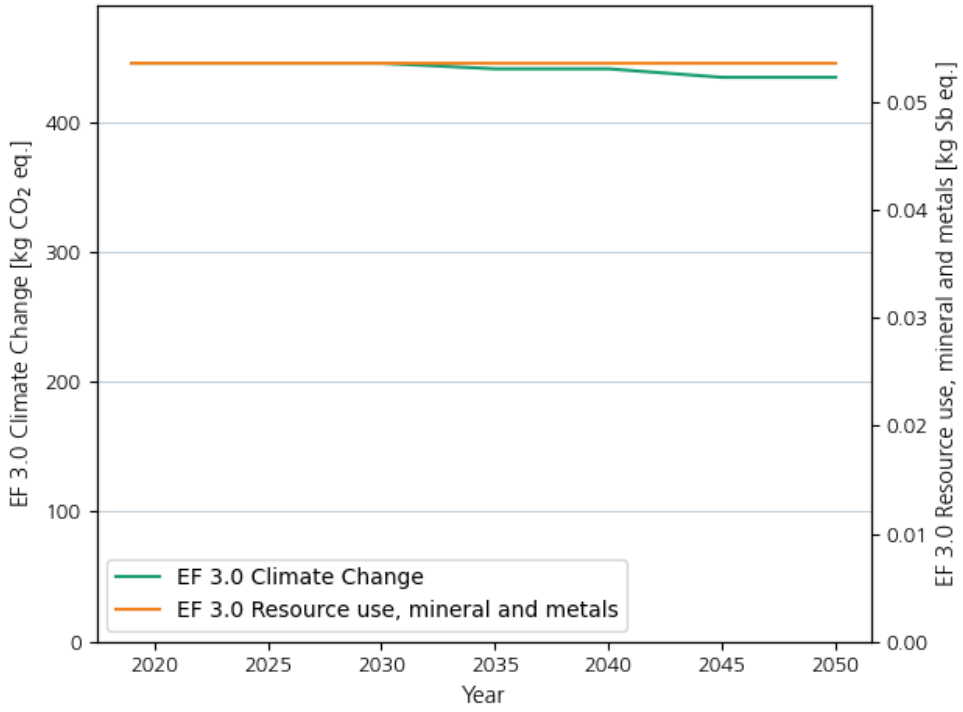


Fig. 56 Environmental impacts of solar thermal system per MW installed capacity.

Figure 57 shows the contribution of the different elements to the environmental impact of Resource Use in solar thermal power plants. Since no absolute change in the amount of elements used can be observed between 2020 and 2050, the relative contribution to the environmental impact remains constant.

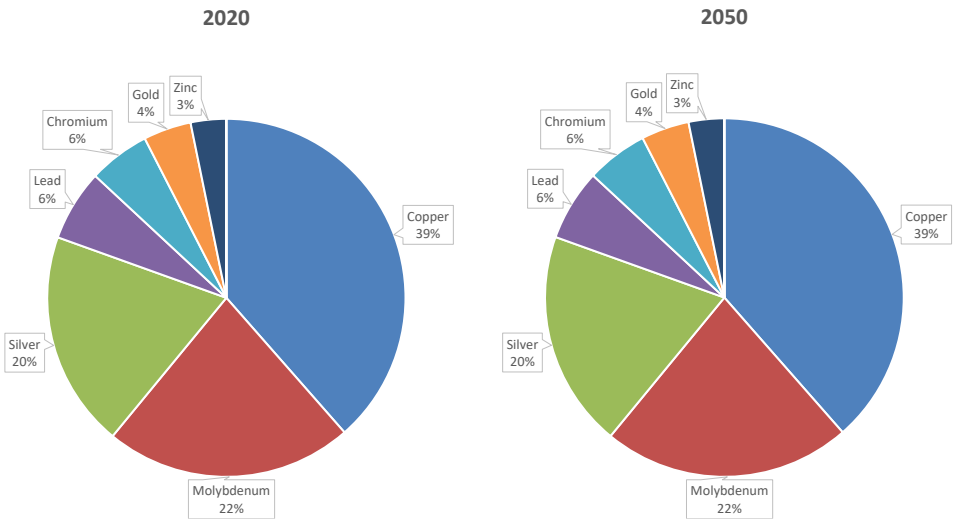


Fig. 57 Contribution of the different elements to Resource Use in solar thermal system.

1 1 Heat Storage

11.1 Hot Water Tank

11.1.1 Description

System boundaries

- Heat storage tank

Parameters for Life cycle Analysis (LCA)

- Production location: Germany

Technical parameters

Tab. 97 Technical properties of the heat storage tank taken as reference for the material composition analysis (Schmidt et al., 2003)

	Reference value
Water capacity [m³]	600
Internal diameter [m]	13
Height [m]	5
Maximum temperature [°C]	95
Operating temperatures [°C]	50-90

11.1.2 Material efficiency

No material efficiency measures are considered.

11.1.3 Material composition

The material composition of a heat storage tank until 2050 is shown hereafter. Metals are the focus of the present analysis. When available, data on other materials are provided as well as they remain relevant for the Life Cycle Analysis (LCA).

Tab. 98 Projected material composition of a heat storage tank. Based on (Schmidt et al., 2003)

	2018 - 2050
Heat tank [t/GWh]	
Stainless steel	238
Concrete	9,510
Mineral wool	103
Extruded polystyrene	64

11.1.4 Environmental impacts

The environmental impact indicators Climate Change and Resource Use of the heat storage tank are shown in Figure 58. The level of Climate Change and Resource Use remains almost constant between 2020 and 2050 (decrease of 0.8%). This change in the environmental impact is solely due to the contribution of electricity, as the environmental impact of the other processes and products remains unchanged. The

largest contribution to the Climate Change indicator is made by stainless steel (approx. 50%) and concrete (36%) during the entire period under review.

The slight change in the environmental impact of the Resource Use indicator (plus 0.04%) is also exclusively due to electricity. During the period under consideration, stainless steel was responsible for almost 100% of the environmental impacts.

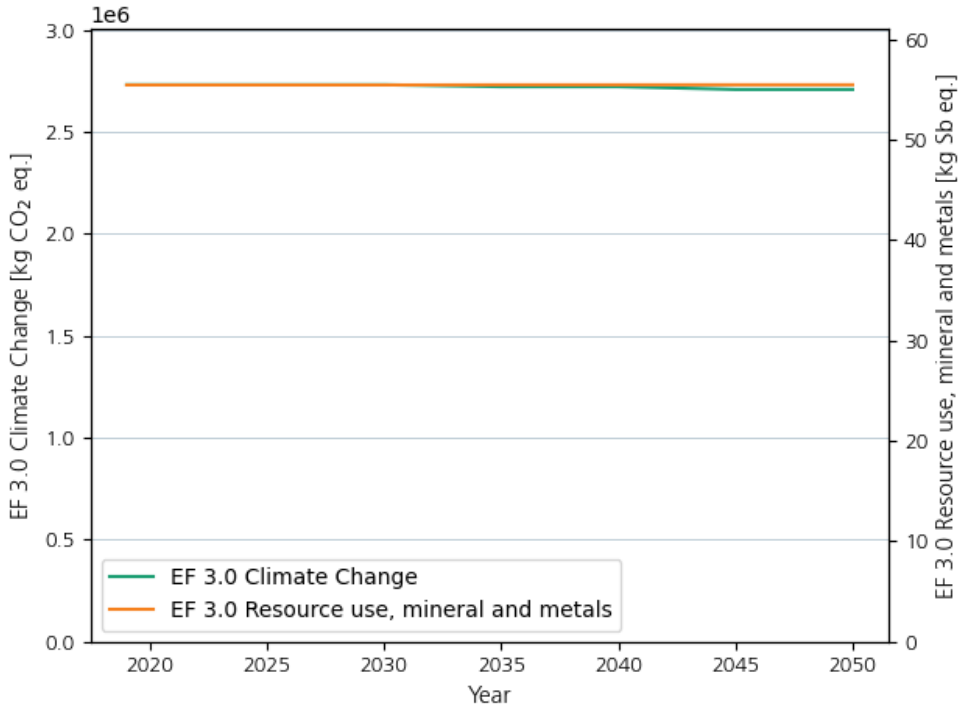


Fig. 58 Environmental impacts of the heat storage tank per GWh of storage capacity.

Figure 59 shows the contribution of the various elements to the environmental impact of Resource Use in a heat storage tank. Since the absolute quantity of the elements used remains almost unchanged between 2020 and 2050, their relative contribution to the environmental impact is also subject to relatively small fluctuations.

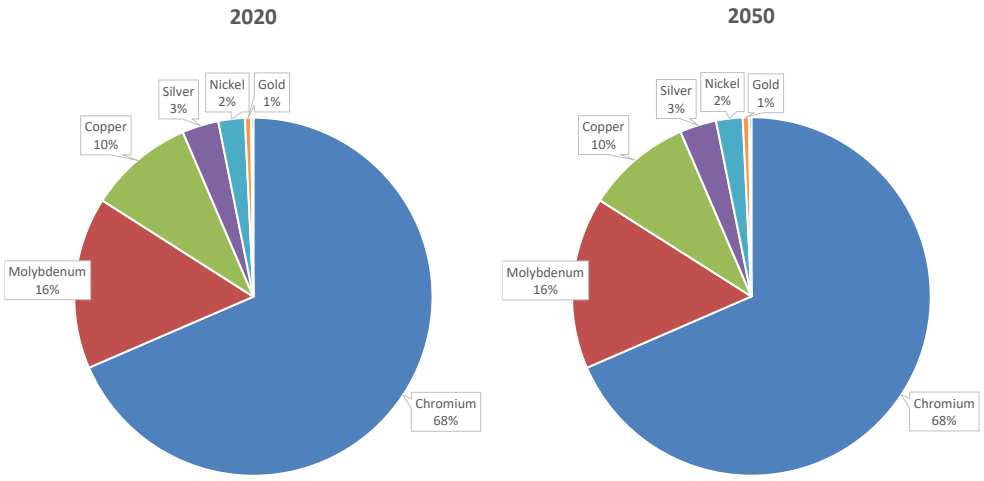


Fig. 59 Contribution of the different elements to the Resource Use of the heat storage tank per GWh of storage capacity.

1 2 Building Retrofitting

12.1 Insulation

12.1.1 Description

Building retrofitting is part of the strategies to achieve the transformation of the energy system, but is not a classic technology per se, rather a series of measures to achieve certain energy-related building values. Retrofitting measures always depend on the initial building situation or starting point before the retrofit.

Five different retrofit levels are hereby considered, based on data from (Fraunhofer ISE, 2020).

Tab. 99 Retrofit measures considered, based on (Fraunhofer ISE, 2020). The German renovation standards characterizing the retrofit levels are indicated in italics.

	Starting point	Target	Measure	Abbr.
Retrofit measure 1	Unrenovated *»Unsaniert« 2011*	Total retrofit *»Vollsaniert« nach EnEV*	Insulation	SAN1
Retrofit measure 2	New construction *„Neubau"*	Total retrofit *»Vollsaniert« nach EnEV*	Insulation	SAN2
Retrofit measure 3	Unrenovated *»Unsaniert« 2011*	Total retrofit, passive house standard *»Vollsaniert-Plus« Passivhaus-Standard*	Insulation	SAN3
Retrofit measure 4	New construction *„Neubau"*	Total retrofit, passive house standard *»Vollsaniert-Plus« Passivhaus-Standard*	Insulation	SAN4
Retrofit measure 5	New construction *„Neubau"*	Unrenovated *»Unsaniert« 2011*	Insulation	SAN5

The approach used to assume the building performance based on the renovation standard is shown hereafter.

Tab. 100 Approach to identify the building performances for each retrofit measure

	German renovation standard	Literature source
SAN1	EnEV2014	Type construction from (Loga et al., 2015)
SAN2	EnEV2014	Type construction from (Fingerling et al., 2000) and adaptation based on (EnEV, 2013)
SAN3	Passivhausstandard	Calculation of the U-values of the insulation layers based on the KfW 70 constructions (Loga et al., 2015). Adjustment to Passive House values via insulation layers thickness (Kaufman et al., 2004)
SAN4	Passivhausstandard	Type construction from (Fingerling et al., 2000)
SAN5	Unsaniert 2011 Standard	Type construction from (EnEV, 2013) und adjustment to the 2011 energy standard for buildings via layer thickness

Tab. 101 U-values for the different retrofit measures

	»Unsaniert« 2011	»Vollsaniert« nach EnEV	»Vollsaniert-Plus« Passivhaus-Standard
Roof/Storey ceiling – U [W/m²*K]	0.20	0.20	0.12
Exterior wall – U [W/m².K]	0.28	0.24	0.12
Window – U [W/m².K]	1.30	1.30	< 0.8
Floor – U [W/m².K]	0.35	0.35	0.184

System boundaries

- Insulation measures

Parameters for Life cycle Analysis (LCA)

- Production location: Germany

12.1.2 Material efficiency

No material efficiency measures are considered. Material efficiencies can only be achieved through material substitution (based on the building performance values). No clear trend is discernible here, which is why substitution has not been considered for insulation materials.

12.1.3 Material composition

The material composition for the different insulation measures until 2050 is shown hereafter based on the sources listed in Table 100. Metals are the focus of the present analysis. When available, data on other materials are provided as well as they remain relevant for the Life Cycle Analysis (LCA).

Tab. 102 Projected material composition of the different retrofit measures considered

Material	Unit	SAN1	SAN2	SAN3	SAN4	SAN5
Cement screed	kg/m²		329.28		28.81	329.28
Polystyrene	kg/m²	2.00	1.24	3.20	43.17	1.62
Concrete ceiling	kg/m²		276.60		138.55	276.60
Plasterboard	kg/m²	142.77	21.42	142.77	21.42	21.42
Mineral plaster	m²/m²	1.02	1.02	1.02	1.02	1.02
Lime sandstone	kg/m²		321.24		321.24	321.24
Lime plaster	kg/m²		9.18		9.18	9.18
Window glass	kg/m²	1.56	1.56	6.45	6.45	11.63
Window frame	kg/m²	14.57	14.57	14.57	14.57	14.57
Window	kg/m²	14.57	14.57	14.57	14.57	14.57

The demand for metallic elements used for retrofitting as built-in materials can further be decomposed as follows based on the inventory data from the LCA models:

Tab. 103 Assumed metal composition of the different retrofit measures considered

Material	Unit	SAN1	SAN2	SAN3	SAN4	SAN5
Fe	kg/m^2	17.73	44.81	17.73	31.29	44.81
Zn	kg/m^2	0.49	0.49	0.49	0.49	0.49

12.1.4 Environmental impacts

The environmental impacts for retrofit options are listed in Tables 114 and 115.

The impact on Climate Change is mainly driven by the production of the cement products and to a minor degree by the retrofitted windows. The reduction comes from the decarbonisation of the background database.

The impact on Resource Use is driven by silver and lead, used in the production of the windows.

1 3 Imports

13.1 Electricity imports

13.1.1 Description

Electricity imports to Germany induce an additional CO2 footprint. The source of these electricity imports by energy type is based on the reference scenario from (BMWi, 2017), with the share of hydropower in electricity generation from (Agora Energiewende and Sandbag, 2020).

Tab. 104 Projected electricity generation in Europe – Germany excluded – in TWh (Agora Energiewende and Sandbag, 2020; BMWi, 2017)

	2020	2030	2040	2050
Nuclear	811.8	613.3	490.0	382.4
Lignite	95.4	34.4	15.2	0.0
Hard coal	495.8	361.4	148.4	9.1
Natural gas	198.6	141.3	23.4	8.3
Wind onshore	449.7	1058.5	1684.2	2012.0
Wind offshore	123.4	126.4	118.7	117.2
Photovoltaics	162.1	315.3	484.5	541.7
Solar thermal	20.5	20.3	137.3	184.4
Biomass	301.7	299.7	284.8	281.2
Hydropower	390.2	387.6	363.9	359.3

System boundaries

- Electricity imports from Europe to Germany

13.1.2 Material efficiency

No material efficiency measures are considered.

13.1.3 Material composition

No physical materials are consumed directly.

13.1.4 Environmental impacts

The environmental impacts from electricity imports are calculated based on the following LCA processes from the GaBi database (Sphera, 2020):

- EU-28: Electricity from biomass (solid) ts
- EU-28: Electricity from hard coal ts
- EU-28: Electricity from hydro power ts
- EU-28: Electricity from lignite ts
- EU-28: Electricity from natural gas ts
- EU-28: Electricity from nuclear ts
- EU-28: Electricity from photovoltaic ts
- EU-28: Electricity from solar thermal ts

- EU-28: Electricity from wind power ts

Imports

The environmental impacts for the specific years from electricity are listed in Tables 114 and 115.

1 4 Material Composition of Alloys and Electronics

The material composition of alloys and electronics can be disaggregated by constituent element.

Tab. 105 Average composition of high alloy steel

	Fe	Ni	Cr
High alloy steel [%]	74	18	8

Tab. 106 Average composition of low alloy steel

	Fe	Cr	Ni	Mo
Low alloy steel [%]	97	1	1	1

Tab. 107 Average composition of low carbon steel

	Fe	C
Low carbon steel [%]	99.7	0.3

Tab. 108 Average composition of cast iron

	Fe	C	Si
Cast iron [%]	95	4	1

Tab. 109 Average composition of messing

	Cu	Zn
Messing [%]	60	40

Tab. 110 Average composition of low alloy steel 28NiCrMo4, e.g., used in Combined Cycle Power Plant (Steel Grades)

	C	Cr	Fe	Mn	Mo	Ni	P	S	Si
Low alloy steel [%] 28NiCrMo4	0.24	1	97.04	0.3	0.2	1	0.035	0.035	0.15

Tab. 111 Average composition of high alloy steel with Chromium X22CrMoV12, e.g., used in Combined Cycle Power Plant (Georg Grimm Edelstahlhandel)

	C	Cr	Fe	Mn	Mo	Ni	P	S	Si	V
High alloy steel with Cr [%] X22CrMoV12	0.24	12.5	83.47	0.9	1.2	0.8	0.025	0.015	0.5	0.35

Tab. 112 Average composition of high alloy steel with Chromium-Nickel NiCr20Co18Ti, e.g., used in Combined Cycle Power Plant (PCC Energy Group, 2020)

	Al	C	Cr	Co	Fe	Mo	Nb	Si	Ti
High alloy steel with Cr-Ni [%] NiCr20Co18Ti	1.35	0.03	24.5	20	51.02	0.1	1.5	0.15	1.35

Tab. 113 Average composition of a printed circuit board (PCB), e.g., used as a proxy for the material composition of electronics. Based on literature review by (Shammugam et al., 2019)

	Cu	Al	Pb	Zn	Ni	Fe	Sn	Cr	Ag	Au	Pt	Pa	Co	Ti
PCB [%]	21.4	3.5	2.3	1.5	1.8	3.7	3.4	0.4	0.001	0.005	0.0002	0.0002	0.005	0.005

1 5 Absolute numbers of environmental impacts by technology

Tab. 114 Environmental impact on Climate Change per technology [kg CO2 eq.]

Technology	Functional Unit	2020	2025	2030	2035	2040	2045	2050
PERC - Roof	MW	1,09E+06	1,00E+06	7,39E+05	5,70E+05	4,46E+05	2,78E+05	2,77E+05
PERC - Ground	MW	1,08E+06	9,94E+05	7,30E+05	5,61E+05	4,37E+05	2,69E+05	2,68E+05
SHJ - Roof	MW	1,30E+06	1,23E+06	9,36E+05	7,45E+05	5,86E+05	3,49E+05	3,30E+05
SHJ - Ground	MW	1,29E+06	1,22E+06	9,26E+05	7,36E+05	5,77E+05	3,40E+05	3,22E+05
CIGS - Roof	MW	6,78E+05	6,39E+05	3,49E+05	2,72E+05	2,59E+05	1,61E+05	1,54E+05
CIGS - Ground	MW	6,23E+05	5,88E+05	3,68E+05	2,90E+05	2,78E+05	1,78E+05	1,71E+05
III-V/Si – Roof	MW	1,23E+06	1,23E+06	1,23E+06	9,41E+05	8,33E+05	4,79E+05	4,63E+05
III-V/Si – Ground	MW	1,31E+06	1,31E+06	1,31E+06	9,96E+05	8,86E+05	4,97E+05	4,81E+05
EESG-DD Onshore	MW	4,09E+05	3,94E+05	4,93E+05	4,71E+05	4,71E+05	4,71E+05	4,71E+05
PMSD-DD Onshore	MW	4,41E+05	5,49E+05	6,89E+05	8,29E+05	8,29E+05	8,29E+05	8,27E+05
PMSD-DD Offshore	MW	3,42E+05	3,58E+05	3,95E+05	3,46E+05	3,93E+05	3,93E+05	3,91E+05
PMSG-MS Offshore	MW	2,93E+05	3,03E+05	3,16E+05	3,23E+05	3,63E+05	3,63E+05	3,62E+05
PEMFC	kW	8,98E+02	6,87E+02	4,40E+02	3,76E+02	3,18E+02	2,59E+02	2,24E+02
AEL	MW	8,68E+04	8,68E+04	8,14E+04	7,80E+04	7,61E+04	7,07E+04	6,91E+04
VRFB	kWh	4,61E+02	3,66E+02	2,92E+02	2,92E+02	2,92E+02	2,92E+02	2,92E+02
NMC	kWh	1,05E+02	1,01E+02	8,41E+01	7,28E+01	7,04E+01	5,59E+01	5,34E+01
AC	km	1,85E+05	1,85E+05	1,85E+05	2,33E+05	2,33E+05	2,11E+05	2,11E+05
DC	km	9,34E+04	9,34E+04	9,34E+04	9,30E+04	9,30E+04	9,23E+04	9,23E+04
NGCC	MW	2,69E+04	2,69E+04	2,65E+04	2,59E+04	2,56E+04	2,47E+04	2,43E+04
Gas Condensing Boiler	kW	7,00E+00	7,00E+00	7,00E+00	6,91E+00	6,91E+00	6,78E+00	6,78E+00
AWHP	kW	4,41E+01	4,17E+01	3,72E+01	3,69E+01	3,69E+01	3,63E+01	3,63E+01
Solar Flat Plate Collector	kW	4,45E+02	4,45E+02	4,45E+02	4,41E+02	4,41E+02	4,34E+02	4,34E+02
Long Term Heat Storage	GWh	2,73E+06	2,73E+06	2,73E+06	2,72E+06	2,72E+06	2,71E+06	2,71E+06
Building Retrofit 1	m2	1,13E+02	1,13E+02	1,13E+02	1,07E+02	1,07E+02	9,85E+01	9,85E+01
Building Retrofit 2	m2	2,33E+02	2,33E+02	2,33E+02	2,27E+02	2,27E+02	2,17E+02	2,17E+02

Building Retrofit 3	m2	1,21E+02	1,21E+02	1,21E+02	1,15E+02	1,15E+02	1,06E+02	1,06E+02
Building Retrofit 4	m2	2,76E+02	2,76E+02	2,76E+02	2,70E+02	2,70E+02	2,62E+02	2,62E+02
Building Retrofit 5	m2	2,45E+02	2,45E+02	2,45E+02	2,38E+02	2,38E+02	2,28E+02	2,28E+02
Import	kWh	2,44E-01	2,08E-01	1,72E-01	1,26E-01	8,10E-02	5,51E-02	2,92E-02

Tab. 115 Environmental impact on Resource Use per technology [kg Sb eq.]

Technology	Functional Unit	2020	2025	2030	2035	2040	2045	2050
PERC - Roof	MW	1,16E+01	1,10E+01	1,27E+01	1,18E+01	1,12E+01	1,09E+01	1,09E+01
PERC - Ground	MW	1,26E+01	1,18E+01	1,34E+01	1,24E+01	1,16E+01	1,13E+01	1,13E+01
SHJ - Roof	MW	1,41E+01	1,34E+01	1,59E+01	1,54E+01	1,50E+01	1,46E+01	1,41E+01
SHJ - Ground	MW	1,48E+01	1,40E+01	1,64E+01	1,58E+01	1,54E+01	1,50E+01	1,44E+01
CIGS - Roof	MW	1,04E+01	9,33E+00	8,59E+00	8,20E+00	7,80E+00	7,53E+00	7,22E+00
CIGS - Ground	MW	8,88E+00	8,09E+00	8,04E+00	7,80E+00	7,55E+00	7,40E+00	7,20E+00
III-V/Si – Roof	MW	1,07E+01	1,07E+01	1,07E+01	1,05E+01	1,00E+01	9,89E+00	9,55E+00
III-V/Si – Ground	MW	1,09E+01	1,09E+01	1,09E+01	1,06E+01	1,01E+01	9,88E+00	9,47E+00
EESG-DD Onshore	MW	2,89E+01	1,98E+01	2,49E+01	2,43E+01	2,43E+01	2,43E+01	2,43E+01
PMSD-DD Onshore	MW	1,96E+01	2,77E+01	3,31E+01	4,17E+01	4,17E+01	4,17E+01	4,17E+01
PMSD-DD Offshore	MW	1,41E+02	1,42E+02	1,43E+02	1,40E+02	1,42E+02	1,42E+02	1,42E+02
PMSG-MS Offshore	MW	1,38E+02	1,39E+02	1,40E+02	1,40E+02	1,43E+02	1,43E+02	1,43E+02
PEMFC	kW	4,54E-02	3,48E-02	2,20E-02	1,89E-02	1,59E-02	1,31E-02	1,10E-02
AEL	MW	1,47E+00	1,47E+00	1,47E+00	1,47E+00	1,47E+00	1,48E+00	1,48E+00
VRFB	kWh	2,39E-03	1,87E-03	1,49E-03	1,49E-03	1,49E-03	1,49E-03	1,49E-03
NMC	kWh	2,99E-03	2,78E-03	2,64E-03	2,48E-03	2,34E-03	2,20E-03	2,09E-03
AC	km	4,96E-02	4,96E-02	4,96E-02	9,41E-02	9,41E-02	1,00E-01	1,00E-01
DC	km	9,84E+01	9,84E+01	9,84E+01	9,84E+01	9,84E+01	9,84E+01	9,84E+01
NGCC	MW	2,17E+00	2,17E+00	2,12E+00	2,12E+00	2,07E+00	2,07E+00	2,02E+00
Gas Condensing Boiler	kW	9,40E-04	9,40E-04	9,40E-04	9,40E-04	9,40E-04	9,40E-04	9,40E-04
AWHP	kW	2,74E-02	2,58E-02	2,41E-02	2,41E-02	2,41E-02	2,41E-02	2,41E-02
Solar Flat Plate Collector	kW	5,36E-02	5,36E-02	5,36E-02	5,36E-02	5,36E-02	5,36E-02	5,36E-02

Absolute numbers of environmental impacts by technology

Long Term Heat Storage	GWh	5,54E+01	5,54E+01	5,54E+01	5,54E+01	5,54E+01	5,55E+01	5,55E+01
Building Retrofit 1	m2	1,48E-03	1,48E-03	1,48E-03	1,49E-03	1,49E-03	1,49E-03	1,49E-03
Building Retrofit 2	m2	1,48E-03	1,48E-03	1,48E-03	1,50E-03	1,50E-03	1,50E-03	1,50E-03
Building Retrofit 3	m2	1,48E-03	1,48E-03	1,48E-03	1,49E-03	1,49E-03	1,49E-03	1,49E-03
Building Retrofit 4	m2	1,49E-03	1,49E-03	1,49E-03	1,50E-03	1,50E-03	1,50E-03	1,50E-03
Building Retrofit 5	m2	1,48E-03	1,48E-03	1,48E-03	1,50E-03	1,50E-03	1,50E-03	1,50E-03
Import	kWh	1,66E-07	2,39E-07	3,11E-07	3,95E-07	4,79E-07	5,13E-07	5,47E-07

1 6 References

Abbas, Q., Mirzaeian, M., Gibson, D., 2020. Vanadium Air/Redox Flow Batteries, in: Reference Module in Materials Science and Materials Engineering. Elsevier.

Agora Energiewende and Sandbag, 2020. The European Power Sector in 2019. Up-to-Date Analysis on the Electricity Transition.

Altun-Çiftçioğlu, G.A., Gökulu, O., Kadırgan, F., Kadırgan, M., 2016. Life cycle assessment (LCA) of a solar selective surface produced by continuous process and solar flat collectors. Solar Energy 135, 284–290.

ANL, 2018. BatPaC: A Lithium-Ion Battery Performance and Cost Model for Electric-Drive Vehicles, in: OECD, International Energy Agency (Eds.), Global EV Outlook 2018.

Aquino, A., Bonamente, E., Rinaldi, S., Nicolini, A., Medaglia, C.M., 2017. Life cycle assessment of a ground-source heat pump including an upstream thermal storage. 17th CIRIAF National Congress. Sustainable Development, Human Health and Environmental Protection, Perugia.

Ardente, F., Beccali, G., Cellura, M., Lo Brano, V., 2005. Life cycle assessment of a solar thermal collector. Renewable Energy 30, 1031–1054.

Ashuri, T., 2012. Beyond classical upscaling. Integrated aeroservoelastic design and optimization of large offshore wind turbines. [s.n.], [S.l.].

BERR, 2008. Review of cabling Techniques and Environmental Effects Applicable to the Offshore Wind Farm Industry: Technical Report.

Betten, T., Shammugam, S., Graf, R., 2020. Adjustment of the Life Cycle Inventory in Life Cycle Assessment for the Flexible Integration into Energy Systems Analysis. Energies 13, 4437.

Birkeland, C., 2011. Assessing the Life Cycle Environmental Impacts of Offshore Wind Power Generation and Power Transmission in the North Sea. Master Thesis.

Blanco, C.F., Cucurachi, S., Dimroth, F., Guinée, J.B., Peijnenburg, W.J.G.M., Vijver, M.G., 2020. Environmental impacts of III-V/silicon photovoltaics: life cycle assessment and guidance for sustainable manufacturing. Energy Environ. Sci. 13, 4280–4290.

Bleck, W., Moeller, E., 2018. Handbuch Stahl. Auswahl, Verarbeitung, Anwendung. Carl Hanser Verlag, München.

BMWi, 2017. Langfristszenarien für die Transformation des Energiesystems in Deutschland. https://www.bmwi.de/Redaktion/DE/Artikel/Energie/langfrist-und-klimaszenarien.html.

Bongartz, L., Shammugam, S., Gervais, E., Schlegl, T., 2021. Multidimensional criticality assessment of metal requirements for lithium-ion batteries in electric vehicles and stationary storage applications in Germany by 2050. Journal of Cleaner Production 292, 126056.

Born, H., Willenbrink, S.S., Lange, H., Bussmann, G., Bracke, R., 2017. Analyse des deutschen Wärmepumpenmarktes - Bestandaufnahme und Trends. 2. Aktualisierung der Studie, Bochum.

Buchert, M., Dolega, P., Degreif, S., 2019. Gigafactories für Lithium-Ionen-Zellen. Rohstoffbedarfe für die globale Elektromobilität bis 2050, Darmstadt. https://www.oeko.de/fileadmin/oekodoc/Fab4Lib-Rohstoffe-Elektromobilitaet.pdf. Accessed October 2, 2019.

Buchert, M., Jenseit, W., Merz, C., Schüler, D., 2011. Ökobilanz zum „Recycling von Lithium-Ionen-Batterien" (LithoRec). Endbericht, Darmstadt. https://www.oeko.de/oekodoc/1500/2011-068-de.pdf. Accessed August 8, 2018.

Buist, J., 2015. Pile testing that suggests monopiles could use 35% less steel. Windpower monthly.

Bundesamt für Seeschifffahrt und Hydrographie. Unterwasserkabel. https://www.bsh.de/DE/THEMEN/Offshore/Offshore-Vorhaben/Unterwasserkabel/unterwasserkabel_node.html. Accessed June 9, 2021.

Bundesnetzagentur, 2016. Netzausbau. Freileitungen.

Bundesnetzagentur, 2019. EEG-Anlagenstammdaten (außer PV-Gebäudeanlagen). Veröffentlichung der Registerdaten - 08/2014 bis 01/2019. https://www.bundesnetzagentur.de/DE/Sachgebiete/ElektrizitaetundGas/Unternehmen_Institutionen/ErneuerbareEnergien/ZahlenDatenInformationen/EEG_Registerdaten/EEG_Registerdaten_node.html. Accessed July 26, 2019.

Bywaters, G., John, V., Lynch, J., Mattila, P., Norton, G., Stowell, J., 2004. Northern Power Systems WindPACT Drive Train Alternative Design Study Report.

Caduff, M., Huijbregts, M.A.J., Althaus, H.-J., Koehler, A., Hellweg, S., 2012. Wind power electricity: the bigger the turbine, the greener the electricity? Environmental science & technology 46, 4725–4733.

Cariou, R., Benick, J., Feldmann, F., Höhn, O., Hauser, H., Beutel, P., Razek, N., Wimplinger, M., Bläsi, B., Lackner, D., Hermle, M., Siefer, G., Glunz, S.W., Bett, A.W., Dimroth, F., 2018. III–V-on-silicon solar cells reaching 33% photoconversion efficiency in two-terminal configuration. Nature Energy 3, 326–333.

Carnevale, E., Lombardi, L., Zanchi, L., 2014. Life Cycle Assessment of solar energy systems: Comparison of photovoltaic and water thermal heater at domestic scale. Energy 77, 434–446.

Carrascal, S.R., 2014. Life Cycle Assessment. 1 Kwh generated by Gamesa G114-2.0MW On-shore wind farm. http://www.gamesacorp.com/recursos/doc/productos-servicios/aerogeneradores/life-cycle-assesment-g114-20-mw.pdf. Accessed 03.04.17.

Chen, Y., 2019. Engineering energy aluminum conductor composite core (ACCC) and its application. Academic Press, an imprint of Elsevier, London, United Kingdom.

CTC Global, 2011. Engineering Transmission Lines with High Capacity Low Sag ACCC® Conductors.

Dilthey, U., 2005. Schweißtechnische Fertigungsverfahren, 3., bearb. Aufl. Springer, Berlin.

Dorenbusch, K., Bohlen, W., Berlin, J., Knobloch, V., Reichhardt, D., Lüninghöner, M., Czerwonka, V., 2019. ENERCON Life Cycle Assessment. (Courtesy of ENERCON).

Elshkaki, A., Graedel, T.E., Ciacci, L., Reck, B.K., 2018. Resource Demand Scenarios for the Major Metals. Environmental science & technology 52, 2491–2497.

ENBW, 2020. EnBW Baltic 1: Technik. https://www.enbw.com/erneuerbare-energien/windenergie/unsere-windparks-auf-see/baltic-1/technik.html. Accessed May 13, 2020.

Enercon. Anlagenkomponenten. https://www.enercon.de/technologie/komponenten/. Accessed July 29, 2019.

Enercon, 2019. WEC Technology. Accessed July 29, 2019.

EnEV, 2013. Beispielhafte Maßnahmen zur Verbesserung der Energieeffizienz von typischen Wohngebäuden. Bundesgesetzblatt Jahrgang 2013 Teil 1 Nr. 67, Bonn.

Essig, S., Allebé, C., Remo, T., Geisz, J.F., Steiner, M.A., Horowitz, K., Barraud, L., Ward, J.S., Schnabel, M., Descoeudres, A., Young, D.L., Woodhouse, M., Despeisse, M., Ballif, C., Tamboli, A., 2017. Raising the one-sun conversion efficiency of III–V/Si solar cells to 32.8% for two junctions and 35.9% for three junctions. Nat Energy 2, 3.

EU Horizon 2020. ReaLCoE. https://www.realcoe.eu/. Accessed July 29, 2019.

FfE, 2017. Kurzstudie Power-to-X: Ermittlung des Potenzials von PtX Anwendungen für die Netzplanung der deutschen ÜNB. Accessed August 16, 2019.

Fingerling, K.-H., Feist, W., Otte, J., Pfluger, R., 2000. Konstruktionshandbuch für Passivhäuser, Teil 1 des Forschungsberichts zum Projekt: Das kostengünstige mehrgeschossige Passivhaus in verdichteter Bauweise.

Fraunhofer ISE, 2020. Wege zu einem klimaneutralen Energiesystem. Die deutsche Energiewende im Kontext gesellschaftlicher Verhaltensweisen, Freiburg. Accessed March 12, 2020.

Fthenakis, V., Kim, H.C., Frischknecht, R., M. Raugei, P. Sinha, M. Stuck, 2011. Life Cycle Inventories and Life Cycle Assessments of Photovoltaic Systems. IEA PVPS Task 12, Subtask 20, LCA, Report IEA-PVPS T12-02:2011. https://www.bnl.gov/pv/files/pdf/226_Task12_LifeCycle_Inventories.pdf.

Garcia Pardo, N., Vatopoulos, K., Krook Riekola, A., Perez Lopez, A., Olsen, L., 2012. Best available technologies for the heat and cooling market in the European Union. Publications Office, Luxembourg.

GE Renewable Energy, 2019. Haliade-X 12 MW: Die zurzeit größte und leistungsstärkste Offshore-Windenergieanlage der Welt. https://www.gerenewableenergy.com/de/wind/windenergieanlagen/haliade-x-12mw-offshore. Accessed July 29, 2019.

Georg Grimm Edelstahlhandel. Das Werkstoffdatenblatt - 1.4923. https://www.grimm-edelstahlhandel.de/1-4923-das-werkstoffdatenblatt/. Accessed August 12, 2022.

Gervais, E., Shammugam, S., Friedrich, L., Schlegl, T., 2021. Raw material needs for the large-scale deployment of photovoltaics – Effects of innovation-driven roadmaps on material constraints until 2050. Renewable and Sustainable Energy Reviews 137, 110589.

Gielen, D., 2021. Critical minerals for the energy transition, Abu Dhabi.

Görner, K., Sauer, D.U., 2016. Konventionelle Kraftwerke. Technologiesteckbrief zur Analyse „Flexibilitätskonzepte für die Stromversorgung 2050". Energiesysteme der Zukunft. Accessed January 8, 2020.

Graedel, T.E., Nassar, N.T., 2015. The criticality of metals. A perspective for geologists. Geological Society, London, Special Publications 393, 291–302.

Greening, B., Azapagic, A., 2012. Domestic heat pumps: Life cycle environmental impacts and potential implications for the UK. Energy 39, 205–217.

Greening, B., Azapagic, A., 2014. Domestic solar thermal water heating: A sustainable option for the UK? Renewable Energy 63, 23–36.

Gregoir, L., van Acker, K., 2022. Metals for Clean Energy: Pathways to solving Europe's raw materials challenge. https://eurometaux.eu/media/jmxf2qm0/metals-for-clean-energy.pdf. Accessed September 15, 2022.

Hertwich, E.G., 2021. Increased carbon footprint of materials production driven by rise in investments. Nat. Geosci. 14, 151–155.

Hofmann, Lutz, 2015. Einsatz von Erdkabeln und Freileitungen in Hochspannungs-Drehstrom- und -Gleichstromübertragungssystemen. Informationstag BNetzA, Hannover. Accessed September 5, 2019.

Huelman, P., Schirber, T., Mosiman, G., Jacobson, R., Smith, T., Li, M., 2016. Residential Ground Source Heat Pump Study: A Comprehensive Assessment of Performance, Emissions, and Economics. Conservation Applied Research & Development (CARD) Final Report. Prepared for: Minnesota Department of Commerce, Division of Energy Resources.

IEA-PVPS Task 12, 2020. Life Cycle Inventories and Life Cycle Assessment of Photovoltaic Systems. Report T12-19:2020. https://iea-pvps.org/wp-content/uploads/2020/12/IEA-PVPS-LCI-report-2020.pdf. Accessed September 15, 2022.

ITRPV, 2019. International Technology Roadmap for Photovoltaic. Tenth Edition.

James, B., 2018. 2018 Cost Projections of PEM Fuel Cell Systems for Automobiles and medium-Duty Vehicles. https://www.energy.gov/eere/fuelcells/downloads/2018-cost-projections-pem-fuel-cell-systems-automobiles-and-medium-duty. Accessed September 2, 2019.

James, B., Jennie M Huya-Kouadio, Cassidy Houchins, Daniel A Desantis, 2017. Mass Production Cost Estimation of Direct H2 PEM Fuel Cell Systems for Transportation Applications: 2017 Update. Accessed August 16, 2019.

James, B., Kalinoski, J., Baum, K., 2010. Mass Production Cost Estimation for Direct H2 PEM Fuel Cell Systems for Automotive Applications: 2010 Update.

Johnson, E.P., 2011. Air-source heat pump carbon footprints: HFC impacts and comparison to other heat sources. Energy Policy 39, 1369–1381.

Jorge, R.S., Hawkins, T.R., Hertwich, E.G., 2012. Life cycle assessment of electricity transmission and distribution—part 1: power lines and cables. The International Journal of Life Cycle Assessment 17, 9–15.

Jungbluth, N., Stucki, M., Flury, K., Frischknecht, R., Büsser, S., 2012. Life Cycle Inventories of Photovoltaics.

Kao, Y.-C., Chou, H.-M., Hsu, S.-C., Lin, A., Lin, C.-C., Shih, Z.-H., Chang, C.-L., Hong, H.-F., Horng, R.-H., 2019. Performance comparison of III-V//Si and III-V//InGaAs multi-junction solar cells fabricated by the combination of mechanical stacking and wire bonding. Scientific Reports 9, 4308.

Kaufman, B., Feist, W., u.a., 2004. Passivhäuser erfolgreich planen und bauen.

Kim, S., 2019. Vanadium Redox Flow Batteries: Electrochemical Engineering, in: Taha Demirkan, M., Attia, A. (Eds.), Energy Storage Devices. IntechOpen.

Koj, J., Wulf, C., Schreiber, A., Zapp, P., 2017. Site-Dependent Environmental Impacts of Industrial Hydrogen Production by Alkaline Water Electrolysis. Energies 10, 860.

Kushnir, D., Sandén, B.A., 2012. The time dimension and lithium resource constraints for electric vehicles. Resources Policy 37, 93–103.

Kwon, H.M., Moon, S.W., Kim, T.S., Kang, D.W., Sohn, J.L., Lee, J., 2019. A study on 65 % potential efficiency of the gas turbine combined cycle. J Mech Sci Technol 33, 4535–4543.

Lakshmanan, B., 2017. 2017 Bipolar Plate Workshop Report. GM Perspective on Bipolar Plate Status and Needs.

Leprich, U., Guss, H., Weiler, K., Ritzau, M., Macharey, U., Igel, M., Diegler, J., 2011. Ausbau elektrischer Netze mit Kabel oder Freileitung unter besonderer Berücksichtigung der Einspeisung Erneuerbarer Energien.

Liang, Y., Kleijn, R., Tukker, A., van der Voet, E., 2022. Material requirements for low-carbon energy technologies: A quantitative review. Renewable and Sustainable Energy Reviews 161, 112334.

Loga, T., Stein, B., Diefenbach, N., Born, R., 2015. Deutsche Wohngebäudetypologie. Beispielhafte Maßnahmen zur Verbesserung der Energieeffizienz von typischen Wohngebäuden.

Lozano Miralles, J.A., Palomar Carnicero, J.M., Lopez Garcia, R., Rey Martinez, F.J., 2018. Análisis del ciclo de vida (acv) de una bomba de calor aire/aire aplicada a un edificio terciario como contribución a una energía renovable. DYNAII (DYNA Ingenieria E Industria), 262–267.

Marscheider-Weidemann, F., Langkau, S., Hummen, T., Erdmann, L., Tercero Espinoza, L.A., Angerer, G., Marwede, M., Benecke, S., 2016. Rohstoffe für Zukunftstechnologien 2016. Auftragsstudie. DERA, Berlin.

Marwede, M., 2013. Cycling critical absorber materials of cdTe- and CIGS-photovoltaics. Material efficiency along the life-cycle. Dissertation.

Meeus, M., 2018. Overview of Battery Cell Technologies, Brussels.

Minke, C., 2016. Techno-ökonomische Modellierung und Bewertung von stationären Vanadium-Redox-Flow-Batterien im industriellen Maßstab, 1st ed. Cuvillier Verlag, Göttingen.

Miotti, M., Hofer, J., Bauer, C., 2017. Integrated environmental and economic assessment of current and future fuel cell vehicles. Int J Life Cycle Assess 22, 94–110.

Mohr, N.J., Schermer, J.J., Huijbregts, M.A.J., Meijer, A., Reijnders, L., 2007. Life cycle assessment of thin-film GaAs and GaInP/GaAs solar modules. Prog. Photovolt: Res. Appl. 15, 163–179.

Moss, R., Willis, P., Tercero, E.L., Tzimas, E., Arendorf, J., Thompson, P., Chapman, A., Morley, N., Sims, E., Bryson, R., Pearson, J., Marscheider-Weidemann, F., Soulier, M., Lüllmann, A., Sartorius, C., Ostertag, K., 2013. Critical metals in the path towards the decarbonisation of the EU energy sector. Assessing rare metals as supply-chain bottlenecks in low-carbon energy technologies. Publications Office of the European Union, Luxembourg.

Nadeem, F., Hussain, S.M.S., Tiwari, P.K., Goswami, A.K., Ustun, T.S., 2019. Comparative Review of Energy Storage Systems, Their Roles, and Impacts on Future Power Systems. IEEE Access 7, 4555–4585.

NKT, 2017. 640 kV XLPE HVDC cable system. Accessed September 5, 2019.

NPE, 2016. Roadmap integrierte Zell- und Batterieproduktion Deutschland, Berlin.

Olivetti, E.A., Ceder, G., Gaustad, G.G., Fu, X., 2017. Lithium-Ion Battery Supply Chain Considerations. Analysis of Potential Bottlenecks in Critical Metals. Joule 1, 229–243.

Parthey, F., 2010. Dissertation - Lebenszyklusanalyse und Bestimmung von Einflussfaktoren zur nachhaltigen Produktgestaltung von GuD-Kraftwerken.

Pavel, C.C., Lacal-Arántegui, R., Marmier, A., Schüler, D., Tzimas, E., Buchert, M., Jenseit, W., Blagoeva, D., 2017. Substitution strategies for reducing the use of rare earths in wind turbines. Resources Policy 52, 349–357.

PCC Energy Group, 2020. INCONEL® ALLOY 740H ®. A Superalloy Specifically Designed For Advanced Ultra Supercritical Power Generation.

Pertti, K., 2017. Raw material needs by the Li-ion battery industry. http://closeloop.fi/wp-content/uploads/2017/05/Li-raw-materials-20170517.pdf. Accessed August 1, 2018.

Pettinger, K.-H., Dong, W., 2017. When Does the Operation of a Battery Become Environmentally Positive? J. Electrochem. Soc. 164, A6274-A6277.

Pillot, C., 2017. Lithium ion battery raw material Supply & Demand 2016-2025, Mainz.

2015. Produktionsprozess einer Lithium-Ionen-Batteriezelle, Frankfurt/Aachen. https://www.pem.rwth-aachen.de/global/show_document.asp?id=aaaaaaaaaoqixv. Accessed November 13, 2019.

Qian, Y., Hu, S., Zou, X., Deng, Z., Xu, Y., Cao, Z., Kang, Y., Deng, Y., Shi, Q., Xu, K., Deng, Y., 2019. How electrolyte additives work in Li-ion batteries. Energy Storage Materials 20, 208–215.

Reuter, B., Riedl, J., Hamacher, T., Lienkamp, M., Bradshaw, A., 2014. COFAT 2014 – Future Resource Availability for the Production of Lithium-Ion Vehicle Batteries, in: Conference on Future Automotive Technology (CoFAT,2014).

Ropenus, S., Godron, P., Deutsch, M., 2018. Toolbox für die Stromnetze. Für die künftige Integration von Erneuerbaren Energien und für das Engpassmanagement.

Salhi, B., 2022. The Photovoltaic Cell Based on CIGS: Principles and Technologies. Materials (Basel, Switzerland) 15.

Schlegl, T., 2013. Entwicklungslinien der PV-Technologien und Materialsubstitutionsmöglichkeiten. Strategische Metalle für die Energiwende, Tuzing. web.ev-akademie-tutzing.de/cms/get_it.php?ID=1760. Accessed June 8, 2017.

Schmidt, K.H., 2013. Komponentenverhalten im 700 °C-Kraftwerk : numerische und experimentelle Untersuchungen.

Schmidt, T., Benner, M., Heidemann, W., Müller-Steinhagen, H., 2003. Saisonale Wärmespeicher – aktuelle Speichertechnologien und Entwicklungen bei Heißwasser-Wärmespeichern, OTTI, Fachseminar Oberflächennahe Geothermie.

Shah, V.P., Debella, D.C., Ries, R.J., 2008. Life cycle assessment of residential heating and cooling systems in four regions in the United States. Energy and Buildings 40, 503–513.

Shammugam, S., 2019. Raw materials and energy transformation process. Analysis of supply bottlenecks and implications on metal markets. Shaker Verlag, Düren.

Shammugam, S., Gervais, E., Schlegl, T., Rathgeber, A., 2019. Raw metal needs and supply risks for the development of wind energy in Germany until 2050. Journal of Cleaner Production 221, 738–752.

Siemens Gamesa Renewable Energy, 2019. SG 10.0-193. Offshore wind turbine. https://www.siemensgamesa.com/products-and-services/offshore/wind-turbine-sg-10-0-193-dd. Accessed July 29, 2019.

Sieros, G., Chaviaropoulos, P., Sørensen, J.D., Bulder, B.H., Jamieson, P., 2012. Upscaling wind turbines. Theoretical and practical aspects and their impact on the cost of energy. Wind Energ. 15, 3–17.

Smolinka, T., Wiebe, N., Sterchele, P., Palzer, A., 2018. Studie IndWEDe. Industrialisierung der Wasser elektrolyse in Deutschland: Chancen und Herausforderungen für nachhaltigen Wasserstoff für Verkehr, Strom und Wärme, Berlin. https://www.google.com/url?sa=t&rct=j&q=&esrc=s&source=web&cd=1&cad=rja&uact=8&ved=2ahUKEwjwib_C3pToAhUNy6QKHVFkDg8QFjAAegQIAhAB&url=https%3A%2F%2Fwww.now-gmbh.de%2Fcontent%2Fservice%2F3-publikationen%2F1-nip-wasserstoff-und-brennstoffzellentechnologie%2Findwede-studie_v04.1.pdf&usg=AOvVaw0pEnVq4htdFaN_7i6HP7BJ. Accessed March 12, 2020.

Sneed, B.T., Cullen, D.A., Mukundan, R., Borup, R.L., More, K.L., 2018. PtCo Cathode Catalyst Morphological and Compositional Changes after PEM Fuel Cell Accelerated Stress Testing. J. Electrochem. Soc. 165, F3078-F3084.

Sphera, 2020. Sphera. GaBi Software and Databases. Service Pack 40. Sphera Solutions GmbH, Leinfelden-Echterdingen, Germany.

Steel Grades. Steel Grades. 28NiCrMo4. https://www.steel-grades.com/Steel-Grades/Carbon-Steel/28NiCrMo4.html. Accessed August 12, 2022.

Stenzel, P., Fleer, J., Linssen, J., 2015. Elektrochemische Speicher, in: Wietschel, M., Ullrich, S., Markewitz, P., Schulte, F., Genoese, F. (Eds.), Energietechnologien der Zukunft. Springer Fachmedien Wiesbaden, Wiesbaden, pp. 157–214.

Sterchele, P., 2019. Analysis of Technology Options to Balance Power Generation from Variable Renewable Energy. Case Study for the German Energy System with the Sector Coupling Model REMod, 1. Auflage. Shaker, Düren.

Stucki, Matthias: Jungbluth, Niels, 2012. Update of the Life Cycle Inventories of Solar Collectors. http://esu-services.ch/fileadmin/download/publicLCI/stucki-2010-Solar-Collector.pdf. Accessed November 20, 2019.

2011. Thermische Solaranlagen. Informationsblatt 17. https://www.bdh-koeln.de/fileadmin/user_upload/Publikationen/Infoblaetter/Infoblatt_Nr_34_Maerz_2011_Betriebssicherheit_thermischer_Solaranlagen.pdf. Accessed November 21, 2019.

Thielmann, A., Neef, C., Hettesheimer, T., Döscher, H., Wietschel, M., Tübke, J., 2017. Energiespeicher-Roadmap. Update 2017, Karlsruhe. Accessed August 21, 2018.

Thielmann, A., Sauer, A., Wietschel, M., 2015. Gesamt-Roadmap Lithium-Ionen-Batterien 2030, Karlsruhe. Accessed August 1, 2018.

Thomas, H., Marian, A., Chervyakov, A., Stückrad, S., Salmieri, D., Rubbia, C., 2016. Superconducting transmission lines – Sustainable electric energy transfer with higher public acceptance? Renewable and Sustainable Energy Reviews 55, 59–72.

Thomitzek, M., Cerdas, F., Thiede, S., Herrmann, C., 2019. Cradle-to-Gate Analysis of the Embodied Energy in Lithium Ion Batteries. Procedia CIRP 80, 304–309.

Tong, C., 2019. Introduction to Materials for Advanced Energy Systems. Springer International Publishing, Cham.

UBA, 2016. Ableitung von Recycling- und Umweltanforderungen und Strategien zur Vermeidung von Versorgungsrisiken bei innovativen Energiespeichern, Dessau-Roßlau. Accessed June 12, 2019.

United Nations Environment Programme, 2020. Global Resources Outlook 2019. Natural Resources for the Future We Want. United Nations, New York.

Vignali, G., 2017. Environmental assessment of domestic boilers: A comparison of condensing and traditional technology using life cycle assessment methodology. Journal of Cleaner Production 142, 2493–2508.

Watari, T., McLellan, B., Ogata, S., Tezuka, T., 2018. Analysis of Potential for Critical Metal Resource Constraints in the International Energy Agency's Long-Term Low-Carbon Energy Scenarios. Minerals 8, 156.

Watari, T., Nansai, K., Nakajima, K., 2020. Review of critical metal dynamics to 2050 for 48 elements. Resources, Conservation and Recycling 155, 104669.

Wuppertal Institut, 2014. KRESSE – Kritische mineralische Ressourcen und Stoffströme bei der Transformation des deutschen Energieversorgungssystems. Abschlussbericht 0325324 an das Bundesministerium für Wirtschaft und Energie (BMWi), Wuppertal. http://wupperinst.org/de/projekte/details/wi/p/s/pd/38/. Accessed August 1, 2018.

Xu, C., Dai, Q., Gaines, L., Hu, M., Tukker, A., Steubing, B., 2020. Future material demand for automotive lithium-based batteries. Commun Mater 1.

Zheng, M., Fang, R., Yu, Z., 2016. Life Cycle Assessment of Residential Heating Systems: A Comparison of Distributed and Centralized Systems. Energy Procedia 104, 287–292.

1 7 Imprint

Recommended citation

Gervais, E., Betten, T., Shammugam, S., Graf, R., Müller, M., Schlegl, T.: Material requirements for the energy transition – Energy technology profiles and environmental impacts (2022)

https://dx.doi.org/10.24406/publica-427

Authors

Estelle Gervais, Shivenes Shammugam, Thomas Schlegl (Fraunhofer ISE)

Thomas Betten, Roberta Graf, Matthias Müller (University of Stuttgart)

Acknowledgement

This research was conducted as part of the InteRessE project (Ressourcenbedarf für die Energiewende: Interdisziplinäre Bewertung von Szenarien für die Bereitstellung von Strom und Wärme), funded by the German Federal Ministry for Economic Affairs and Climate Action under grant no. 03ET4065.

Thanks go to Lisa Bongartz and Daniel Rhein for the support in data collection and formatting.

Contact

Estelle Gervais

Fraunhofer Institute for Solar Energy Systems ISE
E-Mail: estelle.gervais@ise.fraunhofer.de

Thomas Betten

University of Stuttgart – Department Life Cycle Engineering, Institute for Acoustics and Building Physics

E-Mail: thomas.betten@iabp.uni-stuttgart.de